

1 This manuscript is a preprint of a paper that was submitted for publication in Journal  
2 of the Geological Society. Please note that the manuscript is now formally accepted  
3 for publication in JGS and has the doi number:

4  
5 <https://doi.org/10.1144/jgs2020-222>

6  
7 The final version of this manuscript will be available via the 'Peer reviewed Publication  
8 DOI' link on the right-hand side of this webpage. Please feel free to contact any of the  
9 authors. We welcome feedback on this community effort to produce a framework for  
10 future rock record-based subdivision of the pre-Cryogenian geological timescale.  
11

12 **Towards a new geological time scale: A template for improved rock-based subdivision of**  
13 **pre-Cryogenian time**

14

15 Graham A. Shields<sup>1\*</sup>, Robin A. Strachan<sup>2</sup>, Susannah M. Porter<sup>3</sup>, Galen P. Halverson<sup>4</sup>, Francis A.  
16 Macdonald<sup>3</sup>, Kenneth A. Plumb<sup>5</sup>, Carlos J. de Alvarenga<sup>6</sup>, Dhiraj M. Banerjee<sup>7</sup>, Andrey Bekker<sup>8</sup>,  
17 Wouter Bleeker<sup>9</sup>, Alexander Brasier<sup>10</sup>, Partha P. Chakraborty<sup>7</sup>, Alan S. Collins<sup>11</sup>, Kent Condie<sup>12</sup>,  
18 Kaushik Das<sup>13</sup>, Evans, D.A.D.<sup>14</sup>, Richard Ernst<sup>15</sup>, Anthony E. Fallick<sup>16</sup>, Hartwig Frimmel<sup>17</sup>, Reinhardt  
19 Fuck<sup>6</sup>, Paul F. Hoffman<sup>18</sup>, Balz S. Kamber<sup>19</sup>, Anton Kuznetsov<sup>20</sup>, Ross Mitchell<sup>21</sup>, Daniel G. Poiré<sup>22</sup>,  
20 Simon W. Poulton<sup>23</sup>, Robert Riding<sup>24</sup>, Mukund Sharma<sup>25</sup>, Craig Storey<sup>2</sup>, Eva Stueeken<sup>26</sup>, Rosalie  
21 Tostevin<sup>27</sup>, Elizabeth Turner<sup>28</sup>, Shuhai Xiao<sup>29</sup>, Shuanhong Zhang<sup>30</sup>, Ying Zhou<sup>1</sup>, Maoyan Zhu<sup>31</sup>

22

23 <sup>1</sup>Department of Earth Sciences, University College London, UK; [g.shields@ucl.ac.uk](mailto:g.shields@ucl.ac.uk)

24 <sup>2</sup>School of the Environment, Geography and Geosciences, University of Portsmouth, UK

25 <sup>3</sup>Department of Earth Science, University of California at Santa Barbara, USA

26 <sup>4</sup>Department of Earth and Planetary Sciences, McGill University, Canada

27 <sup>5</sup>Geoscience Australia (retired), Canberra, Australia

28 <sup>6</sup>Instituto de Geociências, Universidade de Brasília, Brazil

29 <sup>7</sup>Department of Geology, University of Delhi, India

30 <sup>8</sup>Department of Earth and Planetary Sciences, University of California, Riverside, USA

31 <sup>9</sup>Geological Survey of Canada, Ottawa, Canada

32 <sup>10</sup>School of Geosciences, University of Aberdeen, UK

33 <sup>11</sup>Department of Earth Sciences, The University of Adelaide, Australia

34 <sup>12</sup>New Mexico Institute of Mining and Technology, USA

35 <sup>13</sup>Department of Earth and Planetary System Sciences, Hiroshima University, Japan

36 <sup>14</sup>Department of Earth and Planetary Sciences, Yale University, USA

37 <sup>15</sup>Department of Earth Sciences, Carleton University, Canada; Faculty of Geology and Geography, Tomsk State  
38 University, Tomsk, Russia

39 <sup>16</sup>Isotope Geosciences Unit S.U.E.R.C., East Kilbride, UK

40 <sup>17</sup>Institute of Geography and Geology, University of Würzburg, Germany

41 <sup>18</sup>Department of Earth and Planetary Sciences, Harvard University, USA; University of Victoria, Canada

42 <sup>19</sup>School of Earth and Atmospheric Sciences, Queensland University of Technology, Brisbane, Australia

43 <sup>20</sup>Institute of Precambrian Geology and Geochronology, St. Petersburg, Russia

44 <sup>21</sup>Institute of Geology and Geophysics, Beijing, China

45 <sup>22</sup>Centro de Investigaciones Geológicas–CONICET–FCNyM, (UNLP), La Plata, Argentina

46 <sup>23</sup>School of Earth and Environment, University of Leeds, UK

47 <sup>24</sup>Department of Earth and Planetary Sciences, University of Tennessee, Knoxville, USA

48 <sup>25</sup>Birbal Sahni Institute of Palaeobotany, Lucknow, India

49 <sup>26</sup>Department of Earth Sciences, University of St. Andrews, UK

50 <sup>27</sup>Department of Earth Sciences, University of Cape Town, South Africa

51 <sup>28</sup>Laurentian University, Sudbury, Canada

52 <sup>29</sup>Department of Geosciences, Virginia Tech, USA

53 <sup>30</sup>Institute of Geomechanics, Chinese Academy of Geological Sciences, China

54 <sup>31</sup>Nanjing Institute of Geology and Palaeontology, Nanjing, China

55

56 **Abstract**

57

58 Four eon- and nine era-level units continue to provide intuitive subdivision of geological time. Major  
59 Earth system transitions occurred at approximately 2.5-2.3, 1.8-1.6, 1.0-0.8 and 0.7-0.5 Ga, and so  
60 future rock record-based subdivision of pre-Cryogenian time, eventually by use of global stratotypes  
61 (GSSPs), will likely require only modest deviation from current chronometric era boundaries. Here we  
62 argue that removal of GSSAs could be expedited by establishing event-based concepts and provisional,  
63 approximate ages for eon-, era- and period-level subdivisions as soon as practicable. We also outline  
64 the geological basis behind the current timescale and outline where immediate changes to the present  
65 scheme could be formalised, as a framework for future GSSP development. We agree with previous  
66 workers that the informal four-fold Archean subdivision could be simplified to a tripartite scheme  
67 pending more detailed analysis. Although the ages of period boundaries would inevitably change in a  
68 more closely rock-based or chronostratigraphic scheme, we support retention of all currently ratified  
69 period names. Existing period names, borrowed from the Greek, were chosen to delimit natural  
70 phenomena of global reach. Any new global nomenclature ought to follow this lead for consistency  
71 (e.g., *Scourian*, *Kratian*, *Kleisian*, *Syndian*), and so we discourage the use of both supercontinent names  
72 (e.g., Rodinian, Columbian) and regional phenomena, however exceptional they may be. Here we  
73 propose that a new period could precede the Tonian as the first period of the Neoproterozoic Era and  
74 concur with previous authors that the existing Siderian Period (named for iron formations) would fit  
75 better as a chronostratigraphically defined period of the terminal Archean rather than the basal  
76 Proterozoic. Indeed, all pre-Cryogenian subdivisions will need better conceptual grounding in any  
77 future chronostratigraphic scheme. We conclude that an improved rock-based Proterozoic Eon could  
78 potentially comprise a three-fold, period-level subdivision of the Paleoproterozoic Era (*early*  
79 *Paleoproterozoic* or *Scourian*, Rhyacian, Orosirian), a four-fold subdivision of the Mesoproterozoic  
80 Era (Statherian, Calymmian, Ectasian, Stenian) and potentially four-fold subdivision of the  
81 Neoproterozoic Era (pre-Tonian or *Kleisian*, Tonian, Cryogenian and Ediacaran). Refinements towards  
82 an improved rock-based pre-Cryogenian time scale could potentially use the proposed framework for  
83 further development by international bodies with remit over the 1) pre-Ediacaran Neoproterozoic, 2)  
84 Mesoproterozoic, 3) Paleoproterozoic and 4) Archean (plus Hadean) as few experts and disciplines can  
85 speak to the entire pre-Cryogenian rock record.

86

87 **1. Introduction**

88 The term ‘Precambrian’, or more traditionally ‘pre-Cambrian’ (Glaessner, 1962), is an informal  
 89 geological term that refers to the time before the beginning of the Cambrian Period at c. 0.54 Ga (Peng  
 90 et al., 2020). The two pre-Cambrian eonothems (Archean and Proterozoic) have long pedigrees  
 91 (Sedgwick, 1845; Logan, 1857; Dana, 1872), but, were introduced formally only after extensive  
 92 discussion among members of the Subcommittee on Precambrian Stratigraphy (SPS), which was  
 93 tasked in 1966, with Kalervo Rankama as chair, with standardizing Precambrian nomenclature  
 94 (Trendall, 1966). James (1978), summarising discussions within the subcommittee, outlined five  
 95 categories of proposals: 1) subdivision by intervals of equal duration (Goldich, 1968; see also Hofmann,  
 96 1990; 1992; Trendall, 1991); 2) subdivision by major magmatic-tectonic cycles (Stockwell, 1961;  
 97 1982); 3) subdivision by stratotypes (Dunn et al., 1966; see also Crook, 1989); 4) subdivision by breaks  
 98 in the geological record defined by radiometric ages (James, 1972); and 5) subdivision based on Earth  
 99 evolution concepts (Cloud, 1976). One result of those early discussions was that an approximate  
 100 chronological age of 2500 Ma was assigned to a somewhat transitional Archean-Proterozoic boundary  
 101 (James, 1978). However, further subdivision of the Precambrian in a comparable manner to that  
 102 achieved for younger rocks, although favoured by some (Hedberg, 1974), proved unworkable (James,  
 103 1978) due to 1) the relatively fragmentary nature of the Precambrian rock record, much of which is  
 104 strongly deformed and metamorphosed, and 2) a scarcity of age-diagnostic fossils. For this reason, a  
 105 mixed approach was applied: Global Standard Stratigraphic Ages (GSSAs) were introduced to  
 106 subdivide Precambrian time but the absolute ages of periods were chosen to bracket major magmatic-  
 107 tectonic episodes (Plumb and James, 1986; Plumb, 1991). Since that decision was ratified, all of pre-  
 108 Cryogenian Earth history and its geological record has been subdivided using geochronology rather  
 109 than chronostratigraphy.

110 The principal Precambrian subdivisions now comprise the informal Hadean and formal  
 111 Archean and Proterozoic eons (Fig. 1A), which, following the GSSA concept, are defined as units of  
 112 time rather than stratigraphic packages. The Hadean Eon refers to the interval with no preserved crustal  
 113 fragments that followed formation of the Earth at c. 4.54 Ga (Patterson, 1956; Manhès et al., 1980).  
 114 Because the Hadean Eon left no rock record on Earth (other than reworked mineral grains or  
 115 meteorites), it cannot be regarded as a stratigraphic entity (eonothem) and has never been formally  
 116 defined or subdivided. It is succeeded by the Archean Eon, which is usually taken to begin at 4.0 Ga  
 117 and is itself succeeded at precisely 2.5 Ga by the Proterozoic Eon. The Archean Eon is informally  
 118 divided into four eras (Eoarchean, Paleoarchean, Mesoarchean and Neoarchean; e.g., Bleeker, 2004a),  
 119 although a three-fold subdivision is widely favoured (van Kranendonk et al., 2012; Strachan et al.,  
 120 2020). The Proterozoic Eon is currently subdivided into three eras (Paleoproterozoic, Mesoproterozoic  
 121 and Neoproterozoic) and ten periods (Siderian, Rhyacian, Orosirian, Statherian, Calymmian, Ectasian,  
 122 Stenian, Tonian, Cryogenian and Ediacaran). The era names were conceived after a proposal from Hans

123 Hofmann in 1987 (Hofmann, 1992; Plumb, 1992), while the period names derive from discussions  
124 within the SPS (Plumb 1991). The three Proterozoic eras were originally proposed to begin at 2.5 Ga  
125 (Proterozoic I), 1.6 Ga (Proterozoic II) and 0.9 Ga (Proterozoic III), respectively (Plumb and James,  
126 1986). However, the beginning of the Neoproterozoic Era was subsequently moved to 1.0 Ga in the  
127 final proposal (Plumb, 1991).

128 The ages of Precambrian boundaries were selected to delimit major cycles of sedimentation,  
129 orogeny and magmatism (Plumb, 1991; Fig. 1A). However, knowledge has improved considerably over  
130 the past thirty years due to 1) increasingly precise and accurate U-Pb zircon dating, 2) improved isotopic  
131 and geochemical proxy records of tectonic, environmental and biological evolution, and 3) new rock  
132 and fossil discoveries. As a result, some of these numerical boundaries no longer bracket the events for  
133 which they were named. The International Commission on Stratigraphy (ICS) began to address the  
134 GSSA immobility problem in 2004 when they ratified the basal Ediacaran GSSP (Global Stratotype  
135 Section and Point) on the basis of the stratigraphic expression of a global chemo-oceanographic (and  
136 climatic) event in a post-glacial dolostone unit in South Australia (Knoll et al., 2004). Latest  
137 geochronology and chronostratigraphy confirms that all typical Marinoan ‘cap dolostone’ units were  
138 deposited contemporaneously at c. 635.5 Ma (Xiao and Narbonne, GTS 2020). The Ediacaran GSSP is  
139 thus one of the most highly resolved system-level divisions of the entire geological record.

140 The chronostratigraphic (re)definition of the Ediacaran Period (and System) replaced the  
141 provisional GSSA (650 Ma) that had been used to mark the end of the Cryogenian Period. This allowed  
142 the Marinoan ‘snowball’ glaciation (c. 645 – c. 635.5 Ma) to be included within the geological period  
143 that owed its name to that glaciation. The 850 Ma age marking the beginning of the Cryogenian was  
144 subsequently found to be much older than consensus estimates for the onset of widespread Sturtian  
145 ‘snowball’ glaciation at c. 717 Ma (Macdonald et al., 2010; Halverson et al., 2020) and so it was also  
146 removed, following a proposal from the Cryogenian Subcommittee (Shields-Zhou et al., 2016). A  
147 globally correlative stratigraphic horizon at or beneath this level has not yet been proposed by the  
148 Cryogenian Subcommittee, although an approximate age of c. 720 Ma for the boundary, pending a  
149 ratified GSSP, has been written into the international geological time scale. Despite the lack of a GSSP,  
150 the age revision of the Cryogenian Period by 130 million years has been quickly accepted by the  
151 geological community worldwide, presumably because it now matches the natural phenomena for  
152 which it was named. International geological bodies have yet to tackle other issues of non-alignment  
153 between names and ages for any other Proterozoic period despite occasional challenges, e.g., Bleeker  
154 (2004a,b), van Kranendonk et al. (2012).

155 In both cases (Cryogenian and Ediacaran GSSPs), and in the case of the earlier ratification of  
156 the Precambrian-Cambrian boundary GSSP (Brasier et al., 1994), establishment of a rock-based or  
157 chronostratigraphic concept permitted relatively easy consensus around an approximate,  
158 stratigraphically calibrated age, before more prolonged and detailed discussions could take place  
159 towards eventual GSSP proposal and ratification. In the light of rapidly expanding knowledge about

160 Precambrian Earth history, these three precedents serve to illustrate how the GSSA approach has  
161 become outdated and how it is now evident that all Precambrian subdivisions will require revision to a  
162 more natural, chronostratigraphic framework (e.g., Bleeker 2004a,b; Van Kranendonk et al., 2012;  
163 Ernst et al., 2020). Identified shortcomings with the inflexible GSSA approach include: a) a lack of ties  
164 to the rock record and broader Earth and planetary history, b) the diachronous nature of the tectonic  
165 events on which the current scheme (Fig. 1A) is based, and c) the lack of any major sedimentological,  
166 geochemical and biological criteria that can be used to correlate subdivision boundaries in stratigraphic  
167 records. As a result, Proterozoic period nomenclature, although increasingly used in the scientific  
168 literature, is commonly out of step with the concepts or phenomena for which they were named, while  
169 the underlying basis for both era and period nomenclature is neither universally accepted nor widely  
170 understood.

171 An alternative stratigraphic scheme for the Precambrian was therefore revisited for discussion  
172 based on potential Global Boundary Stratotype Sections and Points (GSSPs) (Fig. 1B) (Van  
173 Kranendonk et al., 2012). Following the rationale of Cloud (1972), the approach taken was to base a  
174 revised Precambrian time scale as closely as possible around geobiological events, such as changes to  
175 oceans, atmosphere, climate or the carbon cycle that would be near instantaneous compared to changes  
176 in geotectonic processes. We agree with the rationale pursued in Van Kranendonk et al. (2012), which  
177 followed an earlier proposal of Bleeker (2004a), while noting that some newly proposed subdivisions  
178 represent a radical departure from standard practice. This is illustrated by the proposal of a new and  
179 exceptionally long ‘Rodinian’ Period between 1800 Ma and 850 Ma Van Kranendonk et al. (2012),  
180 which replaced five of the pre-existing Proterozoic periods. The principle of naming a geological period  
181 after a hypothetical supercontinent set a further precedent that is not widely accepted.

182 Recent progress towards, and widespread acceptance of, chronostratigraphic definitions for two  
183 Precambrian periods suggests that the international community can act expeditiously to address  
184 inadequacies of the chronometric scheme, while overcoming the confusion generated by the informal  
185 erection of new periods and unsupported concepts. This contribution outlines current understanding of  
186 Earth history in order to encourage broader consultation on new recommendations around 1) a time  
187 frame for GSSA removal, 2) rock-based concepts and approximate ages for eon-, era- and possible  
188 period-level subdivision of pre-Cryogenian time, and 3) new international expert bodies to propose  
189 concepts, criteria and candidates for future GSSPs. Our aim is to outline the geological basis behind  
190 current chronometric divisions, explore how boundaries might differ in any future chronostratigraphic  
191 scheme, identify where major issues might arise during the transition to that scheme, and identify where  
192 some immediate changes to the present scheme could be easily updated/formalised, as a framework for  
193 future GSSP development. We note that this is not simply a matter of academic interest for geologists.  
194 Establishing a robust, coherent and intuitive stratigraphic nomenclature is of great importance for  
195 improving understanding of Earth’s history for schools, universities and the wider community alike.

196           Transitioning from a purely chronometric to a chronostratigraphic scheme will inevitably place  
197 more emphasis on the rock record and on precise stratigraphic levels within key successions and their  
198 global equivalents. In this regard, we accept the arguments made by Zalasiewicz et al. (2004) that units  
199 of time and strata are, following the introduction of boundary stratotypes and points or GSSPs,  
200 interchangeable and largely superfluous. Specifically, we agree that chronostratigraphic units such as  
201 eonothem, erathem or system are confusing and argue that they are particularly inappropriate for  
202 subdividing the enormously long time intervals and relatively incomplete rock records of the pre-  
203 Cryogenian archive. As a result, we mainly use time subdivisions below (eons, eras, periods), while  
204 recalling that their precise definitions and stratigraphically calibrated ages would eventually need to be  
205 defined using a level within a global boundary stratotype section.

206

207

## 208           **2. Eon- and Era-level subdivisions of Precambrian time**

### 209           **2.1 Hadean Eon (> c.4.0 Ga)**

210           Spanning the interval between the formation of the Solar System (c. 4.567 Ga) and the first rock-based  
211 evidence for crust on Earth (c. 4.0 Ga), the Hadean Eon was a time of planetary accretion and  
212 differentiation. Defining an absolute time scale for the eon is challenging due to the criterion on which  
213 it is typically defined: the lack of a preserved rock record on Earth (Cloud, 1976; Strachan et al., 2020).  
214 Nevertheless, our understanding of the geological processes that shaped our planet during the Hadean  
215 continues to improve. Neither the beginning nor the end of the Hadean are yet formally defined by the  
216 International Commission on Stratigraphy (ICS) but the end is usually taken as 4.0 Ga (Fig. 1A). It has  
217 been proposed that the Hadean-Archaean boundary be defined as the age of the oldest preserved crustal  
218 rock (van Kranendonk et al., 2012). The oldest unambiguously dated rocks are  $4.031 \pm 0.003$  Ga  
219 orthogneisses from the Acasta gneiss of the Slave Craton, Canada (Stern and Bleeker, 1998; Bowring  
220 and Williams, 1999), which led van Kranendonk et al. (2012) to propose that the boundary be placed at  
221 c. 4.03 Ga (Fig. 1B). However, other authorities have preferred a younger boundary at c. 3.85 Ga to  
222 represent the time when crustal preservation on multiple cratonic fragments increased sharply (Bleeker,  
223 2004a,b; Kamber, 2015). A definition based around the ages of the oldest unambiguous supracrustal  
224 rocks matches closely the ideas of Cloud (1972) and may facilitate more robust linkages with wider  
225 solar system evolution

226           Controversially, older model ages of up to ~4.4 Ga have been inferred for mafic gneisses in the  
227 Nuvvuagittuq Supracrustal Belt in the Superior Province, Canada (O'Neil et al., 2008, 2012), based on  
228 contested interpretations of the short-lived  $^{146}\text{Sm}$ - $^{142}\text{Nd}$  systematics in these highly metamorphosed  
229 rocks (e.g., see Caro et al., 2017). Zircon U-Pb ages from felsic orthogneisses in the Nuvvuagittuq Belt  
230 suggest a formation age of >3.8 Ga (e.g., Darling et al., 2014), and coupled Lu-Hf and Sm-Nd model  
231 ages of ~3.9 Ga for the mafic gneisses have been taken as evidence for an Archaean, rather than Hadean

232 origin (e.g., Guitreau et al., 2013). However, O’Neil et al. (2012) report a  $^{147}\text{Sm}$ - $^{143}\text{Nd}$  isochron from  
233 intrusive gabbro in the Nuvvuagittuq Belt of  $4.115 \pm 0.1$  Ga. Taken together, these studies highlight the  
234 difficulty in unambiguously dating highly deformed and metamorphosed ancient crustal rocks from  
235 very small preserved fragments (Kamber, 2015), while confirming that c. 4.0 Ga (or later) still  
236 represents a suitable approximate age for the Hadean-Archean boundary if defined on the basis of  
237 potentially correlative rock and mineral assemblages. To debate this boundary further, however, lies  
238 beyond the scope and intent of the current paper, as the defining concept of the Hadean remains largely  
239 unchallenged.

240

## 241 **2.2 Archean Eon (c. 4.0 to 2.45/2.5 Ga)**

242 The Archean Eon spans the period of early crustal formation and thickening, leading to the formation  
243 of the first cratons and platform sedimentation. It is characterised by granite-greenstone terranes and  
244 the extrusion of ultramafic lavas (komatiites), which are very rare in post-Archean rocks. Away from  
245 the recognised granite-greenstone terranes or younger platform covers, the Archean is characterised by  
246 high-grade, polymetamorphic granite-gneiss complexes, of various ages.

247 Subdivision of the chronometric Archean Eon was not formalised, pending collection of more  
248 data and analysis (Plumb, 1991). Nevertheless, the Subcommittee on Precambrian Stratigraphy (SPS)  
249 voted in 1991 and again in 1995 to pursue formal subdivision into four eras: Eoarchean (>3.6 Ga),  
250 Paleoarchean (3.6 to 3.2 Ga), Mesoarchean (3.2 to 2.8 Ga), and Neoarchean (2.8 to 2.5 Ga) (Fig. 1A);  
251 no reasons for the choice of these boundaries were given. Since these subdivisions have not been  
252 formally ratified (Robb et al., 2004), they are considered to be recommendations only (Bleeker, 2004a).  
253 An alternative subdivision scheme was proposed by van Kranendonk et al. (2012), which simplified  
254 these to three: the Paleoarchean (4.03 to 3.49 Ga), Mesoarchean (3.49 to 2.78 Ga), and Neoarchean  
255 (2.78 to 2.42 Ga), each composed of a number of periods (Fig. 1B). The base of the Paleoarchean in the  
256 2012 proposal was defined by the age of the oldest extant rocks, the Acasta Gneiss, Canada, while the  
257 base of the overlying Mesoarchean was defined at the oldest microbially-influenced textures or  
258 structures in stromatolites of the North Pole Dome in western Australia, thus representing the oldest  
259 potential “golden spike” (Fig. 1B). The Paleoarchean contained an ‘Acastan Period’, the lower limit of  
260 which was defined by the oldest preserved rocks (Acasta Gneiss, Canada) and an ‘Isuan Period’, the  
261 lower limit of which was defined at 3.81 Ga (the age of the Earth’s oldest supracrustal rocks, the Isua  
262 Supracrustal Belt in Greenland).

263 The problem with this approach is that the oldest occurrence of a particular rock type may identify  
264 chance preservation rather than any fundamental change in geological process, and older terranes may  
265 be identified in the future. It also runs counter to the concept of the international geological time scale  
266 as a correlative ‘stratigraphic’ framework, leading us to support leaving the base of the Archean at ~4.0  
267 Ga, pending formal definition of the Hadean-Archean boundary. This argument also invalidates the  
268 Eoarchean as a fundamental unit of geological time. A similar problem arises with the placement of the



269 base of the Mesoarchean at c. 3.49 Ga for the North Pole Dome stromatolites; not only the problem of  
270 these being the “oldest” stromatolites, but the occurrence of stromatolites is controlled by the particular  
271 environment, rather than being a definable moment in evolution. A less ambiguous boundary for the  
272 base of the Mesoarchean could be the near-coeval base of the first preserved Barberton and Pilbara  
273 granite-greenstone terranes. This is currently considered to be ~3.5 Ga, or perhaps a little older. High-  
274 grade metamorphic-plutonic complexes, with little internal stratigraphic structure (e.g., Limpopo Belt;  
275 Western Gneiss Terranes, Western Australia) become more common toward the top of the interval.

276 Van Kranendonk et al. (2012) also proposed changing the end of the Archean to c. 2.42 Ga, based  
277 on the first widespread appearance of ‘Huronian’ glacial deposits in the rock record (Young, 2019) and  
278 the approximately contemporaneous change to an oxygenated atmosphere (Great Oxidation Event or  
279 GOE), which followed the end of the world’s greatest development of banded iron formation (BIF).  
280 This approach seems reasonable based on the rock record, which constrains globally significant climatic  
281 and atmospheric changes to before this time (Gumsley et al., 2017). Although the GOE is sometimes  
282 taken to refer to a more prolonged interval of the early Paleoproterozoic, we restrict our usage here to  
283 this shorter interval between c. 2.45 to c. 2.32 Ga, with a preference for the earlier age (e.g., Warke et  
284 al., 2020b). The GOE has been defined in various ways but in recent years has been presumed to begin  
285 when atmospheric oxygen had accumulated sufficiently to prevent the formation and/or preservation of  
286 mass independent S-isotope fractionation in sedimentary rocks (Farquhar et al., 2000; Bekker et al.,  
287 2004). However, it is currently unclear whether this was a globally synchronous event, with estimates  
288 for MIF-S disappearance varying from 2.45 to 2.32 Ga due to uncertainties over memory effects caused  
289 by oxidative weathering of sulphides and recycling of the MIF signature or stratigraphic ambiguities  
290 (Reinhard et al., 2013; Philippot et al., 2018; cf. Torres et al., 2018; Warke et al., 2020b). The MIF-S  
291 record has also shown structure within the later Archean (oxygen ‘whiffs’) that could potentially be  
292 used as a future stratigraphic marker (Farquhar et al., 2007; Domagal-Goldman et al., 2008; Halevy et  
293 al., 2010; Kurzweil et al., 2013) if the structure is confirmed as a global phenomenon rather than  
294 superimposed local signals (see e.g., Gallagher et al., 2017).

295 While the precise ages and correlation of the GOE with MIF-S events and Paleoproterozoic tillites  
296 remain uncertain (Young, 2019), an equally significant event in the transition is the end of the major  
297 late Archean BIF deposition. The Archean-Proterozoic boundary might be best constrained/defined by  
298 accurately dated tuffs (~2.45 Ga) at the top of the Hamersley Group BIF (Trendall et al, 2004); BIFs in  
299 the Transvaal Basin of South Africa have similar ages. This would imply redefining the Siderian Period,  
300 named for the global peak in iron formations, and moving it into the Neoproterozoic (van Kranendonk et  
301 al., 2012); a simple solution also to the criticism that 2.5 Ga splits this important rock unit. A 2.45 Ga  
302 date also prevents splitting some younger classic “Archean” terranes which overlap the chronometric  
303 2.5 Ga boundary. We concur with this reasoning and propose that the terminal Archean Siderian Period  
304 end at c. 2.45 Ga, to be followed by a new *Scourian* Period (named after the Greek term for rust  
305 (skouria), as a nod to rock-based evidence for widespread oxidative weathering since the GOE.

306 Signal reworking should not affect other geochemical or isotopic markers of upper ocean  
307 oxygenation, e.g., redox-sensitive elemental and isotopic enrichments. Geochemical signs of oxidation  
308 are recorded intermittently from the Mesoarchean (Ossa Ossa et al., 2019), becoming more expansive  
309 during the Neoproterozoic (Ostrander et al., 2019) and are attributed to transient pulses of oxygen prior to  
310 the GOE (the so-called ‘whiffs of oxygen’) (Anbar et al., 2007; Kendall et al., 2015; Stueeken et al.,  
311 2015) or more persistent oxygenation of shallow marine platform environments (Riding et al., 2014).  
312 Therefore, the Archean-Proterozoic transition interval is characterised as much by the decline of anoxic  
313 shallow marine environments as by the onset of sustained atmospheric oxygenation. The Neoproterozoic  
314 is also remarkable for the highly negative carbon isotope composition of deposited organic carbon  
315 during the interval between c. 2.8 Ga and c. 2.6 Ga (Hayes, 1994) as well as a number of other uniquely  
316 extreme stable isotope signatures, possibly related to nascent stages of local environmental oxidation  
317 (Thomazo et al., 2009).

318 Complementary records of Archean change, which can potentially be divided into three chapters,  
319 are provided by geochemical and isotopic studies of magmatic rocks that appear to indicate major  
320 secular changes in tectonic processes (Kamber and Tomlinson, 2019). On this basis, Griffin et al. (2014)  
321 concurred that the Archean Eon is best divided into three: ‘Paleoarchean’ (4.0-3.6 Ga), ‘Mesoarchean’  
322 (3.6-3.0 Ga) and ‘Neoproterozoic’ (3.0-2.4 Ga) eras. In this interpretation, during the ‘Paleoarchean’ Era,  
323 Earth’s dominantly mafic crust acted as a stagnant-to-sluggish lid. Towards the close of the era, zircon  
324 grains reveal subtle geochemical signs of a change in tectonic regime interpreted as a move away from  
325 granitoid production from oceanic plateaus to some form of arc-like settings (Ranjan et al., 2020). It  
326 has been suggested that the subsequent ‘Mesoarchean’ was dominated by major episodes of mantle  
327 overturn and plume activity (Van Kranendonk, 2011) that led to development of the subcontinental  
328 lithospheric mantle and a steady increase between c. 3.3 and c. 3.0 Ga in the  $K_2O/Na_2O$  ratios of TTG  
329 (tonalite-trondhjemite-granodiorite) rock suites (Johnson et al., 2019). However, early evidence of  
330 subduction is also interpreted at this time, along with diapiric doming, in adjoining terranes of the  
331 Pilbara Craton (Hickman, 2004; Van Kranendonk et al., 2004).

332 The Neoproterozoic witnessed the onset of some form of plate tectonics, and the development of  
333 significant volumes of continental crust, characterised by the first K-rich granitoids (Bédard, 2018).  
334 However, gravity-driven doming and plume activity was still an active process in the formation of  
335 granite-greenstone terranes ~2720-2600 Ga (Jones et al., 2020). Progressive cratonization is reflected  
336 by the development of the first true platform covers – the Witwatersrand and Ventersdorp Supergroups  
337 from ~2.95 Ga on the Barberton Craton, the Mount Bruce Supergroup from ~2770 Ga on the Pilbara  
338 Craton and the c. 2.93 Ga to c. 2.80 Ga successions of Canada, e.g., the Steep Rock Lake Group (Riding  
339 et al., 2014; Fralick and Riding, 2015) or the Central Slave Cover Group (Bleeker et al., 1999; Sircombe  
340 et al., 2001). The Pongola Group (~2980 Ga) probably represents an earlier platform, but is intruded by  
341 late-tectonic granites. Emergence of this more buoyant crust may have led to these early carbonate  
342 platforms, although pre-3.0 Ga fluvial sediments imply at least some earlier regional emergence

343 (Heubeck and Lowe, 1994). The first development of platform covers on stable cratons provides a  
344 logical interim boundary within the Archean and the base of the Neoproterozoic at ~3.1-3.0 Ga. Increasing  
345 lithospheric stability is also represented by the oldest extensive mafic dyke swarms between ~2.8 and  
346 2.7 Ga (Evans et al., 2017; Gumsley et al., 2020).

347 It seems significant that the youngest widespread granite-greenstone terranes (e.g., Yilgarn, southern  
348 Superior craton, Bulawayan) are coeval with the basalt-rich Fortescue and Ventersdorp platform covers.  
349 This could form a basis for future 3-fold subdivision of the Neoproterozoic, into three periods based on the  
350 rock records of a newly defined Siderian Period (see above), the coeval Fortescue–Ventersdorp groups,  
351 and the Witwatersrand-Pongola groups, respectively. To address period-level Archean subdivision any  
352 further lies beyond the scope of the present study, although we note that one of these periods could be  
353 named *Kratian* for the cratonization that typifies the later Archean.

354 Clear evidence for the transport of surface crustal material to the deep mantle is found in diamonds  
355 within kimberlites. Their stable isotope compositions, geochronology and mineral inclusions imply  
356 deep transport to the lower mantle of eclogitized basaltic protoliths that had interacted with seawater as  
357 long ago as 3.0 Ga (Shirey and Richardson, 2011; Schulze et al., 2013). Cratonization culminated in a  
358 globally stable “supercraton” regime around the Archean-Proterozoic boundary (Bleeker, 2003;  
359 Cawood et al., 2018). This configuration set up the lithospheric conditions, due to secular cooling of  
360 the mantle, for a switch to a full mode of plate tectonics, which arguably began with rift and drift of  
361 these Archean cratons and led eventually to prolonged amalgamation after c. 1.9 Ga of Nuna  
362 (Columbia), which is widely considered to have been a true supercontinent as opposed to a  
363 megacontinent comprising <50% of all continental area.

### 364 **2.3 Proterozoic Eon (2.45/2.5 to c. 0.539 Ga)**

365 The Archean and Proterozoic eons represent fundamentally different Earth systems, and the boundary  
366 between the two is currently placed at precisely 2.5 Ga. This boundary approximates the change from  
367 an early Earth that, although still characteristically Archean (e.g., rare K-rich granitoids but widespread  
368 komatiite magmatism, granite-greenstone terranes), had gradually developed many aspects of modern  
369 tectonics, to a plate tectonic regime that was characterised by stabilized, emergent continental  
370 (super)cratons and the onset of a supercontinent cycle as well as a notable paucity of the high-MgO  
371 lavas that are characteristically occur throughout the Archean. The Archean-Proterozoic boundary  
372 precedes quite closely, but does not correspond precisely to a change in surface environments from a  
373 reducing to an oxygenated atmosphere, and from wholly anoxic oceans to a more complex ocean redox  
374 structure characterised by oxic, anoxic-ferruginous and anoxic-euxinic portions. Consequently, the  
375 boundary must represent a planetary step change that significantly transformed, within 100 to 150 Myr,  
376 the Earth’s biogeochemical cycles, presumably accompanied by the development of novel microbial  
377 pathways and metabolisms, leading eventually to larger and more complex (eukaryotic) forms. The  
378 Proterozoic marine sedimentary rock record is also marked by a greater diversity of authigenic minerals

379 (Hazen, 2010; Hazen et al., 2011) and carbonate rock textures (James et al., 1998; Shields, 2002;  
380 Hodgskiss et al., 2018). The Proterozoic Eon is divided into three eras, namely the Paleo-, Meso-, and  
381 Neo-Proterozoic eras.

382

383 **i. Paleoproterozoic Era (2.45/2.5 to 1.8/1.6 Ga)**

384 The Paleoproterozoic Era witnessed the transition from an Archean tectonic regime of scattered, small  
385 supercratons (Bleeker, 2003) to a more conventional form of plate tectonics, which resulted in  
386 formation of Earth's earliest widely accepted supercontinent, Nuna (Hoffman, 1989, 1997; Rogers and  
387 Santosh, 2002; Zhao et al., 2002; Payne et al., 2009; Evans and Mitchell, 2011; Zhang et al., 2012;  
388 Yang et al., 2019), as evidenced by ~2.0-1.6 Ga orogenic belts on all present-day continents. Redefining  
389 the Siderian to contain within it the BIFs at the top of the Neoproterozoic requires a new period to be  
390 defined and named for the earliest Paleoproterozoic. Van Kranendonk et al. (2012) refer to this period  
391 as the Oxygenian Period, although we consider *Scourian* (Skourian), after the Greek word for rust, to  
392 be a suitable, rock-based alternative.

393 The Paleoproterozoic sedimentary record provides clues to significant events, some of which are  
394 likely to have been global in scale and can probably be related to the large-scale tectonic processes  
395 outlined above. Abundances of molybdenum, uranium, selenium, sulfate and iodate increased in marine  
396 sedimentary rocks in multiple Paleoproterozoic basins, indicating increasing ocean reservoirs of those  
397 redox-sensitive species (Scott et al., 2008; Partin et al., 2013; Kipp et al., 2017; Hardisty et al., 2017;  
398 Blättler et al., 2018). This trend has been interpreted as evidence of oxidative weathering caused by  
399 atmospheric oxygenation after the GOE together with expansion of oxic conditions in the marine realm,  
400 which stabilised these elements as oxyanions in solution, while titrating redox-sensitive iron,  
401 manganese and cerium out of solution (Tsikos et al., 2010; Warke et al., 2020a). Accumulation of iron  
402 formations (IFs) peaked around the Archean-Proterozoic boundary, but continued until c. 1.8 Ga (Klein,  
403 2005), after which major BIF deposits are scarce but not entirely absent (Bekker et al., 2010; 2014;  
404 Canfield et al., 2018). The initial decline in the abundance of BIF is widely attributed to the widespread  
405 development of euxinic waters on productive continental shelves at ~1.84 Ga, which titrated ferrous  
406 iron in the form of pyrite (Canfield, 1998; Poulton et al., 2010; Poulton and Canfield, 2011). However,  
407 ferruginous deeper oceans persisted throughout most of the mid-Proterozoic (Poulton et al., 2010;  
408 Planavsky et al., 2011), and the paucity of BIF through this period is likely also related to diminished  
409 hydrothermal sources of iron after c. 1.8 Ga (Cawood and Hawkesworth, 2014). The disappearance of  
410 redox-sensitive detrital minerals, such as pyrite, uraninite and siderite, has long been attributed to the  
411 GOE (Holland, 1984, 2006; Frimmel, 2005; van Kranendonk et al., 2012), although the onset and  
412 duration of the GOE is still inadequately constrained (e.g., Luo et al., 2016) and may not have been  
413 synchronous everywhere (Phillipot et al., 2018; Hodgskiss et al., 2019). The onset of the GOE is  
414 generally considered to have been approximately contemporaneous with what some have interpreted as

415 the Earth's first global scale glaciations (Bekker and Kaufman, 2007; Brasier et al., 2013; Tang and  
 416 Chen, 2013; Bekker, 2014; Young, 2019). The strongest evidence for a Paleoproterozoic Snowball  
 417 Earth comes from South Africa, with evidence of low-latitude glaciation in the Makganyene Formation  
 418 at ~2.43 Ga (Evans et al., 1997). This glaciation is considered to have occurred shortly after the initial  
 419 disappearance of MIF-S isotope fractionation, as recorded in pre-glacial sediments in Karelia (Warke  
 420 et al. 2020b).

421 Paleoproterozoic glacial episodes were followed by the Earth's largest known positive  $\delta^{13}\text{C}$   
 422 excursion (or excursions, see Martin et al., 2015), the Lomagundi-Jatuli Event (LJE) between c. 2.31-  
 423 2.22 and c. 2.11-2.06 Ga (Martin et al., 2013), which accompanied the first major evaporite sulfate  
 424 deposits (Melezhik et al., 2005; Schröder et al., 2008; Brasier et al., 2011; Blättler et al., 2018). The  
 425 LJE is followed by the c. 2.06 Ga Shunga Event that is characterised by a major accumulation of  $\text{C}_{\text{org}}$ -  
 426 rich sedimentary rocks, the generation of giant petroleum deposits (Melezhik et al. 2004) and pyrite-  
 427 rich black shale (Sheen et al., 2019) as well as the first sedimentary phosphorite deposits (Kipp et al.,  
 428 2020). The c. 2.06 Ga Shunga Event interestingly coincides with the emplacement of two Large Igneous  
 429 Provinces (LIPs), the Bushveld LIP (Kaapvaal craton) and the Kevitsa LIP on the Karelian craton (e.g.,  
 430 Ernst et al. 2020), which inspired the name of the chronometric Rhyacian Period (2.3 – 2.05 Ga) after  
 431 the Greek word Rhyax (meaning streams of lava) (Plumb, 1991). One potentially distinctive feature of  
 432 the middle Paleoproterozoic is a disputed tectono-magmatic lull between c. 2.3 to 2.2 Ga (Spencer et  
 433 al., 2018), during which evidence of continental magmatism and orogenesis is scarce, but not entirely  
 434 absent (Partin et al., 2014; Moreira et al., 2018). Juvenile magmatism reinitiated after c. 2.2 Ga (Condie  
 435 et al., 2009; Spencer et al., 2018). The chronometric Rhyacian-Orosirian boundary (2050 Ma) possibly  
 436 correlates also with an abrupt increase in magnitude of a mass-independent O-isotope anomaly of  
 437 photochemical origin that is carried in sedimentary sulfate minerals (gypsum/anhydrite and barite). The  
 438 observed box-like secular shift to a large (negative)  $\Delta^{17}\text{O}$  anomaly is tentatively ascribed to a collapse  
 439 without parallel in global gross primary productivity (Hodgskiss et al., 2019; Crockford et al., 2019)  
 440 and ushering in a period of muted isotopic variability and low oxygen levels.

441 The first macroscopic organic-walled fossils, coiled forms similar to *Grypania spiralis*, appear  
 442 within Paleoproterozoic strata by c. 1.89 Ga (Han and Runnegar, 1992; Javaux and Lepot, 2018) to be  
 443 joined by large, more convincingly eukaryote-grade fossils by the end of the era (Zhu et al., 2016). The  
 444 Paleoproterozoic fossil record contains the c. 1.88 Ga Gunflint fossil microbes, which are taken to be  
 445 the oldest unambiguous evidence of iron-oxidising bacteria and oxygenic cyanobacteria (Planavsky et  
 446 al., 2009; Crosby et al., 2014; Lepot et al., 2017), although cyanobacterial fossils are known also from  
 447 the c. 2.0 Ga Belcher Group in eastern Hudson Bay (Hofmann, 1975; Hodgskiss et al., 2019).

448 A period of worldwide orogeny and major crustal growth from c. 2.06 to 1.78 Ga, and reaching  
 449 maximum intensity between 1.90-1.85 Ga, (Condie, 1998, 2004; Puetz and Condie, 2019; Condie and  
 450 Puetz, 2019) culminated in the formation of the supercontinent Nuna or Columbia (Zhao et al., 2002),

451 speculated to have been Earth's first "true" supercontinent (Hoffman, 1989; Bleeker, 2003; Mitchell,  
452 2014). For example, Nuna assembly is largely constrained to between ca. 2.0-1.8 Ga, from the 1970 Ma  
453 Thelon orogen (Bowring and Grotzinger, 1992), with the Rae craton serving as the upper plate of the  
454 growing Laurentia (Hoffman, 2014) that was central to Nuna (Evans and Mitchell, 2011). Local  
455 orogeny continued through the Statherian, culminating with final suturing events in Australia  
456 continuing into the Calymmian (ca. 1.6-1.4 Ga) (Pourteau et al., 2018; Yang et al., 2019; Gibson et al.,  
457 2020), which were peripheral in Nuna (Kirscher et al., 2019), which were peripheral in Nuna.

458 The end of the Paleoproterozoic Era, as currently defined, is characterised by the widespread  
459 formation of unmetamorphosed, shallow-marine sedimentary basins with expansive carbonate  
460 platforms over increasingly stable cratons, following amalgamation of Nuna. Some such as the c.1.7–  
461 c. 1.4 Ga Changcheng-Jixian groups of the Sino-Korean or North China craton, are traditionally  
462 considered and mapped as Mesoproterozoic successions (Zhao and Cawood, 2012), despite their  
463 slightly earlier origin prior to 1.6 Ga. Many other classic mid-Proterozoic sequences also fall into this  
464 category, having begun their depositional history similarly during the chronometric Statherian Period  
465 (1.8-1.6 Ga). For example, pre-1.6 Ga units originally envisaged to fall within the chronometric  
466 Proterozoic II (Plumb and James, 1986: Figure 1) include the lower McArthur Basin of Australia  
467 (Rawlings, 1999); the lower Riphean Burzyan Group of Russia (Semikhatov et al., 2015); the Espinhaço  
468 Supergroup and Araí Group of Brazil and coeval Chela Group of central Africa (Chemale et al., 2012;  
469 Guadagnin et al., 2015; Pedreira and de Waele, 2008); the Vindhyan and Cuddupah supergroups of  
470 India (Ray, 2006; Collins et al., 2015; Chakraborty et al., 2020) and the Uncompahgre Group of SW  
471 Colorado, USA, which formed during the late stages of the Yavapai orogeny (1.71-1.68 Ga)  
472 (Whitmeyer and Karlstrom, 2007).

473 The difficulty in assigning a precise age for the Paleoproterozoic - Mesoproterozoic boundary due  
474 to the prolonged nature of late Paleoproterozoic orogenies, now interpreted to relate to the  
475 amalgamation of Nuna, was recognized early on by the Precambrian Subcommittee who expressed  
476 "*individual preferences ... from 1400 Ma to 1800 Ma*" (Plumb and James, 1986). In this contribution,  
477 we recommend that the end of the Paleoproterozoic be provisionally redefined as ~1.8 Ga, with the  
478 Statherian placed in the Mesoproterozoic, pending future definition of GSSPs. This age is constrained  
479 by the latest Orosirian magmatic activity dated at ~1.82 Ga and the base of first platform covers ~1.8  
480 Ga.

481

## 482 ii. Mesoproterozoic Era (1.8/1.6 to c. 1.0 Ga)

483 The Mesoproterozoic Era represents a period of seeming overall stability in Earth history, during which  
484 there were long thought to be few changes in the sedimentary record, biogeochemical cycling, climate  
485 and biological evolution (Buick et al., 1995; Brasier and Lindsay, 1998). New platform covers, soon  
486 after Orosirian orogeny, developed across most cratons. For example, the McArthur Basin of North

487 Australia saw up to 10 km of sediments deposited throughout the period from 1.8-1.6 Ga: the Tawallah  
488 Group of sandstone and volcanics from ~1.8-1.7 Ga, succeeded by stromatolitic and evaporitic  
489 carbonates of the McArthur Group (1.7-1.6 Ga), Nathan Group (~1.6-1.55 Ga) and the Roper Group  
490 (~1.55-1.31 Ga). The near basal mafic volcanics and intrusives across the coeval Tawallah and  
491 Kimberley Groups represent the major extensional Carson LIP (Ernst et al., 2020). Detailed studies  
492 show significant breaks throughout which correlate with changes in direction in a polar wander curve  
493 from the same sections, illustrating active plate tectonic control of basins near craton margins (Idnurm  
494 et al., 1995, Page et al, 2000). Relatively thin sandstone-volcanic sequences were initiated about the  
495 same time in Brazil and central Africa, but did not continue up into carbonates (Pedreira et al., 2008).  
496 The arenitic Changcheng Group of China began later, after ~1.7 Ga, and continued through the  
497 carbonate-rich Jixian Group until after ~1.44 Ga (Qu et al., 2014), as did the Lower Riphean of Russia  
498 (Semikhatov et al, 2015).

499 The final assembly of Nuna was probably completed by ~1.6 Ga (Pourteau et al., 2018; Gibson  
500 et al., 2020) and followed soon after by thick terrigenous deposition in the Roper (North Australia) and  
501 Belt-Purcell (western North America) Basins. However, some studies suggest that the West Australian  
502 Craton did not combine with North and South Australia until ~1.4 Ga (Yang et al., 2019). The period  
503 1.4–1.25 Ga saw few short-lived basins worldwide, and was dominated by the breakup of the core of  
504 supercontinent Nuna (Evans and Mitchell, 2011; Pisarevsky et al., 2014), although the breakup may  
505 have been relatively incomplete (Ernst et al., 2016; Li et al., 2019) as it was likely followed by re-  
506 amalgamation into a different configuration by around 1.0 Ga to form the supercontinent Rodinia (Li  
507 et al., 2008). This partial breakup could be reflected in the 1.33-1.30 Ga Derim Derim-Yanliao LIP of  
508 northern Australia and the North China craton (Bodorkos et al., 2020; Yang et al. 2020).

509 The final period of the Mesoproterozoic was named Stenian for the “Grenvillian” worldwide  
510 linear orogenic belts (Plumb, 1991). The type Grenvillian is specifically defined by two events:  
511 Boundary, ~1090 – 1020 Ma and Rigolet, ~1000 – 980 Ma (Rivers, 2015). The Boundary event was  
512 probably the time of collision and is defined by high-grade metamorphic rocks from deep in the crust.  
513 The Rigolet boundary was a higher-level event with less movement. An extensional event separated the  
514 two, and magmatic emplacement of anorthosites, charnockites and metagranites occurred throughout.  
515 Earlier events, integral to the belt, extend back to c. 1200 Ma. The Sunsás and Natal-Namaqua belts  
516 display similar deep-seated metamorphism and magmatism between c. 1200 – 1000 Ma (Cornell et al.,  
517 2006; Teixeira et al., 2010). The continuity and contemporaneity of these orogens was challenged by  
518 Fitzsimons (2000) who demonstrated that the apparent linear, linked, nature of these belts encircling  
519 Antarctica was an artifact of imprecise dating and lack of outcrop. For example, in Central Australia,  
520 the high-grade 1240-1120 Ma Musgrave Orogeny is followed by the Warkuma LIP. The mafic-  
521 ultramafic Giles Complex was emplaced at various levels into the metamorphic rocks, coeval with high-  
522 level post-tectonic granites and the bimodal Bentley Supergroup (Howard et al, 2014).

523           Increasingly convincing discoveries of fossil eukaryotes, in the form of large, multicellular  
524 organic-walled fossil fronds and ornamented acritarchs (Zhu et al., 2016; Miao et al. 2019), first occur  
525 in rocks that straddle the chronometric Paleoproterozoic–Mesoproterozoic boundary at 1.6 Ga, and  
526 suggest that much of the Mesoproterozoic fossil record remains undiscovered. Current fossil and  
527 molecular evidence agree that crown group Archaeplastida (a group that includes the red, green and  
528 glaucophyte algae) emerged during the Mesoproterozoic Era (Butterfield, 2000; Eme et al. 2014), or  
529 possibly even earlier in non-marine environments (Sánchez-Baracaldo et al., 2017). Multicellular  
530 eukaryotic algae appear before 1.0 Ga in the form of isolated examples of red algae (*Bangiomorpha*  
531 *pubescens* at c. 1.05 Ga) and green algae (*Proterocladus antiquus* at c. 1.0 Ga) (Butterfield et al., 1994;  
532 Tang et al., 2020), with possibly earlier examples of red algae from India (*Rafatazmia chitrakootensis*  
533 and *Ramathallus lobatus*) at c. 1.6 Ga (Bengtson et al., 2017). Ornamented acritarchs are more common  
534 eukaryote-grade fossils and some may prove useful for biostratigraphy, e.g., *Tappania plana* is a widely  
535 reported Mesoproterozoic fossil taxon, which has been found in the Ruyang Group of China (Yin, 1997;  
536 Yin et al., 2018), Roper Group of Australia (Javaux et al., 2001; Javaux and Knoll, 2017); Siberia  
537 (Nagovitsin, 2009), USA (Adam et al., 2017) and Singhora Group, India (Singh et al., 2019). Therefore,  
538 the Mesoproterozoic Era, although often given the epithet ‘boring’, marks the point in geological time  
539 when biostratigraphy begins to seem possible.

540           As summarised by Cawood and Hawkesworth (2014), the period from 1.7 to 0.75 Ga is  
541 characterised by a paucity of passive margins (Bradley, 2008), anoxic-ferruginous and regionally  
542 euxinic marine environments, an absence of significant Sr isotope deviations in the seawater record,  
543 few highly evolved  $\epsilon_{\text{Hf}(t)}$  values in zircon grains, limited orogenic gold and VHMS (but major  
544 sedimentary exhalative Pb-Zn) deposits, an absence of glacial deposits and a paucity of massive BIF.  
545 Although thought to be Paleoproterozoic in age (Bekker et al., 2003; Papineau, 2010), some of the  
546 oldest significant phosphorite deposits may instead have formed around the 1.6 Ga mark in India and  
547 Australia (McKenzie et al., 2013; Crosby et al., 2014; Chakraborty et al., 2020; Fareeduddin and  
548 Banerjee, 2020). Anorthosites and related intrusive rocks are characteristic of the middle  
549 Mesoproterozoic (c. 1.5 – 1.2 Ga) and are in places spatially and temporally linked to convergent plate  
550 margins (Whitmeyer and Karlstrom, 2007; McLelland et al., 2010; Ashwal and Bybee, 2017). Their  
551 development during the Mesoproterozoic was attributed by Cawood and Hawkesworth (2014) to  
552 secular cooling of the mantle to a temperature at which continental lithosphere was strong enough to be  
553 thickened, but still warm enough to result in melting of the lower thickened crust.

554           A lack of stratigraphically useful new life forms, major climatic changes, and demonstrably  
555 global C isotope excursions throughout the Mesoproterozoic makes it particularly difficult to subdivide.  
556 However, the Mesoproterozoic C-isotope record may have been less invariant than has been appreciated  
557 until now as exceptions to the apparent monotony are emerging (e.g., Zhang, K. et al., 2018; Shang et  
558 al., 2019). Regional scale magmatic events such as the c. 1320 Ma and c. 1230 Ma dyke swarms of  
559 North China (Zhai et al., 2015; Peng et al., 2015; Wang et al., 2016), the 1320 Ma swarm also found



560 throughout northern Australia (Yang et al. 2020; Bodorkos et al. 2020), the Mackenzie dyke swarm in  
561 Canada (c. 1.27 Ga) and the approximately contemporaneous Ghanzi-Chobe-Umkondo and  
562 Midcontinent Rift Systems (c. 1.12-1.08 Ga) have not been linked to any global-scale isotopic  
563 excursions that could be used for correlation, although the coincidence of widespread ca. 1385 Ma LIPs  
564 and black shales has been proposed as potential rock-based markers of Mesoproterozoic subdivision,  
565 e.g., at the Calymmian-Ectasian boundary (Zhang, S. et al., 2018).

566 The final period of the Mesoproterozoic was named ‘Stenian’ for a series of orogenies (Plumb,  
567 1991) that led eventually to formation of the supercontinent Rodinia, which completed its final  
568 amalgamation phase by c. 950 Ma (Li et al., 1999; Evans et al., 2016; Merdith et al. 2017a). The first  
569 period of the Neoproterozoic was named ‘Tonian’, due to the lithospheric stretching now known to be  
570 related to the break-up of Rodinia, and originally placed at 0.9 Ga (Plumb and James, 1986).

571

572 **iii. Neoproterozoic Era (c.1.0 – c.0.54 Ga)**

573 The subdivision of Neoproterozoic time has largely been informed by 1) the occurrence of widespread  
574 glacial units now known to be of late Precambrian age (Thomson, 1871; 1877; Reusch, 1891; Kulling,  
575 1934; Lee, 1936; Howchin, 1901; Mawson, 1949) and 2) fossils of metazoan affinity that postdate those  
576 glaciogenic deposits but predate Cambrian strata (Glaessner, 1962). Harland (1964) first proposed the  
577 term “infra-Cambrian” or “Varangian” for the late Precambrian system (Fig. 2) based on two discrete  
578 diamictite units, the Smalfjord (Bigganjargga) and Mortensnes, although these are now known to be of  
579 late Cryogenian (Marinoan) and Ediacaran age, respectively. Harland proposed that the start of this new  
580 period should correspond to the base of the lower of these two glacial horizons on the Varanger  
581 Peninsula, NE Norway, first described by Reusch (1891). Dunn et al. (1971) subsequently introduced  
582 the terms “Sturtian” and “Marinoan” (named after Sturt Gorge and Marino Rocks near Adelaide) for  
583 the two glacial epochs recorded in the late Proterozoic strata of the Adelaide Geosyncline of South  
584 Australia, emphasizing their utility as chronostratigraphic markers. Cloud and Glaessner (1982)  
585 proposed the term “Ediacarian” for the interval spanning from the upper limit of the last late  
586 Precambrian glacial deposit to the base of the Cambrian. This term also originates from South Australia  
587 (the Ediacaran Hills) where Ediacara-type fossils were recognized (Sprigg, 1947). Plumb (1991) penned  
588 the name “Cryogenian” for the period that included the more widespread of the late Neoproterozoic ice  
589 ages and the term “Tonian” (meaning stretching in Greek and in reference to the onset of rifting, now  
590 related to the break-up of Rodinia) for the preceding period, setting the chronological boundary between  
591 them at precisely 850 Ma. These terms and GSSA boundaries were revised from previously suggested  
592 period-rank subdivisions on the geological time scale by the Subcommittee on Precambrian  
593 Stratigraphy (Plumb and James, 1986).

594 The number, duration, and intensity of the glaciations have been intensely debated (e.g.,  
595 Kaufman et al., 1997; Kennedy et al., 1998; Halverson et al., 2005), particularly in the light of the

596 Snowball Earth hypothesis (Hoffman et al., 1998; Hoffman and Schrag, 2002; Fairchild and Kennedy,  
597 2007; Etienne et al., 2007). Notwithstanding these debates, the base of the Ediacaran System (Period)  
598 was formally ratified in 2004 in the Adelaide Geosyncline (Knoll et al., 2004; 2006) at the same  
599 stratigraphic level as originally proposed by Cloud and Glaessner (1982) for their “Ediacarian” period.  
600 The terms Cryogenian and Tonian are now widely accepted for the two preceding periods (Shields-  
601 Zhou et al., 2012, 2016). Recent proliferation of radioisotopic ages spanning Neoproterozoic glacial  
602 deposits has largely resolved the question of the number and timing of late Precambrian glacial  
603 intervals. It is now well established that two discrete glaciations of global extent occurred during the  
604 Cryogenian Period (i.e., between c. 717 Ma and c. 635 Ma). Despite initial reservations, the  
605 international community generally uses the terms *Sturtian* and *Marinoan* to refer to these two glacial  
606 events (“cryochrons”, cf. Hoffman et al., 2017) of the Cryogenian Period. This subdivision, though still  
607 informal, appears justifiable in light of the geochronological evidence that 1) the Sturtian glaciation is  
608 now thought to have begun at c. 717 Ma (Macdonald et al., 2010, 2018; McLennan et al., 2018) and  
609 ended at c. 660 Ma (Rooney et al., 2015; 2020; Cox et al., 2018; Wang et al., 2019) synchronously  
610 worldwide, within the uncertainty of available ages, and that 2) the Marinoan glaciation, though shorter-  
611 lived and of uncertain duration (between about 4 and 17 Myr; Hoffmann et al., 2004; Condon et al.,  
612 2005; Prave et al., 2016; Nelson et al., 2020) also ended synchronously at c. 635.5 Ma (Crockford et  
613 al., 2018; Zhou et al., 2019). The start of the Cryogenian Period has now been changed to c. 720 Ma so  
614 as to encompass only the glacigenic sequences, pending proposal and ratification of a GSSP.

615 The preceding Tonian Period now lasts 280 million years. Having originally been envisaged to  
616 encapsulate a period of lithospheric thinning (supercontinent break-up), the Tonian now covers the final  
617 amalgamation of Rodinia (Evans et al., 2016; Merdith et al. 2017) and a prolonged interval of relative  
618 stability prior to the onset of major break-up after 0.85 Ga, and perhaps as late as 0.75 Ga (Jing et al.,  
619 2020; Merdith et al 2017b).

620 A proliferation of sedimentary basins in Rodinia between c. 850 and c. 800 Ma (e.g., the  
621 Centralian Superbasin of Australia, the East-Svalbard-East Greenland basin, the Mackenzie Mountains-  
622 Amundsen and associated basins of northern-northwestern Canada, the Nanhua rift basin of South  
623 China and the Central Africa Copperbelt (Lindsay, 2002, Hoffman et al., 2012; Rainbird et al., 1996;  
624 Wang et al., 2011; Bull et al., 2011; Li et al., 2013) were originally interpreted to record an initial phase  
625 of Rodinia break-up (Li et al., 1999; Macdonald et al., 2012), perhaps related to insulation of the  
626 underlying mantle (Lindsay, 2002) and/or the influence of a series of similarly aged mantle plumes and  
627 associated LIP events that impinged on Rodinia at this time (Li et al., 1999, 2003). The existence of  
628 widespread basin-scale evaporite deposits with ages ranging from c. 830 to c. 730 Ma (Prince et al.,  
629 2019) is consistent with rifting around this time. However, aside from the western margin of North  
630 America (e.g., Macdonald et al., 2012; Timmons et al., 2001; Jefferson et al., 1998) evidence of  
631 extension leading to continental separation is lacking and true break-up probably began in earnest only  
632 around the start of the Cryogenian (e.g., Merdith et al., 2017a,b), followed by a peak in passive margin

633 abundance at c. 600 Ma (Bradley, 2008). Therefore, Rodinia's tenure as a supercontinent coincided  
634 with the Tonian Period, as currently defined, which was named for the tectonic stretching that led to its  
635 break-up. Division of the long Tonian into two periods is therefore desirable, although at present most  
636 c. 850-800 Ma basins lack adequate geochronological control.

637

638

### 639 **3. Tracers of crustal evolution: cornerstone of the geological time scale**

640 Recent research has focused on understanding episodicity and secular trends in the Precambrian  
641 geological record, recognising that the supercontinent cycle and mantle dynamics exert a fundamental  
642 control on the evolution of not only the Earth's lithosphere, but also the atmosphere and biosphere,  
643 including the spatial distribution of elements and therefore the evolution of mineral deposits (e.g.,  
644 Huston et al., 2016; Frimmel, 2018), via a series of complex, incompletely understood feedbacks (e.g.,  
645 Worsley et al., 1985; Lindsay and Brasier, 2002; Cawood et al., 2013; Young 2013; Grenholm and  
646 Schersten, 2015; O'Neill et al., 2015; Hawkesworth et al. 2016; van Kranendonk and Kirkland 2016;  
647 Gumsley et al., 2017; Nance and Murphy 2018; Alcott et al., 2019).

648 Various workers have proposed that the Precambrian can be divided into a number of major  
649 intervals based on the dominant tectonic process at any one time. Hawkesworth et al. (2016) suggested  
650 five intervals: 1) initial accretion, core/mantle differentiation, development of magma ocean and an  
651 undifferentiated mafic crust; 2) plume-dominated tectonics (pre-subduction) at c. 4.5–3.0 Ga; 3)  
652 stabilisation of cratons and onset of “hot subduction” between c. 3.0 and c. 1.7 Ga; 4) the “boring  
653 billion” at 1.7–0.75 Ga; and 5) Rodinia breakup and development of “cold subduction” from 0.75 Ga  
654 onwards. Similarly, van Kranendonk and Kirkland (2016) suggested five intervals, each of which starts  
655 with a pulse of mafic-ultramafic magmatism, includes the formation of a supercontinent, and ends with  
656 an often protracted period of relative quiescence as the previously formed supercontinent drifts and  
657 breaks apart. Following c. 4.03–3.20 Ga – the period from the start of the preserved rock record to the  
658 onset of modern-style plate tectonics – these stages are: 1) 3.20–2.82 Ga – the onset of modern-style  
659 plate tectonics and the oldest recognised Wilson cycle; 2) 2.82–2.25 Ga – commencing with major  
660 crustal growth, emergence of the continents and formation of Superior-type BIFs, and closing with  
661 magmatic slowdown and stagnant-lid behaviour; 3) 2.25–1.60 Ga – global mafic/ultramafic magmatism  
662 followed by global terrane accretion and the formation of Nuna; 4) 1.60–0.75 Ga – the “Boring Billion”  
663 but included partial break-up of Nuna and subsequent formation of Rodinia during the Grenvillian and  
664 other orogenies; 5) 0.75 Ga to present – breakup of Rodinia, the Pangean supercontinent cycle and  
665 present transition to Amasia (Safonova and Maruyama 2014; Mitchell et al., 2012; Merdith et al. 2019).

666 Worsley et al. (1985) and Nance et al. (1986) pointed out that processes associated with the  
667 supercontinent cycle can be tracked by several isotopic proxies. For example, the distribution of U-Pb  
668 zircon ages for the past 4.0 Ga (Fig. 3) in orogenic granitoids and detrital sedimentary rocks record

669 similar peaks at 2.7 Ga (and 2.5 Ga), 1.87 Ga, 1.0 Ga, 0.6 Ga and 0.3 Ga, which correspond to the times  
 670 of global-scale collisional orogenesis and magmatism associated with the amalgamations of Kenora  
 671 (Kenorland), Nuna (Columbia), Rodinia, Gondwana and Pangea, respectively. A more recent  
 672 compilation (Condie and Puetz, 2019) interprets these peaks to be pulses of crustal growth and revises  
 673 the timing of later peaks to 1875 Ma, 1045 Ma, 625 Ma, 265 Ma and 90 Ma. A kernel density estimation  
 674 analysis (Vermeesch et al., 2016) of almost 600,000 detrital zircons (Spencer et al., 2020) confirms  
 675 similar peaks at 2.69 Ga, 2.50 Ga, 1.86 Ga, 1.02 Ga, 0.61 Ga, 0.25 Ga and 0.1 Ga, and troughs at 2.27  
 676 Ga, 1.55-1.28 Ga, 0.88-0.73 Ga, 0.38 Ga and 0.20 Ga. Variations in the mean initial  $\epsilon_{\text{Hf}}$  and  $\delta^{18}\text{O}$  values  
 677 from detrital zircon grains in recent sediments show negative troughs and positive peaks, respectively,  
 678 that correspond to times of supercontinent assembly (Fig. 3). Both proxies are consistent with extensive  
 679 crustal re-working at the time of assembly with more juvenile contributions representing times of  
 680 supercontinent breakup and dispersal. Most importantly, all current major subdivisions of geological  
 681 time, 2.5 Ga, 1.6 Ga, 1.0 Ga, c.539 Ma, c.252 Ma and c.66 Ma, sit within the downslope of troughs that  
 682 follow peaks in zircon abundance. Note, however, that the time between the ‘Nuna’ peak at 1.87 Ga  
 683 and the currently defined Paleoproterozoic-Mesoproterozoic boundary, which precedes a long-lived  
 684 abundance trough, is anomalously long, and reflects protracted assembly of the Nuna supercontinent.

685 The effect of crustal processes on seawater composition is recorded by the  $^{87}\text{Sr}/^{86}\text{Sr}$  ratios of  
 686 marine carbonates. High  $^{87}\text{Sr}/^{86}\text{Sr}$  values are attributed to times of increased exhumation of old  
 687 radiogenic crystalline rocks that would accompany supercontinent amalgamation and disaggregation,  
 688 while low  $^{87}\text{Sr}/^{86}\text{Sr}$  values signify reduced exhumation of old crustal domains that occur when  
 689 supercontinent breakup is accompanied by enhanced ocean ridge hydrothermal activity, rift-related  
 690 magmatism and sea level rise (Veizer, 1989). Although commonly used seawater  $^{87}\text{Sr}/^{86}\text{Sr}$  curves  
 691 (Veizer et al., 1999; Shields and Veizer, 2002; Shields 2007) imply that continental weathering had  
 692 little influence before the end of the Archean, recent studies (e.g., Satkoski et al., 2016) suggest that  
 693 continental weathering and low-temperature surface alteration were more important than previously  
 694 suspected during the Archean. Two prolonged peaks in the Sr isotope composition of seawater  
 695 correspond with the Paleoproterozoic-Mesoproterozoic and Neoproterozoic-Phanerozoic transitions  
 696 (Shields, 2007; Kuznetsov et al., 2018). These intervals of enhanced continental weathering of more  
 697 radiogenic rocks coincide with the amalgamation of Nuna and Gondwana, respectively (e.g., Cawood  
 698 et al., 2013; Nance and Murphy, 2018). The widespread orogenesis that accompanied amalgamation of  
 699 Rodinia (Namaqua-Natal (Africa), Grenville-Sveconorwegian (North America-Europe) and Sunsás  
 700 (South America) does not feature prominently in the seawater Sr isotope curve or zircon  $\epsilon_{\text{Hf}}$   
 701 compilations, likely because these orogens primarily involved juvenile arcs in external orogens (e.g.,  
 702 Spencer et al, 2013) rather than old radiogenic crustal domains. The dominant influence of lithology  
 703 over weathering rates on the  $^{87}\text{Sr}/^{86}\text{Sr}$  record is consistent with the observed negative covariation  
 704 between  $^{87}\text{Sr}/^{86}\text{Sr}$  and zircon  $\epsilon_{\text{Hf}}$  records (Hawkesworth et al., 2016).

705 Supercontinent amalgamation has been proposed to increase nutrient availability (including  
706 important bio-limiting nutrients such as iron and phosphorus, e.g., Tyrell, 1999) and organic production  
707 via higher rates of chemical weathering, leading to pulses of oxygenation (Campbell and Allen, 2008).  
708 However, the concept of greatly increased weathering rates would appear to be in conflict with the  
709 silicate weathering feedback, which regulates the long-term carbon cycle (Walker et al., 1981).  
710 Moreover, carbon isotope trends, which are commonly used to mirror changes in organic burial and  
711 therefore oxygenation (e.g., Des Marais et al., 1992; Lyons et al., 2014), may relate instead to tectonic  
712 forcing of carbonate weathering, resulting in an inverse (or no) covariation between  $\delta^{13}\text{C}$  and carbon  
713 burial (Shields and Mills, 2017). The relationship between  $\delta^{13}\text{C}$  excursions and oxygenation is made  
714 more complex when we consider that oxidative weathering of organic carbon could have been limited  
715 by low atmospheric oxygen (Bekker and Holland, 2012; Daines et al., 2017). As a consequence,  
716 negative as well as positive carbon isotope excursions could indicate Proterozoic oxygenation events,  
717 driven instead by pyrite burial, particularly at times of enhanced evaporite sulfate weathering since  
718 about 2.0 Ga (Shields et al., 2019). Despite the widespread acceptance of a two-step rise in atmospheric  
719 oxygen during the Proterozoic Eon (Lyons et al., 2014), sophisticated biogeochemical models have  
720 seldom been applied to the Precambrian Earth system and few proxies exist to constrain absolute  
721 atmospheric oxygen levels (Planavsky et al., 2014).

722 Geochemical evidence indicates that during much of the Proterozoic Eon, upper oceans were  
723 oxygenated due to mixing with the atmosphere, but the deep ocean in contrast still tended towards  
724 anoxia with local euxinia (Canfield, 1998; Shen et al., 2002; Arnold et al., 2004; Poulton et al., 2004;  
725 Farquhar et al., 2010). However, the extent of surface oxygenation is still highly disputed (Slack et al.,  
726 2007; Planavsky et al., 2014; Tang et al., 2016; Zhang et al., 2016; Daines et al., 2017). Deep ocean  
727 anoxia suggests that atmospheric oxygen levels were low enough that oxygen became easily exhausted  
728 at productive margins where organic remineralisation scavenged first oxygen then sulphate. After the  
729 assembly of Rodinia, euxinia became less common, leading to mostly ferruginous conditions (Guilbaud  
730 et al., 2015). Under such conditions efficient phosphorus removal may have helped to sustain low  
731 atmospheric oxygen levels (Guilbaud et al., 2020). A two-step oxygenation history (first surface oceans  
732 and atmosphere and then deep oceans) has also been supported by Fe speciation studies, which show  
733 increased amounts of Fe (III) relative to Fe (II) in subaerial volcanic rocks after the GOE, but no change  
734 in submarine volcanics until after the NOE (Stolper and Brenhin-Keller, 2018).

735 How environmental parameters, such as climate and redox conditions, were modulated by the  
736 supercontinent cycle remains uncertain but tectonic and environmental changes track the same  
737 episodicity, providing optimism that natural subdivision of the Proterozoic Eon would be geologically  
738 meaningful. Plume generated LIP magmatism could also help define natural Precambrian (and  
739 Phanerozoic) boundaries through their likely effects on the wider environment (Horton, 2015; Ernst  
740 and Youbi 2017; Ernst et al. 2020). Examples include the Archean-Siderian boundary LIPs (2460-2450

741 Ma Matachewan and coeval events in Karelia-Kola and Pilbara cratons), Rhyacian-Orosirian boundary  
742 LIPs (2058 Ma Bushveld and Kevitsa events), Orosirian-Statherian boundary (1790 Ma LIPs on many  
743 blocks), Statherian-Calymmian boundary (1590 Ma LIPs), Calymmian-Ectasian boundary (1385 Ma  
744 LIPs on many cratons), Ectasian-Stenian boundary (c. 1205 Ma Marnda Moorn LIP), Stenian-Tonian  
745 boundary (c. 1005 Ma Sette Daban event or c. 925 Ma Dashigou event), and Tonian-Cryogenian (720  
746 Ma Franklin LIP and other related LIPs (Ernst and Youbi 2017). Despite the difficulty of matching the  
747 isotopic record with LIP emplacement and weathering, the 720 Ma Tonian-Cryogenian boundary, now  
748 defined by the start of the Sturtian glaciation, has been linked to the Franklin Large Igneous Province  
749 (LIP) of northern Laurentia (Macdonald et al., 2010; Macdonald and Wordsworth, 2017; Ernst and  
750 Youbi, 2017) and potentially other LIP fragments (Ernst et al., 2020) either through an increase in  
751 planetary albedo associated with the release of aerosols or an increase in global weatherability  
752 associated with the tropical emplacement of soluble Ca- and Mg-rich flood basalts. This discovery  
753 builds on the recognition that LIPs are coeval with many Phanerozoic chronostratigraphic boundaries  
754 and that, although regional in scale, LIPs can have global environmental effects and leave global  
755 sedimentary records. Thus, while LIPs are not “golden spikes” in themselves, they can represent proxies  
756 for golden spikes in the sedimentary record, which bodes well for Proterozoic stratigraphic correlation  
757 along Phanerozoic lines.

758         There is a clear consensus that the Earth’s surface environment evolved in a series of events  
759 that were controlled ultimately by magmatism and tectonics. In this, there appears to be no essential  
760 difference between major geological transitions of the Phanerozoic and Proterozoic, all of which reflect  
761 complex interactions and feedbacks between the lithosphere, atmosphere and biosphere. Despite  
762 significant gaps in understanding, various isotopic and geochemical proxies track tectonic  
763 (supercontinent) cyclicity and offer prospects for a more robust, rock-based pre-Cryogenian time scale.  
764

#### 765 **4. Nascent potential of Proterozoic biostratigraphy and chemostratigraphy**

766 Stromatolite textures (and structures) were once thought to be age-diagnostic, although this is now more  
767 frequently interpreted to reflect a general tendency towards greater biological control over calcium  
768 carbonate precipitation through time (Grotzinger, 1990; Arp et al., 2001; Riding, 2008). Coarse sparry  
769 texture (botryoidal fans and microdigitate stromatolites, dendrites, isopachous laminites, and  
770 herringbone calcite) is common in Late Archean-Mesoproterozoic carbonate systems. Although such  
771 textures have commonly been referred to as seafloor cement, they formed at the open sediment-water  
772 interface rather than as void-fills, unlike later calcite microspar cements, which peaked in the early  
773 Neoproterozoic (James et al., 1998), just as cyanobacterial sheaths began to be calcified, forming  
774 clotted, ‘thrombolite’ mounds of calcimicrobial fabric (Arp et al., 2001). Despite evident trends, few if  
775 any sharp temporal divisions can be identified in stromatolite type or microbially induced sedimentary  
776 structures (MISS). For example, abiotically controlled seafloor carbonate precipitation did not entirely

777 disappear at the end of the Archean, while the first occurrence of fossilised bacteria (or stromatolites)  
778 cannot be used to date the evolutionary origins of cyanobacteria (Blank, 2013; Sánchez-Baracaldo et  
779 al., 2017; although see Ward et al., 2016), which from geochemical data ought to predate Neoproterozoic  
780 evidence of oxygenation (Farquhar et al., 2011; Riding et al., 2014). Supposedly age-diagnostic  
781 sedimentary textures, like stromatolite fabrics, have lost favour, while discoveries of new fossils each  
782 year continually resurrect the hope that Precambrian biostratigraphy will be a genuine possibility.

783         Although Precambrian paleontology is a relatively young field, with only belated acceptance  
784 of Ediacaran body fossils (Glaessner, 1962), tremendous advances have been made in recent years.  
785 Nevertheless, Precambrian biostratigraphy is still in its infancy with respect to fossil discovery and  
786 systematic description. It is not unusual, for example, for a new discovery to extend the stratigraphic  
787 range of fossil species by tens or even hundreds of millions of years. Macroscopic forms are too rare or  
788 simple to be of stratigraphic use, and while organic-walled microfossils are common in both fine-  
789 grained siliciclastic sedimentary rocks or concretions, assemblages are typically dominated by simple,  
790 smooth-walled vesicles known as *Leiosphaeridia*, a biologically uninformative acritarch taxon.  
791 Nonetheless, with a growing number of taxonomic studies linked to new paleoenvironmental,  
792 chemostratigraphic and geochronologic constraints (e.g., Sergeev et al., 2012; Tang et al., 2013, 2015;  
793 Baludikay et al., 2016; Porter and Riedman 2016; Riedman and Porter, 2016; Beghin et al. 2017a, b;  
794 Loron and Moczyłowska, 2017; Loron et al., 2019a; Cohen et al. 2017a,b; Javaux and Knoll, 2017;  
795 Miao et al., 2019), a nascent Proterozoic biostratigraphic record is beginning to take shape.

796

797

#### 798         **4.1 Biostratigraphy of the Proterozoic Eon (Eonothem)**

799 The oldest macroscopic organic-walled fossils are known from Paleoproterozoic rocks (Han and  
800 Runnegar, 1992; Javaux and Lepot, 2018), now dated to  $<1891 \pm 3$  Ma (Pietrzak-Renaud and Davis,  
801 2014). However, these simple coils and spirals, similar in appearance to *Grypania spiralis* (e.g., Walter  
802 et al., 1976; Sharma and Shukla, 2009), are not diagnostically eukaryotic in affinity. Decimeter-sized  
803 seaweed-like compressions (Zhu et al., 2016) and ornamented acritarchs occur in rocks at c. 1.6 Ga  
804 (e.g., Miao et al., 2019) and are widely considered to be the first convincing fossilised eukaryotes  
805 (Javaux and Lepot, 2018).

806         Molecular clock analyses place the origin of crown-group eukaryotes sometime in the  
807 Mesoproterozoic or late Paleoproterozoic (e.g., Berney and Pawłowski, 2006; Parfrey et al., 2011; Eme  
808 et al., 2014; Betts et al., 2018). Some phylogenetic data suggest that the first photosynthetic eukaryotes  
809 may have emerged in freshwater habitats (Blank, 2013; Sanchez-Baracaldo et al., 2017), which may  
810 lower their preservation potential in the rock record. The Stenian-Tonian transition interval is  
811 increasingly being viewed as a time of crown group eukaryote diversification (e.g., Knoll et al., 2006;  
812 Cohen and Macdonald, 2015; Butterfield, 2015; Xiao and Tang, 2018). Latest Mesoproterozoic and

813 earliest Neoproterozoic rocks are the first to preserve fossils with clear similarities to particular modern  
814 eukaryotic clades, including red and green algae, fungi, amoebozoans, and stramenopiles (Butterfield  
815 et al., 1994; Butterfield, 2004; Porter et al., 2003; Nagovitsin, 2009; Loron et al., 2019b; Tang et al.,  
816 2020), though the affinities of most early Neoproterozoic fossils remain enigmatic. A number of  
817 eukaryotic innovations also appear in the record during this time, including scales, tests,  
818 biomineralization, and eukaryovory (Porter and Knoll, 2000; Cohen and Knoll, 2012; Cohen et al.,  
819 2017a,b; Porter, 2016). In addition, eukaryote-derived sterane biomarkers appear for the first time c.  
820 810 Ma (Brocks, 2018; Zumberge et al., 2019).

821         Given these evolutionary changes, it is not surprising that late Mesoproterozoic/early  
822 Neoproterozoic fossil assemblages are largely distinct from those of early Mesoproterozoic age  
823 (Sergeev et al., 2017), and that several organic-walled microfossils have been proposed as index fossils  
824 for this interval. These include the acritarch *Trachyhystrichosphaera aimika* (spheroidal vesicles with  
825 sparse, irregularly distributed, hollow processes), which is found in more than 20 sections worldwide  
826 in Stenian and Tonian strata, aged c. 1100 to c. 800 Ma (Butterfield et al., 1994; Tang et al., 2013;  
827 Riedman and Sadler, 2018) or c. 1150 to c. 720 Ma (Pang et al., 2020) and *Cerebrosphaera globosa*  
828 (= *C. buickii*), robust spheroidal vesicles with distinctive wrinkles, common in late Tonian units c. 800–  
829 740 Ma (Hill et al., 2000; Grey et al., 2011; Riedman and Sadler, 2018) (Fig. 4).

830         Several other distinctive fossils from rocks c. 780–740 Ma have potential in subdividing the  
831 Tonian, but there are too few occurrences known at present to have confidence in their ranges (Riedman  
832 and Sadler, 2018). Vorob'eva et al. (2009) noted that many long-ranging early Neoproterozoic and late  
833 Mesoproterozoic taxa may be biostratigraphically useful with respect to their last appearances, and in  
834 this regard it is worth noting that Riedman and Sadler (2018) found that the disappearance of many  
835 ornamented taxa in the later Tonian occurred just before or around the time that distinctive vase-shaped  
836 microfossils appear. The vase-shaped microfossils, constrained to range from c. 790–730 Ma (Riedman  
837 and Sadler, 2018; Riedman et al., 2018), provide the most promising biostratigraphic marker for  
838 subdividing Tonian time, and may be useful in defining the Cryogenian GSSP (Strauss et al., 2014),  
839 although the extent to which the range is controlled by taphonomic factors is not clear.

840

#### 841 **4.2 Chemostratigraphy of the Proterozoic Eon (Eonothem)**

842 With the possible exception of the Neoproterozoic, chemostratigraphy of the Precambrian is restricted to  
843 the Proterozoic Eon. The GOE can be traced using a number of redox-sensitive geochemical proxies,  
844 e.g., mass-independent fractionation of sulfur isotopes, trace metal concentrations and isotopes, while  
845 related changes to microbial metabolisms and biogeochemical cycles may be apparent in nitrogen, iron  
846 and other isotope records.

847         For later portions of the sedimentary archive, the carbon isotope record has most potential for  
848 identifying chemo-oceanographic events during the Proterozoic, beginning with the widespread  
849 positive anomaly (anomalies), referred to the Lomagund-Jatuli Event (LJE), which started before c.



850 2.22 Ga and ended by 2.06 Ga (Karhu and Holland, 1996; Melezhik et al., 2007; Martin et al., 2013).  
 851 Later negative anomalies have been reported at about 2.0 Ga (Kump et al., 2011; Ouyang et al., 2020),  
 852 1.6 Ga (Zhang, K. et al., 2018; Kunzmann et al., 2019) and 0.93 Ga (Park et al., 2016). Carbon and  
 853 strontium isotope stratigraphy (mainly on marine carbonates) are the most widely applied  
 854 chemostratigraphic tools in the Neoproterozoic, and notwithstanding challenges to their general  
 855 robustness to diagenetic alteration (e.g., Knauth and Kennedy, 2009; Derry, 2010) and reliability as  
 856 global seawater proxies (Ahm et al., 2019), consistently reveal similar secular trends at both basinal  
 857 and global scales.

858 The early Neoproterozoic carbon isotope record is identified by its sustained intervals of high  
 859  $\delta^{13}\text{C}_{\text{carb}} \geq +5\text{‰}$  (Fig. 4; Kaufman et al., 1997; Halverson et al., 2005). The shift towards the high  $\delta^{13}\text{C}_{\text{carb}}$   
 860 values appears to be transitional, with moderate fluctuations ( $\leq 4\text{‰}$ ) in  $\delta^{13}\text{C}_{\text{carb}}$  beginning in the late  
 861 Mesoproterozoic (Knoll et al., 1995; Bartley et al., 2001; Kah et al., 2012) and continuing into the early  
 862 Neoproterozoic (Kuznetsov et al., 2006). However, due to a paucity of earliest Neoproterozoic marine  
 863 carbonate successions globally and poor age control on those successions that do exist, the  $\delta^{13}\text{C}_{\text{carb}}$   
 864 record for the interval c. 1100–850 Ma is still poorly constrained. Available data indicate that significant  
 865  $\delta^{13}\text{C}_{\text{carb}}$  excursions could have taken place during this interval but values remained between  $-5\text{‰}$  and  
 866  $5\text{‰}$ , while  $^{87}\text{Sr}/^{86}\text{Sr}$  fluctuated between 0.7052 and 0.7063 (Fig. 5; Cox et al., 2016; Kuznetsov et al.,  
 867 2017; Zhou et al., 2020).

868 The shift towards higher sustained  $\delta^{13}\text{C}_{\text{carb}} (\geq 5\text{‰})$  values occurred at c. 850 Ma (though not  
 869 directly dated), as recorded in the Little Dal Group and equivalent strata of northwestern Canada (Fig.  
 870 5; Halverson, 2006; Macdonald et al., 2012; Thomson et al., 2015). However, this trend to high  $\delta^{13}\text{C}_{\text{carb}}$   
 871 values is punctuated by a discrete and long-lived interval of near zero to negative  $\delta^{13}\text{C}_{\text{carb}}$  values, referred  
 872 to as the Bitter Springs Anomaly (BSA) (Halverson et al., 2005) after the Bitter Springs Formation in  
 873 the Amadeus Basin of central Australia where it was first documented (Hill and Walter, 2000). The  
 874 BSA is well documented in central Australia, Svalbard, northwestern Canada, Ethiopia (Swanson-  
 875 Hysell et al., 2012, 2015; and references therein) and possibly India (George et al., 2018). It is  
 876 constrained by U-Pb zircon CA-TIMS ages to have initiated after 811.5 Ma (Macdonald et al., 2010)  
 877 and terminated prior to 788.7 Ma (MacLennan et al., 2018). Using a thermal subsidence-type age model  
 878 applied to Svalbard, Halverson et al. (2018) estimated the BSA to have begun c. 810 Ma and ended c.  
 879 802 Ma, for a duration of 8 million years.

880 Available strontium isotope data show a plateau near 0.7070 following recovery from the Bitter  
 881 Springs anomaly that is punctuated by a few minor downturns. A larger decline to 0.7064–0.7065  
 882 broadly coincides with the recovery from the c. 738–735 Ma Russøya negative  $\delta^{13}\text{C}_{\text{carb}}$  excursion  
 883 (Halverson et al., 2018; MacLennan et al., 2018). Cox et al. (2016) suggested that these late Tonian  
 884 declines in  $^{87}\text{Sr}/^{86}\text{Sr}$  were driven by preferential silicate weathering of continental flood basalt  
 885 associated with the breakup of Rodinia, with the larger late Tonian drop to 0.7064 corresponding to  
 886 weathering of juvenile arcs in the Arabian-Nubian Shield (Park et al., 2019). Furthermore, the early

887 Neoproterozoic  $^{87}\text{Sr}/^{86}\text{Sr}$  record is strongly biased by data from a small handful of successions (mainly  
888 Svalbard and NW Canada) and suffers from poor age control. Additional high-quality Sr isotope data  
889 are necessary to fill in the secular record of Neoproterozoic seawater  $^{87}\text{Sr}/^{86}\text{Sr}$ , and have been  
890 forthcoming from Russia (Kuznetsov et al., 2017) and the North China craton (Zhou et al., 2020).

891 The broad contours of the secular trend in Tonian–Cryogenian seawater  $^{87}\text{Sr}/^{86}\text{Sr}$  are now well  
892 established, dominated by a long-term rise in  $^{87}\text{Sr}/^{86}\text{Sr}$  (from  $\sim 0.7052$  to  $\sim 0.7073$ ; Fig. 5). However,  
893 strontium isotope chemostratigraphy in the Neoproterozoic is severely limited by the small number of  
894 stratigraphic intervals containing limestones that are sufficiently well preserved (i.e., with high Sr/Ca  
895 and low Mn/Sr) to record reliably the  $^{87}\text{Sr}/^{86}\text{Sr}$  of contemporaneous seawater. Therefore, the record is  
896 constructed typically from small numbers of data points from discrete intervals in different successions.  
897 When combined with limited age control on most samples, the result is an irregular record with a large  
898 number of temporal gaps and limited verification of trends among coeval successions (Fig. 5).  
899 Moreover, due to the near absence of syn-glacial carbonate strata, no proxy data for seawater exist for  
900 the Cryogenian glacial intervals (i.e. c.717–660 and c. $\geq$ 640–635.5 Ma). Nevertheless, due to the  
901 prominent rise in  $^{87}\text{Sr}/^{86}\text{Sr}$  through the Neoproterozoic, the strontium isotopic record can potentially  
902 distinguish between the early Tonian (i.e., 1000–810 Ma), late Tonian (810–720 Ma) and Cryogenian  
903 non-glacial interval (c. 660–650 Ma).

904

## 905 **5. Discussion**

906 The embryonic nature of Proterozoic bio- and chemostratigraphy outlined above illustrates how  
907 ratification of pre-Cryogenian GSSPs lies far in the future and beyond the scope of the current review,  
908 which is focussed on a template for agreed rock-based criteria to permit the removal of current GSSAs,  
909 to be replaced by interim chronostratigraphic units, bounded by approximate ages. Development of a  
910 natural Precambrian time scale, especially for periods (systems), is still a ‘work in progress’ but we  
911 consider nevertheless that improved rock-based subdivision is already possible, desirable and overdue.  
912 In working towards this aim, it is however important not to lose sight of the merits of the established  
913 chronometric scheme, which has served geologists well over the last 30 years. Indeed, it would appear  
914 that most boundaries would change by only small degrees. In order for future units of time (and strata)  
915 to be both widely acceptable and scientifically meaningful, they need to be fully defined conceptually,  
916 as has been done for the Cryogenian, Ediacaran and Cambrian periods, before they can be pinned down  
917 numerically.

918 As detailed above, the boundary definitions for the Hadean, Archean, Proterozoic and  
919 Phanerozoic eons help to broadly delimit four distinct parts of Earth history that are characterised by  
920 particular tectonic and biogeochemical regimes. Similarly, the eras of the Proterozoic Eon are  
921 recognised to be distinct intervals of tectonic, environmental and biological significance. The goal of  
922 any revision to the Precambrian geological time scale should therefore be to minimise disruption to

923 both the current international time scale and existing regional and national stratigraphic norms. In this  
924 vein, it may be pertinent to recall the advice given by James (1978), following Trendall (1966), that:  
925 (1) “the classification should be the simplest possible that will meet immediate needs [as] every  
926 additional complexity provides a basis for disagreement or rejection; (2) The subdivision of time  
927 embodied in the classification should reflect major events in Earth's history, yet not be in such a form  
928 as to inhibit critical review of that history; (3) The classification must be acceptable to most students of  
929 the Precambrian; (4) The nomenclature should not be identified closely with one particular region; and  
930 (5) The subdivision scheme should be accompanied by operational criteria, so that assignment to the  
931 classification will be guided by objective rather than theoretical considerations”. It is in this spirit that  
932 we explore below how an improved rock-based geological time scale might depart from the existing  
933 chronometric time scale.

934

### 935 **5.1 Tripartite rock-based subdivision of Archean time**

936 The current geological time scale divides the Archean into four eras, although none of these eras (or the  
937 preceding Hadean Eon) has been formally defined or ratified. Successive studies of crustal evolution  
938 have tended to favour a simpler three-fold subdivision of the Archean even if the precise numerical  
939 boundaries of those eras differ in each study. We support a tripartite subdivision because the rationale  
940 for the Eoarchean is conceptually unsound as it seems to be based on the chance preservation of crustal  
941 fragments rather than on any fundamental change in Earth history. Although a rock-based onset for the  
942 Archean Eon at c. 3.85 Ga is supported by some (Bleeker, 2004b; Kamber, 2015), proposing a specific  
943 age for the Hadean-Archean boundary lies outside the scope of the current discussion. Moreover it is  
944 also too difficult at present to propose a robust subdivision of Archean time based on diagnostic rock  
945 assemblages with the possible exception of the Neoproterozoic Era. We consider that three rock-based  
946 Archean eras of equal duration would constitute a robust subdivision to be characterised by the  
947 following rock types and geological processes, while acknowledging that future advances in knowledge  
948 may amend these preferences in the future:

949

950 **Paleoarchean** (c. 4.0 Ga – c. 3.5 Ga) Oldest crustal fragments of largely mafic composition, widespread  
951 TTG (Tonalite-Trondhjemite-Granodiorite) granitization; remnants of metamorphosed supracrustals.

952

953 **Mesoarchean** (c. 3.5 Ga – c. 3.0 Ga) Development of the subcontinental lithospheric mantle.  
954 Appearance of granite-greenstone terranes (coeval Pilbara and Barberton cratons) with high-grade,  
955 polymetamorphic granite-gneiss complexes elsewhere. Widespread uncontroversial stromatolite and  
956 other microbial fabrics, largely submerged continents, pulses in TTG magmatism that become  
957 progressively more potassium-rich. The base of the Mesoarchean could potentially be chosen for the  
958 base of a granite-greenstone terrane

959

960 **Neoproterozoic** (c. 3.0 Ga – c. 2.45/2.5 Ga) The Neoproterozoic witnessed a major pulse of (more felsic)  
961 crustal growth and the first platform covers on stable Archean cratons (Witwatersrand, Transvaal,  
962 Pongola Supergroups, South Africa; Mount Bruce Supergroup, Western Australia). Coeval  
963 “youngest” widespread granite-greenstone terranes (Kenoran, North America; Eastern Goldfields,  
964 Western Australia; Bulawayan, Zimbabwe); largest Superior-type BIFs in Earth history (Hamersley  
965 and Transvaal groups); initiation of a nascent form of plate tectonics; first passive margins; oldest  
966 large carbonate platforms; oldest mafic dyke swarms; methanogenic C-isotope signatures in kerogen;  
967 and traces of free oxygen from c. 3.0 Ga. We propose that the Neoproterozoic should include a redefined  
968 c. 2.63-2.45 Ga Siderian Period, encompassing BIF deposition of the Hamersley Group and coeval  
969 Transvaal. There is also potential for additional, as yet unnamed periods from c. 2.78-2.63 Ga,  
970 encompassing the basalt-rich Fortescue and Ventersdorp groups and coeval youngest widespread  
971 granite-greenstone terranes as well as prominent cratonization events; and c. 3.0-2.78 Ga  
972 encompassing the first platform covers (Witwatersrand and Pongola Groups). The base of the  
973 Neoproterozoic could potentially be chosen for the first appearance of carbonate platform covers.  
974 Depending on the outcome of further research on the global distribution of cratonization events, the  
975 term *Kratian*, after the Greek root ‘kratos’ or strength, could be reserved as a possible name for one  
976 of these older periods.

977

## 978 **5.2 Tripartite rock-based subdivision of Proterozoic time**

979 The current three-fold subdivision of the Proterozoic Eon is broadly accepted with each era following  
980 prolonged orogenesis, interpreted to represent supercontinent amalgamation and marked by zircon  
981 abundance peaks at around 2.7-2.5 Ga, 1.90-1.85 Ga and 1.05-1.00 Ga, respectively. The Archean-  
982 Proterozoic boundary follows two major zircon abundance peaks associated with the amalgamation of  
983 the putative megacontinent Kenora (Kenorland). Rock-based characteristics of the three Proterozoic  
984 eras might include:

985

986 **Paleoproterozoic** ( $\leq 2.5$  Ga to  $\leq 1.8$  Ga) Plate tectonic regime switch; new platform covers accompanied  
987 by onset of widespread (global?) glaciation, oxygenation of the atmosphere (crossing the threshold of  
988 disappearance of mass-independent S-isotope fractionation), first widespread sulfate evaporites,  
989 putative rise in continental freeboard (rising seawater  $^{87}\text{Sr}/^{86}\text{Sr}$ ), positive  $\delta^{13}\text{C}$  excursions (LJE). Era  
990 ends with widespread orogenesis, interpreted to mark major stages in Nuna assembly.

991

992 **Mesoproterozoic** ( $\leq 1.8$  Ga to  $\leq 1.0$  Ga) Widespread stable cratons and major platform covers, coeval  
993 with orogenesis, interpreted to represent final stages in the amalgamation of Nuna. Incorporates thick  
994 stromatolitic carbonate systems, with megascopic organic-walled fronds, beads, discs and coils, first  
995 ornamented microscopic acritarchs, appearance of multicellular red and green algae; rare negative

996  $\delta^{13}\text{C}$  excursions, widespread euxinia. Era ends with widespread orogenesis, interpreted to mark the  
997 assembly of Rodinia.

998

999 **Neoproterozoic** ( $\leq 1.0$  Ga to c. 0.539 Ga) New platform covers, interpreted to coincide with final  
1000 amalgamation, tenure and break-up of Rodinia. Diversification of eukaryotic algae and metazoans,  
1001 rising but unstable seawater  $^{87}\text{Sr}/^{86}\text{Sr}$ , high-amplitude  $\delta^{13}\text{C}$  excursions ( $>8\%$ ) and climate  
1002 perturbations, episodic ocean oxygenation. Following a prolonged interval of worldwide glaciation  
1003 (Snowball Earth), the era ends with evolution of the unique Ediacaran multicellular biota, as well as  
1004 widespread orogenesis, uplift and erosion throughout the late Ediacaran to early Cambrian interval.

1005

### 1006 **5.3 Rock-based period subdivisions of the Proterozoic Eon**

1007 Existing period-level GSSAs could be replaced by approximate chronostratigraphic ages as has been  
1008 done for the Cryogenian Period. The Proterozoic period names of Plumb (1991) are retained below,  
1009 with the addition of the *Scourian* Period, cf. Oxygenian Period of van Kranendonk et al. (2012):

1010 **Paleoproterozoic Era** (currently from 2.5 Ga, but interim boundary proposed at c. 2.45 Ga)

1011 **Scourian Period** (after *Skouria*, the Greek word for rust) replaces the Siderian Period (currently 2500  
1012 Ma – 2300 Ma) after *Sideros* (= iron), named for the voluminous “Banded Iron Formations” (BIFs)  
1013 deposited between c. 2.6 and c. 2.4 Ga, and peaking at c. 2.45 Ga. The *Scourian* Period was marked  
1014 by widespread glaciation and oxygenation as evidenced from a range of redox-sensitive elemental and  
1015 isotopic proxies, the decline of redox-sensitive detrital minerals such as pyrite and the eventual  
1016 appearance of red beds, oxidised paleosols and evaporite sulfate minerals.

1017 **Rhyacian Period** (currently 2300 Ma – 2050 Ma) after *Rhyax* (= stream of lava), named for the  
1018 “injection of layered complexes”. The name ‘Rhyacian’ was coined specifically for the exceptional c.  
1019 2.054 Ga Bushveld Igneous Complex of South Africa. The period is a generally quiet interval in terms  
1020 of basin formation and orogeny. 2.2 Ga marks the onset of increased magmatism globally (Spencer,  
1021 2018) with the major Bushveld LIP emplaced near the end of the period. The most characteristic  
1022 feature of this period is arguably the widespread occurrence of very high  $\delta^{13}\text{C}$  values in marine  
1023 carbonate rocks (the Lomagundi-Jatuli Event) and the approximately contemporaneous appearance of  
1024 major evaporite sulfate deposits.

1025 **Orosirian Period** (currently 2050 Ma – 1800 Ma) after *Orosira* (= mountain range), named for a  
1026 “global orogenic period”. This period is characterised by widespread orogenic events, reflected in an  
1027 exceptional zircon abundance peak (Fig. 3), and interpreted to mark the main assembly of Nuna. The  
1028 period incorporates the appearance of the first macroscopic fossils.

1029 **Mesoproterozoic Era** (to begin at or after c. 1.8 Ga)

1030 **Statherian Period** (c. 1800 Ma – c. 1600 Ma) after *Statheros* (= stable), named for “stabilization of  
1031 cratons”. This period is characterized on most continents by new platforms and by coeval orogeny  
1032 marginal to Nuna (e.g., North America; Kimban Orogeny, South Australia). The McArthur Basin of  
1033 northern Australia represents a suitable candidate ‘stratotype’. The sandstone-volcanic Tawallah  
1034 Group and Carson LIP, pass up into stromatolitic carbonates of the McArthur Group, encompassing  
1035 the full interval from 1800 -1600 Ma with several age-constrained sequence breaks. Coeval sandstone-  
1036 volcanic sequences in Brazil (Diamantina Group), central Africa (Chela Group), Russia (Lower  
1037 Riphean), and north China (Changcheng Group) (north China). Macroscopic and microscopic fossils  
1038 with diagnostically indicative eukaryote features appear in rocks towards the end of this period.

1039 **Calymmian Period** (c. 1600 Ma – c. 1400 Ma) after *Calymma* (= cover), named for “platform covers”.  
1040 This period is characterized by the expansion of existing platform covers. Microbially influenced  
1041 carbonates of the Jixian Group (North China) could provide a suitable ‘stratotype’, although there are  
1042 similar carbonate successions in coeval Lower Riphean (Russia). Suturing events, interpreted to  
1043 represent final stages of Nuna amalgamation, were followed by thick terrigenous basins that emerged  
1044 during this period; e.g, Roper Group (North Australia), Belt-Purcell Supergroups (North America),  
1045 Paraguacu-Chapada Diamantina Groups (Brazil). The Statherian- Calymmian boundary is represented  
1046 by a regional unconformity between the McArthur and Nathan Groups (McArthur Basin) in northern  
1047 Australia.

1048 **Ectasian Period** (c.1400 Ma – c. 1200 Ma) after *Ectasis* (= extension), named for “continued expansion  
1049 of platform covers”. A tectonically quiet period, with little basin development or orogeny; e.g., upper  
1050 Roper Group (Australia), Xiamaling Group (North China), Yurmatau Group (Russia), Kibaran  
1051 Supergroup (central Africa). Derim Derim-Yanliao and 1230 Ga Maojiagou LIPs. Although there is  
1052 currently little to distinguish it from the Calymmian Period, it is retained in Figure 6B. No suitable  
1053 “stratotype” exists for now, although some authors have proposed a level close to the Jixian-  
1054 Xiamaling group boundary on the North China craton, inferred to be c. 1400 Ma (between 1380 and  
1055 1440 Ma).

1056 **Stenian Period** (c. 1200 Ma – c. 1000 Ma) after *Stenos* (= narrow), named for “narrow belts of intense  
1057 metamorphism and deformation”, e.g., Grenville, Musgrave, Sunsás, Namaqua orogenies.  
1058 Conselheiro Mata Group (Brazil) and Keweenawan mafic rift (North America) elsewhere. Defining a  
1059 chronostratigraphy from high-grade, deep crustal metamorphic rocks is problematic and specifically  
1060 discouraged by ICS. An interim arbitrary base at c. 1200 Ma is assigned to encompass all the events  
1061 across the “Grenvillian” belts, and coeval Conselheiro Mata Group. The end of the period marks the  
1062 appearance of stem group multicellular red and green algae in the fossil record.

1063 **Neoproterozoic Era** (to begin at or after c. 1.0 Ga).

1064 **Tonian Period** (currently 1000 Ma – c. 720 Ma) after *Tonas* (= stretch), named for the lithospheric  
1065 stretching that we now associate with the breaking apart of the supercontinent Rodinia, now thought  
1066 to have occurred largely after c. 800 Ma based on estimated rift lengths, evaporite deposits and flood  
1067 basalts (Merdith et al., 2019). Although not currently essential, a new period might conceivably cover  
1068 the preceding interval of cratonization from the final amalgamation to initial rupture of Rodinia, i.e.  
1069 approximately  $\leq 1.0$  Ga to  $\geq 0.8$  Ga, with a revised Tonian Period from  $\geq 0.8$  Ga to c. 0.72 Ga. We  
1070 tentatively propose either of the terms *Kleisian* or *Syndian* in Figure 6B, following the Greek words  
1071 respectively for the ‘closure’ or ‘connection’ that naturally followed the narrowing of Grenvillian-  
1072 closing oceans in the final assembly phase of Rodinia. The Tonian Period saw the first appearance of  
1073 mineralised scales and vase-shaped tests in the fossil record, suggesting nascent stages of  
1074 biomineralization and heterotrophic protistan evolution.

1075

## 1076 **6. Concluding remarks and recommendations**

1077

1078 1) The four major divisions of Earth history are the Hadean, Archean, Proterozoic and Phanerozoic  
1079 eons, whereby the Hadean-Archean boundary is taken to represent the start of the terrestrial rock  
1080 record at c. 4.0 Ga.

1081

1082 2) Two first-order (*Archean and Proterozoic eon*) and six second-order (*Palaeoarchean,*  
1083 *Mesoarchean, Neoarchean, Palaeoproterozoic, Mesoproterozoic, Neoproterozoic era*)  
1084 stratigraphic intervals provide intuitive subdivision of post-Hadean / pre-Phanerozoic time. We  
1085 consider that the Archean Eon would be more parsimoniously subdivided into three informal units  
1086 of equal duration (Fig. 6B) instead of the current four eras, to be defined further after detailed  
1087 discussions by a commission of international experts.

1088

1089 3) Major transitions in Earth’s tectonic, biological and environmental history occurred at  
1090 approximately 2.5-2.3, 1.8-1.6 and 1.0-0.8 Ga. We consider, therefore, that current GSSAs at 2.5,  
1091 1.6 and 1.0 Ga could be replaced expeditiously by rock-based Proterozoic eras beginning at or  
1092 after c. 2.5 Ga, c. 1.8 Ga and c. 1.0 Ga, respectively, based around these major transitions, all of  
1093 which occurred following orogenic peaks and during times of waning zircon abundance (post-  
1094 acme, but not yet zenith) in line with Phanerozoic boundaries.

1095

1096 4) We suggest that current period-level GSSAs be replaced by improved rock-based concepts and  
1097 interim chronostratigraphic units as soon as practicable, continuing recent progress towards that

1098 goal, illustrated, for example, by the establishment of an Ediacaran GSSP in 2004 and  
1099 chronostratigraphic definition of the base of the Cryogenian at c. 720 Ma in 2012. Although all  
1100 existing period names could be retained in a future chronostratigraphic scheme, some will need  
1101 more conceptual underpinning, which would likely result in movement of the Siderian Period into  
1102 the Archean Eon.

1103

1104 5) We recommend that a future Paleoproterozoic Era contain only three periods beginning at or after  
1105 c. 2.45 Ga, c. 2.3 Ga and c. 2.05 Ga, respectively, so that the era begins near the end of major  
1106 Archean BIF deposition, the onset of widespread glaciation and the Great Oxidation Event, but  
1107 ends close to the onset of a prolonged period of cratonic, climatic and isotopic stability. Future  
1108 attention will likely focus on ensuring that rock-based Paleoproterozoic periods (currently  
1109 Siderian, Rhyacian and Orosirian) bracket the natural phenomena for which they were named (iron  
1110 formation, magmatism and orogenies, respectively). We propose therefore that the Siderian Period  
1111 be moved into the Neoproterozoic, in which case a new period, potentially the *Scourian* Period (Fig.  
1112 6B), would become the first period of the Paleoproterozoic Era.

1113

1114 6) We recommend that a future Mesoproterozoic Era contain four periods (Statherian at, or more  
1115 likely, after 1.8 Ga, Calymmian at c. 1.6 Ga, Ectasian at c. 1.4 Ga and Stenian at c. 1.2 Ga) so that  
1116 it begins after major orogenic climax but before putative eukaryote-grade fossil assemblages, in  
1117 the form of ornamented acritarchs and megascopic fronds, and ends after the Grenville orogeny  
1118 near the time of final stages of supercontinent amalgamation.

1119

1120 7) We recommend that a future Neoproterozoic Era contain four periods (a pre-Tonian period at or  
1121 after c. 1.0 Ga, Tonian at c. 0.85 Ga, Cryogenian at c. 0.72 Ga and Ediacaran, which has a ratified  
1122 GSSP dated at c. 0.635 Ga) so that it begins around the final amalgamation of Rodinia and ends  
1123 traditionally at the Ediacaran-Cambrian boundary. We tentatively propose that the pre-Tonian  
1124 period could be named the *Kleisian* Period (Fig. 6B), although *Syndian* might also be considered.

1125

1126 8) These and further refinements of pre-Cryogenian time and strata could be developed by new expert  
1127 subcommissions to cover the 1) pre-Ediacaran Neoproterozoic (currently, the Cryogenian  
1128 Subcommission), 2) Mesoproterozoic, 3) Paleoproterozoic and 4) Archean (+ Hadean).

1129

1130



1131

1132 **Acknowledgements**

1133 The authors represent the core of a working group of the International Commission on Stratigraphy for  
1134 pre-Cryogenian chronostratigraphic subdivision. We are greatly indebted to many people who have  
1135 provided comments and helpful advice on various drafts of this article from its early green paper stage,  
1136 including David Harper, Brian Huber, Phil Gibbard, Stan Finney, Phil Donoghue, A.K. Jain, Vivek  
1137 Kale, Mihir Deb, M. Jayananda, Jyotiranjana Ray, Aivo Lepland, Peter Haines, Martin Whitehouse. New  
1138 period names were suggested by A. Bekker (*Scourian*), D. Evans (*Kleisian*, *Syndian*) and G. Shields  
1139 (*Kratian*).

1140

1141 **References**

1142

1143 Adam, Z.R., Skidmore, M.L., Mogk, D.W., Butterfield, N.J., 2017. A Laurentian record of the earliest  
1144 fossil eukaryotes. *Geology* 45, 387-390.

1145 Ahm, A.-S. C., Maloof, A. C., Macdonald, F. A., Hoffman, P. F., Bjerrum, C. J., Bold, U., Rose, C. V.,  
1146 Strauss, J. V., Higgins, J. A., 2019. An early diagenetic deglacial origin for basal Ediacaran “cap  
1147 dolostones”. *Earth and Planetary Science Letters* 506, 292–307.

1148 Alcott, L.J., Mills, B.J.W., Poulton, S.W., 2019. Stepwise Earth oxygenation is an inherent property of  
1149 global biogeochemical cycling. *Science*, 6471, 1333-1337 doi: 10.1126/science.aax6459.

1150 Anbar, A.D., Duan, Y., Lyons, T.W., Arnold, G.L., Kendall, B., Creaser, R.A., Kaufman, A.J., Gordon,  
1151 G.W., Scott, C., Garvin, J., Buick, R., 2007. A whiff of oxygen before the Great Oxidation Event.  
1152 *Science*, 317, 1903-1906.

1153 Arnold, G. L., Anbar, A. D., Barling, J. and Lyons, T. W. 2004. Molybdenum isotope evidence for  
1154 widespread anoxia in mid-Proterozoic oceans. *Science*, 304, 87–90.

1155 Arp, G., Reimer, A., Reitner, J., 2001. Photosynthesis-induced biofilm calcification and calcium  
1156 concentrations in Phanerozoic oceans. *Science*, 292, 1701-1074.

1157 Ashwal, L.D., Bybee, G.M., 2017. Crustal Evolution and the temporality of anorthosites. *Earth Science*  
1158 *Reviews* 173: 307-330.

1159 Baludikay, B.K., Storme, J.Y., François, C., Baudet, D., Javaux, E.J., 2016. A diverse and exquisitely  
1160 preserved organic-walled microfossil assemblage from the Meso–Neoproterozoic Mbuji-Mayi  
1161 Supergroup (Democratic Republic of Congo) and implications for Proterozoic biostratigraphy.  
1162 *Precambrian Research* 281, 166–184.

1163 Bartley, J.K., Semikhatov, M.A., Kaufman, A.J., Knoll, A.H., Pope, M.C., Jacobsen, S.B., 2001. Global  
1164 events across the Mesoproterozoic–Neoproterozoic boundary: C and Sr isotopic evidence from  
1165 Siberia. *Precambrian Research* 111, 165–202.

- 1166 Bédard, J.H., 2018. Stagnant lids and mantle overturns: Implications for Archean tectonics,  
1167 magmatogenesis, crustal growth, mantle evolution, and the start of plate tectonics. *Geoscience Frontiers*,  
1168 9, 19-49.
- 1169 Beghin, J., Guilbaud, R., Poulton, S.W., Gueneli, N., Brocks, J.J., Storme, J.-Y., Blanpied, C., Javaux,  
1170 E.J., 2017a. A palaeoecological model for the late Mesoproterozoic – early Neoproterozoic Atar/El  
1171 Mreïti Group, Taoudeni Basin, Mauritania, northwesternAfric. *Precambrian Research* 299, 1–14.
- 1172 Beghin, J., Storme, J.-Y., Blanpied, C., Gueneli, N., Brocks, J.J., Poulton, S.W., Javaux, E.J., 2017b.  
1173 Microfossils from the late Mesoproterozoic – early Neoproterozoic Atar/El Mreïti Group, Taoudeni  
1174 Basin, Mauritania, northwesternAfric. *Precambrian Research* 291, 63–82.
- 1175 Bekker, A., 2014. Great Oxygenation Event. In: *Encyclopedia of Astrobiology* (eds: R. Amils et al.),  
1176 Springer-Verlag, Berlin, Heidelberg, pp. 1-9.
- 1177 Bekker, A., Holland, H.D., 2012. Oxygen overshoot and recovery during the early Paleoproterozoic.  
1178 *Earth and Planetary Science Letters*, 317, 295-304.
- 1179 Bekker, A, Holland, H.D, Wang, P.L., Ruble, D., Stein, H.J., Hannah, J.L., Coetzee, L.L., Beukes, N.J.,  
1180 2004. Dating the rise of atmospheric oxygen. *Nature*, 427, 117-120.
- 1181 Bekker, A., Karhu, J.A., Eriksson, K.A., Kaufman, A.J., 2003. Chemostratigraphy of Paleoproterozoic  
1182 carbonate successions of the Wyoming Craton: tectonic forcing of biogeochemical change?  
1183 *Precambrian Research*, 120: 279-325.
- 1184 Bekker, A., Kaufman, A.J., 2007. Oxidative forcing of global climate change: a biogeochemical record  
1185 across the oldest Paleoproterozoic ice age in North America. *Earth and Planetary Science Letters*, 258,  
1186 486-499.
- 1187 Bekker, A., Planavsky, N., Rasmussen, B., Krapez, B., Hofmann, A., Slack, J.F., Rouxel, O.J.,  
1188 Konhauser, K.O., Iron formations: Their origins and implications for ancient seawater chemistry.  
1189 *Treatise on Geochemistry*, 12, 561-628.
- 1190 Bekker, A., Slack, J.F., Planavsky, N., Krapez, B., Hofmann, A., Konhauser, K.O., Rouxel, O.J., 2010.  
1191 Iron formation: the sedimentary product of a complex interplay among mantle, tectonic, oceanic, and  
1192 biospheric processes. *Economic Geology*, 105, 467-508.
- 1193 Bengtson, S., Sallstedt T., Belivanova V., Whitehouse M., 2017. Three-dimensional preservation of  
1194 cellular and subcellular structures suggests 1.6 billion-year-old crown-group red algae. *PLoS Biol*  
1195 15(3):e2000735.doi:10.1371/ journal.pbio.2000735.
- 1196 Berney, C., Pawlowski, J., 2006. A molecular time-scale for eukaryote evolution recalibrated with the  
1197 continuous microfossil record. *Proceedings of the Royal Society B* 273, 1867–1872.
- 1198 Betts, H.C., Puttick, M.N., Clark, J.W., Williams, T.A., Donoghue, P.C.J., Pisani, D., 2018. Integrated  
1199 genomic and fossil evidence illuminates life’s early evolution and eukaryote origin. *Nature Ecology  
1200 & Evolution* 2, 1556–1562.

- 1201 Blank, C.E., 2013. Origin and early evolution of photosynthetic eukaryotes in freshwater environments:  
1202 reinterpreting Proterozoic paleobiology and biogeochemical processes in light of trait evolution.  
1203 *Journal of Phycology*, 49(6), 1040-1055.
- 1204 Blättler, C.L., Claire, M.W., Prave, A.R., Kirsimäe, K., Higgins, J.A., Medvedev, P.V., 2018. Two-  
1205 billion-year-old evaporites capture Earth's great oxidation. *Science*, 360: 320-323.
- 1206 Bleeker, W., 2003. The late Archean record: a puzzle in c. 35 pieces. *Lithos*, 71: 99-134.
- 1207 Bleeker, W., 2004a. Towards a "natural" Precambrian time scale. In: Gradstein, F.M., Ogg, J.G., Smith,  
1208 A.G. (Eds.), *A Geologic Time Scale 2004*. Cambridge University Press, Cambridge, pp. 141-146.
- 1209 Bleeker, W., 2004b. Towards a 'natural' time scale for the Precambrian – A proposal. *Lethaia*, 219-  
1210 222.
- 1211 Bleeker, W., Ketchum, J.W.F., Jackson, V.A., Villeneuve, M.E., 1999. The Central Slave Basement  
1212 Complex, Part 1: Its structural topology and autochthonous cover. *Canadian Journal of Earth Sciences*  
1213 36 (7), 1083-1109.
- 1214 Bodorkos, S., Crowley, J.L., Claoue-Long, J.C., Anderson, J.R., Magee, C.W. Jr., 2020. Precise U-Pb  
1215 baddelyite dating of the Derim Derim dolerite, McArthur Basin, Northern Territory: old and new  
1216 SHRIMP and ID-TIMS constraints. *Australian Journal of Earth Sciences*,  
1217 doi:10.1080/08120099.2020.1749929.
- 1218 Bowring, S. A., Grotzinger, J. P., 1992. Implications of new chronostratigraphy for tectonic evolution  
1219 of Wopmay orogen, northwest Canadian Shield. *American Journal of Science*, 292, 1-20.
- 1220 Bowring, S.A., Williams, I.S., 1999. Priscoan (4.00–4.03 Ga) orthogneisses from northwestern,  
1221 Canada. *Contributions Mineralogy and Petrology*, 134, 3–16.
- 1222 Bradley, D. C., 2008. Passive margins through earth history. *Earth-Science Reviews*, 91, 1–26.
- 1223 Brasier, M., Cowie, J., Taylor, M., 1994. Decision on the Precambrian-Cambrian boundary stratotype.  
1224 *Episodes*, 17, 3-8.
- 1225 Brasier, A.T., Fallick, A.E., Prave, A.R., Melezhik, V.A., Lepland, A., FAR-DEEP scientists, 2011.  
1226 Coastal sabkha dolomites and calcitised sulphates preserving the Lomagundi-Jatuli carbon isotope  
1227 signal. *Precambrian Research*, 189, 193-211.
- 1228 Brasier, A.T., Martin, A.P., Melezhik, V.A., Prave, A.R., Condon, D.J., Fallick, A.E., 2013. Earth's  
1229 earliest global glaciation? Carbonate geochemistry and geochronology of the Polisarka Sedimentary  
1230 Formation, Kola Peninsula, Russia. *Precambrian Research*, 235, 278-294.
- 1231 Brocks, J.J., 2018. The transition from a cyanobacterial to algal world and the emergence of animals.  
1232 *Emerging Topics in Life Sciences* 2, 181–190.
- 1233 Bull, S., Selley, D., Broughton, D., Hitzman, M., Cailteux, J., Large, R., McGoldrick, P., 2011.  
1234 Sequence and carbon isotopic stratigraphy of the Neoproterozoic Roan Group strata of the Zambian  
1235 copperbelt. *Precambrian Research* 190, 70–89.
- 1236 Butterfield, N.J., 2000. *Bangiomorphapubescens* n. gen., n. sp.: implications for the evolution of sex,  
1237 multicellularity, and the Mesoproterozoic radiation of eukaryotes. *Paleobiology*, 26, 386-404.

- 1238 Butterfield, N.J., 2004. A vaucheriacean alga from the middle Neoproterozoic of Spitsbergen:  
1239 implications for the evolution of Proterozoic eukaryotes and the Cambrian explosion. *Paleobiology*,  
1240 30, 231–252.
- 1241 Butterfield, N.J., 2015. Early evolution of the Eukaryota. *Palaeontology*, 58, 5–17.
- 1242 Butterfield, N.J., Knoll, A.H., Swett, K., 1994. Paleobiology of the Neoproterozoic Svanbergfjellet  
1243 Formation, Spitsbergen. *Fossils and Strata*, 34, 1–84.
- 1244 Campbell, I.H., Allen, C.A., 2008. Formation of supercontinents linked to increases in atmospheric  
1245 oxygen. *Nature Geoscience*, 1, 554–558.
- 1246 Canfield, D.E., 1998. A new model for Proterozoic ocean chemistry. *Nature*, 396, 450–453.
- 1247 Canfield, D.E., Zhang, S., Wang, H., Wang, X., Zhao, W., Su, J., Bjerrum, C.J., Haxen, E.R.,  
1248 Hammarlund, E.U., 2018. A Mesoproterozoic iron formation. *PNAS*, doi:10.1073/pnas.1720529115.
- 1249 Caro, G., Morino, P., Mojzsis, S.J., Cates, N.L. and Bleeker, W., 2017. Sluggish Hadean  
1250 geodynamics: Evidence from coupled 146,147 Sm–142,143 Nd systematics in Eoarchean  
1251 supracrustal rocks of the Inukjuak domain (Québec). *Earth and Planetary Science Letters*,  
1252 457, 23–37.
- 1253 Cawood, P.A., Hawkesworth, C.J., 2014. Earth’s middle age. *Geology*, 42, 503–506.
- 1254 Cawood, P.A., Hawkesworth, C.J., Dhuime, B. 2013. The continental record and the generation of  
1255 continental crust. *Geological Society of America Bulletin* 125: 14–32.
- 1256 Cawood, P.A., Hawkesworth, C.J., Pisarevsky, S.A., Dhuime, B., Capitanio, F.A., Nebel, O., 2018.  
1257 Geological archive of the Onset of Plate Tectonics. *Philosophical Transactions of the Royal Society*  
1258 A, 376, 20170405.
- 1259 Chakraborty, P.P., Mukhopadhyay, J., Paul, P., Banerjee, D.M., Bera, M.K., 2020. Early atmosphere  
1260 and hydrosphere oxygenation: Clues from Precambrian paleosols and chemical sedimentary records  
1261 of India. *Episodes*, 43, 175–186.
- 1262 Chemale, F., Dussin, I.A., Alkmim, F.F., Martins, M.S., Queiroga, G., Armstrong, R., Santos, M.N.,  
1263 2012. Unravelling a Proterozoic basin history through detrital zircon geochronology: The case of the  
1264 Espinhaço Supergroup, Minas Gerais, Brazil. *Gondwana Research* 22, 200–206.
- 1265 Cloud, P., 1972. A working model of the primitive Earth. *American Journal of Science*, 272: 537–548.
- 1266 Cloud, P., 1976. Major features of crustal evolution. *Geol. Soc. South Africa, Alex L. Du Toit Mem.*  
1267 *Lect. Ser.*, 14, 33pp.
- 1268 Cloud, P., Glaessner, M.F., 1982. The Ediacarian Period and System: Metazoa inherit the Earth. *Science*  
1269 217, 783–792.
- 1270 Cohen, P.A., Knoll, A.H., 2012. Scale Microfossils from the Mid-Neoproterozoic Fifteenmile Group,  
1271 Yukon Territory. *Journal of Paleontology* 86, 775–800.
- 1272 Cohen, P.A., Macdonald, F.A., 2015. The Proterozoic record of eukaryotes. *Paleobiology* 41, 610–632.

- 1273 Cohen, P.A., Irvine, S.W., Strauss, J.V., 2017a. Vase-shaped microfossils from the TonianCallison  
 1274 Lake Formation of Yukon, Canada: taxonomy, taphonomy and stratigraphic palaeobiology.  
 1275 *Palaeontology* 60, 683–701.
- 1276 Cohen, P. A., Strauss, J. V., Rooney, A. D., Sharma, M., Tosca, N., 2017b. Controlled hydroxyapatite  
 1277 biomineralization in an 810 million-year-old unicellular eukaryote. *Science Advances* 3, e1700095.
- 1278 Collins, A.S., Patranabis-Deb, S., Alexander, E., Bertram, C., Falster, G., Gore, R., Mackintosh, J.,  
 1279 Dhang, P.C., Saha, D., Payne, J., Jourdan, F., Backé, G., Halverson, G.P., Wade, B.P., 2015. Detrital  
 1280 Mineral Age, Radiogenic Isotopic Stratigraphy and Tectonic Significance of the Cuddapah Basin,  
 1281 India. *Gondwana Research*, 28, 1294-1309.
- 1282 Condie, K. C., 1998. Episodic continental growth and supercontinents: a mantle avalanche connection?  
 1283 *Earth and Planetary Science Letters* 163, 97–108.
- 1284 Condie, K.C., 2004. Supercontinents and superplume events: distinguishing signals in the geologic  
 1285 record. *Physics of the Earth and Planetary Interiors*, 146, 319–332.
- 1286 Condie, K.C., 2014. Growth of continental crust: a balance between preservation and recycling.  
 1287 *Mineralogical Magazine* 78, 623–637.
- 1288 Condie, K.C., Aster, R.C., 2010. Episodic zircon age spectra of orogenic granitoids: the supercontinent  
 1289 connection and continental growth. *Precambrian Research*, 180: 227-236.
- 1290 Condie, K.C., O’Neill, C. Aster, R.C., 2009. Evidence and implications for a widespread magmatic  
 1291 shutdown for 250 Myr on Earth. *Earth and Planetary Science Letters*, 282, 294-298.
- 1292 Condie, K.C., Puetz, S.J., 2019. Time series analysis of mantle cycles II: The geologic record in zircons,  
 1293 large igneous provinces and mantle lithosphere. *Geoscience Frontiers*, 10, 1327-1336.
- 1294 Condon, D., Zhu, M., Bowring, S., Jin, Y., Wang, W., Yang, A., 2005. From the Marinoan glaciation  
 1295 to the oldest bilaterians: U-Pb ages from the Doushantuo Formation, China. *Science* 308, 95–98.
- 1296 Cornell, D.H., Thomas, R.J., Gibson, R., Moen, H.F.G., Moore, J.M., Reid, D.L., 2006. Namaqua-Natal  
 1297 Province. In: Johnson, M.R., Anhaeuser, C.R., Thomas, R.J. (Eds.), *The Geology of South Africa*.  
 1298 *Geol. Soc. S. Afr, Johannesburg/Council for Geoscience, Pretoria*, pp. 325–379.
- 1299 Cox, G. M., Halverson, G. P., Stevenson, R. K., Vokaty, M., Poirier, A., Kunzmann, M., Li, Z.-X.,  
 1300 Denyszyn, S. W., Strauss, J. V., Macdonald, F. A., 2016. Continental flood basalt weathering as a  
 1301 trigger for Neoproterozoic Snowball Earth. *Earth and Planetary Science Letters* 446, 89–99.
- 1302 Cox, G.M., Isakson, V., Hoffman, P.F., Gernon, T.M., Schmitz, M.D., Shahin, S., Collins, A.S., Preiss,  
 1303 W., Blades, M.L., Mitchell, R.N., Nordsvan, A., 2018. South Australian U-Pb zircon (CA-ID-TIMS)  
 1304 age supports globally synchronous Sturtian deglaciation. *Precambrian Research* 315, 257–263.
- 1305 Crockford, P.W., Hodgskiss, M.S.W., Uhlein, G.J., Caxito, F., Hayles, J.A., Halverson, G.P., 2018.  
 1306 Linking paleocontinents through  $\Delta^{17}\text{O}$  anomalies. *Geology* 46, 179–182.
- 1307 Crockford, P.W, Kunzmann, M., Bekker, A., Hayles, J., Bao, H., Halverson G.P., Peng, Y., Bui,  
 1308 T.H., Cox, G., Gibson T.M., Worndle, S., Rainbird, R., Lepland, A., Swanson-Hysell, N., Master,

- 1309 S., Sreevanis, B., Kuznetsov, A., Krupenik, V., Wing, B.A., 2019. Claypool Continued:  
 1310 Extending the isotopic record of sedimentary sulfate. *Chemical Geology*, 514, 200-225
- 1311 Crosby, C.H., Bailey, J.V., Sharma, M., 2014. Fossil evidence of iron-oxidizing chemolithotrophy  
 1312 linked to phosphogenesis in the wake of the Great Oxidation Event. *Geology* 42, 1015-1018.
- 1313 Crook, K.A.W., 1989. Why the Precambrian time-scale should be chronostratigraphic: A response to  
 1314 recommendations by the Subcommittee on Precambrian stratigraphy. *Precambrian Research*, 43,  
 1315 143-150.
- 1316 Darling, J. R., Moser, D. E., Heaman, L. M., Davis, W. J., O’Neil, J., Carlson, R. (2014). Eoarchean to  
 1317 Neoproterozoic evolution of the Nuvvuagittuq Supracrustal belt: New insights from U-Pb zircon  
 1318 geochronology. *American Journal of Science*, 313(9), 844–876.
- 1319 Daines, S.J., Mills, B.J.W., Lenton, T.M., 2017. Atmospheric oxygen regulation at low Proterozoic  
 1320 levels by incomplete oxidative weathering of sedimentary organic carbon. *Nature Communications*,  
 1321 8, 14379, doi: 10.1038/ncomms14379.
- 1322 Dana, J.D. (1872) *American Journal of Science and Arts*. 3rd series, 3, 16, 250–257.
- 1323 Derry, L.A., 2010. A burial diagenesis origin for the Ediacaran Shuram-Wonoka carbon isotope  
 1324 anomaly, *Earth and Planetary Science Letters* 292, 152–172.
- 1325 Des Marais, D.J., Strauss, H., Summons, R.E., Hayes, J.M., 1992. Carbon isotope evidence for the  
 1326 stepwise oxygenation of the Proterozoic environment. *Nature*, 359, 605-609.
- 1327 Domagal-Goldman, S.D., Kasting, J.F., Johnston, D.T., Farquhar, J., 2008. Organic haze, glaciations  
 1328 and multiple sulfur isotopes in the Mid-Archean Era. *Earth and Planetary Science Letters*, 269(1-2),  
 1329 pp.29-40.
- 1330 Dunn, P.R., Plumb, K.A., Roberts, H.G., 1966. A proposal for time-stratigraphic classification of the  
 1331 Australian Precambrian. *Geol. Soc. Aust. J.*, 13, 593-608.
- 1332 Dunn, P., Thomson, B., Rankama, K., 1971. Late Pre-Cambrian glaciation in Australia as a stratigraphic  
 1333 boundary. *Nature* 231, 498–502.
- 1334 Eme, L., Sharpe, S.C., Brown, M.W., Roger, A.J., 2014. On the age of eukaryotes: evaluating evidence  
 1335 from fossils and molecular clocks. *Cold Spring Harbor Perspectives in Biology* 6, a016139.
- 1336 Ernst, R.E. and Youbi, N., 2017. How large igneous provinces affect global climate, sometimes cause  
 1337 mass extinctions, and represent natural markers in the geological record. *Palaeogeography,*  
 1338 *Palaeoclimatology, Palaeoecology*, 478, 30-52.
- 1339 Ernst, R.E., Wingate, M.T.D., Buchan, K.L., Li, Z.-X. 2008. Global record of 1600–700 Ma Large  
 1340 Igneous Provinces (LIPs): Implications for the reconstruction of the proposed Nuna (Columbia) and  
 1341 Rodinia supercontinents. *Precambrian Research* 160, 159–178.
- 1342 Ernst, R.E., Bond, D.P.G., Zhang, S.H., 2020. Influence of Large Igneous Provinces. From: F.M.  
 1343 Gradstein, J.G. Ogg, M.D. Schmitz, G.M. Ogg. (Eds). *The Geologic Time Scale 2020 volume 2*,  
 1344 Elsevier Science Limited, pp. 345-356.

- 1345 Etienne, J.L., Allen, P.A., Rieu, R., Le Guerroué, E., 2007. Neoproterozoic glaciated basins: a critical  
1346 review of the Snowball Earth hypothesis by comparison with Phanerozoic basins, in: Hambrey, M.J.,  
1347 Christoffersen, P., Glasser, N.F., Hubbard, B. (Eds.), *Glacial Sedimentary Processes and Products*.  
1348 Volume 39 of International Association of Sedimentologists Special Publication, pp. 343–399.
- 1349 Evans, D.A.D., Beukes, N.J., Kirschvink, J.L., 1997. A Paleoproterozoic Snowball Earth. *Nature*, 386,  
1350 262-266.
- 1351 Evans, D.A.D., Mitchell, R.N., 2011. Assembly and breakup of the core of Paleoproterozoic-  
1352 Mesoproterozoic supercontinent Nuna. *Geology*, 39, 443-446.
- 1353 Evans, D.A.D., Smirnov, A.N., Gumsley, A.P., 2017. Paleomagnetism and U–Pb geochronology of  
1354 the Black Range dykes, Pilbara Craton, Western Australia: a Neoproterozoic crossing of the polar circle.  
1355 *Australian Journal of Earth Sciences*, v. 64, p. 225–237, doi:10.1080/08120099.2017.1289981.
- 1356 Evans, D.A.D., Trindade, R.I.F., Catelani, E.L., D-Agrella-Filho, M.S., Heaman, L.M., Oliveira, E.P.,  
1357 Soderlund, U., Ernst, R.E., Smirnov, A.V., Salminen, J.M., 2016. Return to Rodinia? Moderate to  
1358 high palaeolatitude of the São Francisco / Congo craton at 920 Ma. From: Z. Li, D.A.D. Evans, J.B.  
1359 Murphy (eds) *Supercontinent Cycles Through Earth History*, Geological Society, London, Special  
1360 Publications, 424, 167-190.
- 1361 Fairchild, I.J., Kennedy, M.J., 2007. Neoproterozoic glaciation in the Earth system. *Journal of the*  
1362 *Geological Society, London* 164, 895–921.
- 1363 Fareeduddin, Banerjee, D.M., 2020. Aravalli craton and its mobile belts: An update. *Episodes*, 43, 88-  
1364 108.
- 1365 Farquhar, J., Bao, H., Thiemens, M., 2000. Atmospheric influence of Earth's earliest sulphur cycle.  
1366 *Science*, 289, 756-758.
- 1367 Farquhar, J., Nanping, W., Canfield, D.E., Oduro, H., 2010. Connections between Sulfur Cycle  
1368 Evolution, Sulfur Isotopes, Sediments, and Base Metal Sulfide Deposits. *Economic Geology* 105:  
1369 509-533.
- 1370 Farquhar, J., Peters, M., Johnston, D.T., Strauss, H., Masterson, A., Wiechert, U. and Kaufman, A.J.,  
1371 2007. Isotopic evidence for Mesoarchean anoxia and changing atmospheric sulphur chemistry.  
1372 *Nature*, 449, 706-709.
- 1373 Farquhar, J., Zerkle, A.L., Bekker, A., 2011. Geological constraints on the origin of oxygenic  
1374 photosynthesis. *Photosynthesis Research*, 107, 11-36.
- 1375 Fitzsimons, I.C.W., 2010. Grenville-age basement provinces in East Antarctica: evidence for three  
1376 separate collisional orogens. *Geology*, 28 (10), 879-882.
- 1377 Fralick, P. and Riding, R. 2015. Steep Rock Lake: Sedimentology and geochemistry of an Archean  
1378 carbonate platform. *Earth-Science Reviews*, 151, 132-175.
- 1379 Frimmel, H.E., 2005. Archean atmospheric evolution: evidence from the Witwatersrand gold fields,  
1380 South Africa. *Earth Science Reviews* 70, 1-46.

- 1381 Frimmel, H.E., 2018. Episodic concentration of gold to ore grade through Earth's history. *Earth Science*  
1382 *Reviews* 180, 148-158.
- 1383 Gallagher, M., Whitehouse, M.J., Kamber, B.S., 2017. The Neoproterozoic surficial sulphur cycle: An  
1384 alternative hypothesis based on analogies with 20th-century atmospheric lead. *Geobiology*, 15, 385-  
1385 400.
- 1386 George, B.G., Ray, J.S., Shukla, A.D., Chatterjee, A., Awasthi, N. Laskar, A.H., 2018. Stratigraphy and  
1387 geochemistry of the Balwan Limestone, Vindhyan Supergroup, India: Evidence for the Bitter Springs  
1388  $\delta^{13}\text{C}$  anomaly. *Precambrian Research*, 313, 18-30.
- 1389 Gibson, T.M., Wörndle, S., Crockford, P.W., Bui, T.H., Creaser, R.A., Halverson, G.P., 2019.  
1390 Radiogenic isotope chemostratigraphy reveals marine and nonmarine depositional environments in  
1391 the late Mesoproterozoic Borden Basin, Arctic Canada. *Geological Society of America Bulletin*,  
1392 131(11-12), 1965-1978, doi: 10.1130/B35060.1.
- 1393 Gibson, G.M., Champion, D.C., Huston, D.L., Withnall, I.W., 2020. Orogenesis in Paleo-  
1394 Mesoproterozoic Eastern Australia: A response to arc-continent and continent-continent collision  
1395 during assembly of the Nuna supercontinent. *Tectonics*, doi: 10.1029/2019TC005717
- 1396 Glaessner, M.F., 1962. Pre-Cambrian fossils. *Biological Reviews*, 37, 467-494.
- 1397 Goldich, S.S., 1968. Geochronology in the Lake Superior region. *Canadian Journal of Earth Science*,  
1398 5, 715-724.
- 1399 Grenholm, M., Schersten, A., 2015. A hypothesis for Proterozoic-Phanerozoic supercontinent cyclicality,  
1400 with implications for mantle convection, plate tectonics and Earth system evolution. *Tectonophysics*,  
1401 662, 434-453.
- 1402 Grey, K., Hill, A.C., Calver, C., 2011. Biostratigraphy and stratigraphic subdivision of Cryogenian  
1403 successions of Australia in a global context. In: E. Arnaud, G.P. Halverson and G. Shields-Zhou  
1404 (Editors), *The Geological Record of Neoproterozoic Glaciations*. Geological Society, London,  
1405 *Memoirs*, 36, pp. 113–134.
- 1406 Griffin, W.L., Belousova, E.A., O'Neill, C., O'Reilly, S.Y., Malkovets, V., Pearson, N.J., Spetsius, S.,  
1407 Wilde, S.A., 2014. The world turns over: Hadean-Archean crust-mantle evolution. *Lithos*, 189, 2-15.
- 1408 Grotzinger, J.P., 1990. Geochemical model for Proterozoic stromatolite decline. *Am. J. Sci.*, 290-A,  
1409 80–103.
- 1410 Guadagnin, F., Chemale Jr., F., Magalhães, J., Santana, A., Dussin, I., Takehara, L., 2015. Age  
1411 constraints on crystal-tuff from the Espinhaço Supergroup - insight into the Paleoproterozoic to  
1412 Mesoproterozoic intracratonic basin cycles of the Congo-São Francisco Craton. *Gondwana Research*  
1413 27, 363-376.
- 1414 Guilbaud, R., Poulton, S.W., Butterfield, N.J., Zhu, M., Shields, G.A., 2015. A global transition into  
1415 ferruginous conditions in the early Neoproterozoic oceans. *Nature Geoscience*, 8(6), 466-470  
1416 doi:10.1038/NGEO2434.



- 1417 Gumsley, A., Stamsnijder, J., Larsson, E., Söderlund, U., Naeraa, T., de Kock, M., Salacinska, A.,  
1418 Gaweda, A., Humbert, F., Ernst, R., 2020. Neoproterozoic large igneous provinces on the Kaapvaal  
1419 Craton in southern Africa re-define the formation of the Ventersdorp Supergroup and its temporal  
1420 equivalents. *Geological Society of America Bulletin*, v. 132; no. 9/10; p. 1829–1844;  
1421 <https://doi.org/10.1130/B35237.1>.
- 1422 Guitreau, M., Blichert-Toft, J., Mojzsis, S. J., Roth, A. S. G., & Bourdon, B., 2013. A legacy of Hadean  
1423 silicate differentiation inferred from Hf isotopes in Eoarchean rocks of the Nuvvuagittuq supracrustal  
1424 belt (Québec, Canada). *Earth and Planetary Science Letters*, 362, 171–181.
- 1425 Gumsley, A.P., Chamberlain, K.R., Bleeker, W., Söderlund, U., de Kock, M.O., Larsson, E.R., Bekker,  
1426 A., 2017. Timing and tempo of the Great Oxidation Event. *PNAS*, 114: 1811-1816,
- 1427 Halevy, I., Johnston, D.T., Schrag, D.P., 2010. Explaining the structure of the Archean mass-  
1428 independent sulfur isotope record. *Science* 329, 204-207.
- 1429 Halverson, G.P., 2006. A Neoproterozoic chronology. In: Xiao, S., Kaufman, A. (Eds.), *Neoproterozoic*  
1430 *Geobiology and Paleobiology*. Vol. 27 of *Topics in Geobiology*. Springer, Dordrecht, the Netherlands,  
1431 pp. 231–271.
- 1432 Halverson, G.P., Hoffman, P.F., Schrag, D.P., Maloof, A.C., Rice, A.H., 2005. Towards a  
1433 Neoproterozoic composite carbon isotope record. *Geological Society of America Bulletin* 117, 1181–  
1434 1207.
- 1435 Halverson, G. P., Kunzmann, M., Strauss, J. V., Maloof, A. C., 2018. The Tonian-Cryogenian transition  
1436 in Svalbard. *Precambrian Research* 319, 79–95.
- 1437 Halverson, G.P., Porter, S.M., Shields, G.A. (2020) The Tonian and Cryogenian periods. From: F.M.  
1438 Gradstein, J.G. Ogg, M.D. Schmitz, G.M. Ogg (Eds.). *The Geologic Time Scale 2020 volume 1*.  
1439 Elsevier Science Limited 495-519pp.
- 1440 Han, T., Runnegar, B., 1992. Megascopic eukaryotic algae from the 2.1-billion-year-old Negaunee  
1441 Iron-Formation, Michigan. *Science* 257:232–235.
- 1442 Hardisty, D.S., Lu, Z., Bekker, A., Diamond, C.W., Gill, B.C., Jiang, G., Kah, L.C., Knoll, A.H., Loyd,  
1443 S.J., Osburn, M.R. and Planavsky, N.J., 2017. Perspectives on Proterozoic surface ocean redox from  
1444 iodine contents in ancient and recent carbonate. *Earth and Planetary Science Letters*, 463, pp.159-170.
- 1445 Harland, W., 1964. Critical evidence for a great infra-Cambrian glaciation. *Geologische Rundschau* 54,  
1446 45–61.
- 1447 Hawkesworth, C.J., Cawood, P.A., Dhuime, B., 2016. Tectonics and crustal evolution. *GSA Today*,  
1448 26(9), 4-11, doi: 10.1130/GSATG272A.1.
- 1449 Hayes, J.M., 1994. Global methanotrophy at the Archean-Proterozoic transition, in: S. Bengtson (Ed.),  
1450 *Early life on Earth*, Columbia University Press, New York, 1994, pp. 220–236.
- 1451 Hazen, R.M., 2010. The evolution of minerals. *Scientific American* 303(3), 58-65.

- 1452 Hazen, R.M., Bekker, A., Bish, D.L., Bleeker, W., Downs, R.T., Farquhar, J., Ferry, J.M., Grew, E.S.,  
1453 Knoll, A.H., Papoineau, D., Ralph, J.P., Sverjensky, D.A., Valley, J.W., 2011. Needs and  
1454 opportunitires in mineral evolution research. *American Mineralogist*, 96, 953-963.
- 1455 Hedberg, H., 1974. Basis for chronostratigraphic classification of the Precambrian. *Precambrian*  
1456 *Research*, 1, 165-177.
- 1457 Heubeck, C., Lowe, D.R., 1994. Depositional and tectonic setting of the Archean Moodies Group,  
1458 Barberton greenstone belt, South Africa. *Precambrian Research*, 68(3-4), 257-290.
- 1459 Hill, A.C., Cotter, K.L., Grey, K., 2000. Mid-Neoproterozoic biostratigraphy and isotope stratigraphy  
1460 in Australia. *Precambrian Research* 100, 28–298.
- 1461 Hill, A. C., Walter, M. R., 2000. Mid-Neoproterozoic (~830-750 Ma) isotope stratigraphy of Australia  
1462 and global correlation. *Precambrian Research* 100, 181–211.
- 1463 Hodgskiss, M.S.W., Crockford, P.W., Peng, Y., Wing, B.A., Horner, T.J., 2019. A productivity collapse  
1464 to end Earth's Great Oxidation. *PNAS*, 116, 17207-17212, doi: 10.1073/pnas.1900325116.
- 1465 Hodgkiss, M.S.W., Kunzmann, M., Poirier, A., Halverson, G.P., 2018. The role of microbial iron  
1466 reduction in the formation of Proterozoic molar tooth structures. *Earth and Planetary Science Letters*,  
1467 482, 1-11.
- 1468 Hofmann, H.J., 1975. Precambrian microflora, Belcher Islands, Canada: significance and systematics.  
1469 *Journal of Paleontology* 50, 1040-1071.
- 1470 Hofmann, H.J., 1990. Precambrian time units and nomenclature – the geon concept. *Geology*, 18, 340-  
1471 341.
- 1472 Hofmann, H.J., 1992. New Precambrian time scale: Comments. *Epsiodes*, 15(2), 122-123.
- 1473 Hoffman, P. F., 1989. Speculations on Laurentia's first gigayear (2.0 to 1.0 Ga): *Geology*, 17, 135-138.
- 1474 Hoffman, P.F. 1997, Tectonic genealogy of North America, *in* van der Pluijm, B.A., and Marshak, S.,  
1475 eds., *Earth Structure: An Introduction to Structural Geology and Tectonics*: New York, McGraw-Hill,  
1476 p. 459–464.
- 1477 Hoffman, P.F., 2014. The origin of Laurentia: Rae craton as the backstop for proto-Laurentian  
1478 amalgamation by slab suction: *Geoscience Canada*, 41, 313-320.
- 1479 Hoffman, P.F., Abbott, D.S., Ashkenay, Y., Benn, D. I., Brocks, J.J., Cohen, P.A., Cox, G.M.,  
1480 Creveling, J.R., Donnadiou, Y., Erwin, D.H., Fairchild, I.J., Ferreira, D., Goodman, J.C., Halverson,  
1481 G.P., Jansen, M.F., Le Hir, G., Love, G.D., Macdonald, F.A., Maloof, A.C., Partin, C.A., Ramstein,  
1482 G., Rose, B.E.J., Rose, C.V., Sadler, P.M., Tziperman, E., Voigt, A., and Warren, S.G. (2017)  
1483 Snowball Earth climate dynamics and Cryogenian geology and geobiology. *Science Advances* 3,  
1484 e1600983.
- 1485 Hoffman, P.F., Halverson, G. P., Domack, E. W., Maloof, A. C., Swanson-Hysell, N. L., Cox, G. M.,  
1486 2012. Cryogenian glaciations on the southern tropical paleomargin of Laurentia (NE Svalbard and  
1487 East Greenland), and a primary origin for the upper Russøya (Islay) carbon isotope excursion.  
1488 *Precambrian Research* 206-207, 137–158.

- 1489 Hoffman, P., Kaufman, A., Halverson, G., 1998. Comings and goings of global glaciations on a  
1490 Neoproterozoic tropical platform in Namibia. *GSA Today* 8, 1–9.
- 1491 Hoffman, P.F., Schrag, D.P., 2002. The snowball Earth hypothesis: testing the limits of global change.  
1492 *Terra Nova*, 14, 129-155.
- 1493 Hoffmann, K.H., Condon, D.J., Bowring, S.A., Crowley, J.L., 2004. A U-Pb zircon date from the  
1494 Neoproterozoic Ghaub Formation, Namibia: Constraints on Marinoan glaciation. *Geology* 32, 817–  
1495 820.
- 1496 Holland, H.D., 1984. *The Chemical Evolution of the Atmosphere and Oceans*. Princeton University  
1497 Press, Princeton, pp. 582.
- 1498 Holland, H.D., 2006. The oxygenation of the atmosphere and oceans. *Philosophical Transactions of the*  
1499 *Royal Society B*, 361: 903-915.
- 1500 Horton, F., 2015. Did phosphorus derived from the weathering of large igneous provinces fertilize the  
1501 Neoproterozoic ocean? *Geochemistry, Geophysics, Geosystems* 16, 1723–1738.
- 1502 Howard, H.M., Smithies, R.H., Kirkland, C.L., Kelsey, D.E., Aitken, A., Wingate, M.T.D., Quentin de  
1503 Gromard, R., Spaggiari, C.V., Maier, W.D., 2014. The burning heart: The Proterozoic geology and  
1504 geological evolution of the west Musgrave region, central Australia. *Gondwana Research* 27, 64-94.
- 1505 Howchin, W., 1901. Preliminary note on the evidence of glacial beds of Cambrian age in South  
1506 Australia. *Transactions of the Royal Society of South Australia*, 25, 10-13.
- 1507 Huston, D.L., Mernagh, T.P., Hagemann, S.G., Doublier, M.P., Fiorentini, M.L., Champion, D.C.,  
1508 Jaques, A.L., Czarnota, K., Cayley, R., Skirrow, R., Bastrakov, E. (2016) Tectono-metallogenic  
1509 systems — The place of mineral systems within tectonic evolution, with an emphasis on Australian  
1510 examples. *Ore Geology Reviews* 76, 168-210.
- 1511 Idurnum et al., 1995.
- 1512 James, H.L., 1972. Note 40 – Subdivision of Precambrian: an interim scheme to be used by U.S.  
1513 Geological Survey. *Amer. Assoc. Petrol. Geol. Bull.*, 56, 1128-1133.
- 1514 James, H.L., 1978. Subdivision of the Precambrian - a brief review and a report on recent decisions by  
1515 the Subcommittee on Precambrian Stratigraphy. *Precambrian Research*, 7, 193--204.
- 1516 James, N.P., Narbonne, G.M., Sherman, A.G., 1998. Molar-tooth carbonates: shallow subtidal facies of  
1517 the mid- to late Proterozoic. *Journal of Sedimentary Research*, 68, 716-722.
- 1518 Javaux, E.J., Knoll, A.H., 2017. Micropaleontology of the lower Mesoproterozoic Roper Group,  
1519 Australia, and implications for early eukaryotic evolution. *Journal of Paleontology* 91, 199–229.
- 1520 Javaux, E.J., Knoll, A.H., Walter, M.R. 2001. Morphological and ecological complexity in early  
1521 eukaryotic ecosystems. *Nature*, 412, 66-69.
- 1522 Javaux, E.J., Lepot, K., 2018. The Paleoproterozoic fossil record: Implications for the evolution of the  
1523 biosphere during Earth’s middle-age. *Earth Science Reviews*, 176, 68-86.

- 1524 Jing, X., Yang, Z., Evans, D.A.D., Tong, Y., Xi, Y., Wang, H., 2020. A pan-latitude Rodinia in the  
1525 Tonian true polar wander frame. *Earth and Planetary Science Letters*, 530, 115880.
- 1526 Johnson, T.E., Kirkland, C.L., Gardiner, N.J., Brown, M., Smithies, R.H., Santosh, M., 2019. Secular  
1527 change in TTG compositions: Implications for the evolution of Archaean geodynamics. *Earth and*  
1528 *Planetary Science Letters*, 505: 66-75.
- 1529 Jones et al (2020)
- 1530 Kah, L.C., Bartley, J.K., Teal, D. A., 2012. Chemostratigraphy of the Late Mesoproterozoic Atar Group,  
1531 Taoudeni Basin, Mauritania: Muted isotopic variability, facies correlation, and global isotopic trends.  
1532 *Precambrian Research* 200-203, 82–103.
- 1533 Kamber, B.S., 2015. The evolving nature of terrestrial crust from the Hadean, through the Archean, into  
1534 the Proterozoic. *Precambrian Research*, 258, 48-82.
- 1535 Kamber, B.S., Tomlinson, E.L., 2019. Petrological, mineralogical and geochemical peculiarities of  
1536 Archean cratons. *Chemical Geology*, 511, 123-151.
- 1537 Karhu, J., Holland, H.D., 1996. Carbon isotopes and the rise of atmospheric oxygen. *Geology*, 24, 867-  
1538 870.
- 1539 Kaufman, A.J., Knoll, A.H., Narbonne, G.M., 1997. Isotopes, ice ages, and terminal Proterozoic Earth  
1540 history. *Proceedings of the National Academy of Sciences* 95, 6600–6605.
- 1541 Kendall, B., Creaser, R.A., Reinhard, C.Y., Lyons, T.W., Anbar, A.D., 2015. Transient episodes of mild  
1542 environmental oxygenation and oxidative weathering during the late Archean. *Science Advances*,  
1543 1(10), 1500777 doi: 10.1126/sciadv.1500777.
- 1544 Kennedy, M.J., Runnegar, B., Prave, A.R., Hoffmann, K.H., Arthur, M., 1998. Two or four  
1545 Neoproterozoic glaciations? *Geology* 26, 1059–1063.
- 1546 Kipp, M.A., Lepland, A., Buick, R., 2020. Redox fluctuations, trace metal enrichment and  
1547 phosphogenesis in the ~2.0 Ga Zaonega Formation. *Precambrian Research*, 343, 105716.
- 1548 Kipp, M.A., Stüeken, E.E., Bekker, A., Buick, R., 2017. Selenium isotopes record extensive marine  
1549 suboxia during the Great Oxidation Event. *Proceedings of the National Academy of Sciences*, 114(5),  
1550 pp.875-880.
- 1551 Kirscher, U., Liu, Y., Li, Z. X., Mitchell, R. N., Pisarevsky, S., Denyszyn, S. W., Nordsvan, A., 2019.  
1552 Paleomagnetism of the Hart Dolerite (Kimberley, Western Australia) - A two-stage assembly of the  
1553 supercontinent Nuna?: *Precambrian Research*, 329, 170-181.
- 1554 Klein, C., 2005. Some Precambrian banded iron-formations (BIFs) from around the world: Their age,  
1555 geologic setting, mineralogy, metamorphism, geochemistry, and origin. *American Mineralogist*, 90:  
1556 1473-1499.
- 1557 Knauth, P., Kennedy, M.J., 2009. The late Precambrian greening of the Earth. *Nature* 460, 728–732.
- 1558 Knoll, A.H., Javaux, E.J., Hewitt, D., Cohen, P., 2006. Eukaryotic organisms in Proterozoic oceans.  
1559 *Philosophical Transactions of the Royal Society B* 361, 1023–1038.

- 1560 Knoll, A., Kaufman, A., Semikhatov, M., 1995. The carbon-isotopic composition of Proterozoic  
1561 carbonates: Riphean successions from northwestern Siberia (Anabar Massif, Turukhansk Uplift).  
1562 *American Journal of Science* 295, 823–850.
- 1563 Knoll, A., Walter, M., Christie-Blick, N., 2004. A new period for the geological time scale. *Science*  
1564 305, 621–622.
- 1565 Knoll, A.H., Walter, M.R., Narbonne, G.M., Christie-Blick, N., 2006. The Ediacaran Period: a new  
1566 addition to the geologic time scale. *Lethaia* 39, 13–30.
- 1567 Kulling, O., 1934. The Hecla Hoek Formation around Hinlopenstredet. *Geografiska Annaler* 14, 161–  
1568 253.
- 1569 Kump, L.R., Junium, C., Arthur, M.A., Brasier, A., Fallick, V., Lepland, A., Crne, A.E., Luo, G., 2011.  
1570 Isotopic evidence for massive oxidation of organic matter following the great oxidation event. *Science*  
1571 334, 1694-1696.
- 1572 Kunzmann, M., Schmid, S., Blaikie, T.N., Halverson, G.P., 2019. Facies analysis, sequence  
1573 stratigraphy, and carbon isotope chemostratigraphy of a classic Zn-Pb host succession: The  
1574 Proterozoic middle McArthur Group, McArthur Basin, Australia. *Ore Geology Reviews*, 106, 150-  
1575 175.
- 1576 Kurzweil, F., Claire, M., Thomazo, C., Peters, M., Hannington, M. and Strauss, H., 2013. Atmospheric  
1577 sulfur rearrangement 2.7 billion years ago: Evidence for oxygenic photosynthesis. *Earth and Planetary*  
1578 *Science Letters*, 366, 17-26.
- 1579 Kuznetsov, A.B., Semikhatov, M.A., Maslov, A.V., Gorokhov, I.M., Prasolov, E.M., Krupenin, M.T.,  
1580 Kislova, I.V., 2006. New data on Sr- and C-isotopic chemostratigraphy of the Upper Riphean type  
1581 section (southern Urals). *Stratigraphy and Geological Correlation* 14, 602–628.
- 1582 Kuznetsov, A.B., Bekker, A., Ovchinnikova, G.V., Gorokhov, I.M., Vasilyeva, I.M., 2017.  
1583 Unradiogenic strontium and moderate-amplitude carbon isotope variations in early Tonian seawater  
1584 after the assembly of Rodinia and before the Bitter Springs Excursion. *Precambrian Research* 298,  
1585 157–173.
- 1586 Kuznetsov, A.B., Semikhatov, M.A., Gorokhov, I.M., 2018. Strontium isotope stratigraphy: principles  
1587 and state-of-the-art. *Stratigraphy and Geological Correlation* 26, 367-386.
- 1588 Lee, C.T.A., Yeung, L.Y., McKenzie, N.R., Yokoyama, Y., Ozaki, K., Lenardic, A., 2016. Two-step  
1589 rise of atmospheric oxygen linked to the growth of continents. *Nature Geoscience*, 9: 417–424
- 1590 Lee, Y.Y., 1936. The Sinian glaciation in the lower Yangtze Valley. *Bulletin of the Geological Society*  
1591 *of China* 15, 131–134.
- 1592 Li, Z.X., Bogdanova, S.V., Collins, A.S., Davidson, A., DeWaele, B., Ernst, R.E., Fitzsimmons, C.W.,  
1593 Fuck, R.A., Gladkochub, D.P., Jacons, J., Karlstrom, K.E., Lu, S., Natapov, L.M., Pease, V.,  
1594 Pisarevsky, S.A., Thrane, K., Vernikovsky, V., 2008. Assembly, configuration and break-up history  
1595 of Rodinia: a synthesis. *Precambrian Research*, 160: 179-210.

- 1596 Li, Z.X., Evans, D.A.D., Zhang, S., 2004. A 90° spin on Rodinia: possible causal links between the  
 1597 Neoproterozoic supercontinent, superplume, true polar wander and low-latitude glaciation. *Earth and*  
 1598 *Planetary Science Letters* 220, 409–421.
- 1599 Li, Z.X., Evans, D.A.D., Halverson, G. P., 2013. Neoproterozoic glaciations in a revised global  
 1600 palaeogeography from the breakup of Rodinia to the assembly of Gondwanaland. *Sedimentary*  
 1601 *Geology* 294, 219–232.
- 1602 Li, Z.X., Li, X.H., Kinny, P.D., Wang, J., 1999. The breakup of Rodinia: did it start with a mantle plume  
 1603 beneath South China? *Earth and Planetary Science Letters* 173, 171–181.
- 1604 Li, Z.X., Mitchell, R.N., Spencer, C.J., Ernst, R., Pisarevsky, S., Kirscher, K., Murphy, J.B., 2019.  
 1605 Decoding Earth’s rhythms: modulation of supercontinent cycles by longer superocean episodes.  
 1606 *Precambrian Research*, 323, 1-5 doi: 10.1016/j.precamres.2019.01.009.
- 1607 Lindsay, J.F., 1987. Upper Proterozoic evaporites in the Amadeus basin, central Australia, and their  
 1608 role in basin tectonics. *Geological Society of America Bulletin*, 99, 852–865.
- 1609 Lindsay, J.F., 2002. Supersequences, superbasins, supercontinents—evidence from the Neoproterozoic-  
 1610 Early Palaeozoic basins of central Australia. *Basin Research* 14, 207–223.
- 1611 Lindsay, J.F., Brasier, M.D., 2002. Did global tectonics drive early biosphere evolution? Carbon isotope  
 1612 record from 2.6 to 1.9 Ga carbonates of Western Australian basins. *Precambrian Research*, 114, 1-34.
- 1613 Logan, W.E., 1857. On the division of Azoic rocks of Canada into Huronian and Laurentian. *Proc. Am.*  
 1614 *Assoc. Adv. Sci.*, 1857, 44-47.
- 1615 Loron, C., Moczyłowska, M., 2017. Tonian (Neoproterozoic) eukaryotic and prokaryotic organic-  
 1616 walled microfossils from the upper Visingsö Group, Sweden. *Palynology*, 42, 220-254, doi:  
 1617 10.1080/01916122.2017.1335656.
- 1618 Loron, C.C., François, C., Rainbird, R.H., Turner, E.C., Borensztajn, S., Javaux, E.J., 2019b. Early  
 1619 fungi from the Proterozoic Era in Arctic Canada. *Nature* 270, 232–235.
- 1620 Loron, C.C., Rainbird, R.H., Turner, E.C., Greenman, J.W., Javaux, E.J., 2019a. Organic-walled  
 1621 microfossils from the late Mesoproterozoic to early Neoproterozoic lower Shaler Supergroup (Arctic  
 1622 Canada): diversity and biostratigraphic significance. *Precambrian Research* 321, 349–374.
- 1623 Luo, G., Ono, S., Beukes, N.J., Wang, D.T., Xie, S., Summons, R.E., 2016. Rapid oxygenation of  
 1624 Earth’s atmosphere 2.33 billion years ago. *Scientific Advances*, 2: e1600134.
- 1625 Lyons, T.W., Reinhard, C.T., Planavsky, N.J., 2014. The rise of oxygen in Earth’s early ocean and  
 1626 atmosphere. *Nature*, 506: 307–315.
- 1627 Macdonald, F.A., Halverson, G.P., Strauss, J., Smith, E., Cox, G., Sperling, E., 2012. Early  
 1628 Neoproterozoic basin formation in Yukon, Canada: Implications for the make-up and break-up of  
 1629 Rodinia. *Geoscience Canada*, 39, 77-100.

- 1630 Macdonald, F.A., Schmitz, M.D., Crowley, J.L., Roots, C.F., Jones, D.S., Maloof, A.C., Strauss, J.V.,  
1631 Cohen, P.A., Johnston, D.T., Schrag, D.P., 2010. Calibrating the Cryogenian. *Science* 327, 1241–  
1632 1243.
- 1633 Macdonald, F.A., Schmitz, M.D., Strauss, J.V., Halverson, G.P., Gibson, T.M., Eyster, A., Cox, G.,  
1634 Mamrol, P., Crowley, J.L., 2018. Cryogenian of Yukon. *Precambrian Research* 319, 114–143.
- 1635 Macdonald, F.A., Wordsworth, R., 2017. Initiation of Snowball Earth with volcanic sulfur aerosol  
1636 emissions. *Geophysical Research Letters*, 44, 1938-1946.
- 1637 MacLennan, S., Park, Y., Swanson-Hysell, N., Maloof, A., Schoene, B., Gebreslassie, M., Antilla, E.,  
1638 Tesema, T., Alene, M., Haileab, B., 2018. The arc of the Snowball: U-Pb dates constrain the Islay  
1639 anomaly and the initiation of the Sturtian glaciation. *Geology* 46, 539–542.
- 1640 Manhès, G., Allègre, C., Dupré, C., Hamelin, B., 1980. Lead isotope study of basic-ultrabasic layered  
1641 complexes: Speculations about the age of the earth and primitive mantle characteristics. *Earth and*  
1642 *Planetary Science Letters*, 47, 370-382.
- 1643 Martin, A.P., Condon, D.J., Prave, A.R., Lepland, A., 2013. A review of temporal constraints for the  
1644 Palaeoproterozoic large, positive carbonate carbon isotope excursion (the Lomagundi-Jatuli Event.  
1645 *Earth Science Reviews*, 127, 242-261.
- 1646 Martin, A.P., Prave, A.R., Condon, D.J., Lepland, A., Fallick, A.E., Romashkin, A.E., Medvedev, P.V.,  
1647 Rychanchik, D.V., 2015. Multiple Palaeoproterozoic carbon burial episodes and excursions. *Earth*  
1648 *and Planetary Science Letters*, 424, 226-236.
- 1649 Mawson, D., 1949. The Late Precambrian ice age and glacial record of the Bibliando dome. *Journal*  
1650 *and Proceedings of the Royal Society of New South Wales* 82, 150–174.
- 1651 McKenzie, R.N., Hughes, N.C., Myrow, P.M., Banerjee, D.M., Deb, M., and Planavasky, N.J., 2013,  
1652 New age constraints for the Proterozoic-Delhi successions of India and their implications.  
1653 *Precambrian Research*, 238, 120–128.
- 1654 McLelland, J.M., Selleck, B.W., Hamilton, M.A., Bickford, M.E., 2010. Late- to post-tectonic setting  
1655 of some major Proterozoic anorthosite-mangerite-charnokite-granite (AMCG) suites. *Canadian*  
1656 *Mineralogist*, 48: 729-750.
- 1657 Meert, J.G., Santosh, M., 2017. The Columbia supercontinent revisited. *Gondwana Research*, 50, 67-  
1658 83.
- 1659 Melezhik, V.A., Fallick, A.E., Hanski, E.J., Kump, L.R., Lepland, A., Prave, A.R., Strauss, H., 2005.  
1660 Emergence of the aerobic biosphere during the Archean-Proterozoic transition: Challenges of future  
1661 research. *GSA Today*, 15, 11, 4-11.
- 1662 Melezhik, V.A., Filippov, M.M., Romashkin, A.E., 2004. A giant Palaeoproterozoic deposit of shungite  
1663 in NW Russia: Genesis and practical applications. *Ore Geology Reviews*, 24, 135-154.
- 1664 Melezhik, V.A., Huhma, H., Condon, D.J., Fallick, A.E., Whitehouse, M.J., 2007. Temporal constraints  
1665 on the Paleoproterozoic Lomagundi-Jatuli carbon isotopic event. *Geology*, 35, 655-658.

- 1666 Merdith, A. S., Collins, A. S., Williams, S. E., Pisarevsky, S., Foden, J. D., Archibald, D. B., Blades,  
 1667 M. L., Alessio, B. L., Armistead, S., Plavsa, D., Clark, C., Müller, D., 2017a. A full-plate global  
 1668 reconstruction of the Neoproterozoic. *Gondwana Research* 50, 84–134.
- 1669 Merdith, A.S., Williams, S.E., Müller, R.D., Collins, A.S., 2017b. Kinematic constraints on the Rodinia  
 1670 to Gondwana transition. *Precambrian Research*, 299, 132-150.
- 1671 Merdith, A.S., Williams, S. E., Brune, S., Collins, A.S., Müller, R.D., 2019. Rift and plate boundary  
 1672 evolution across two supercontinent cycles. *Global and Planetary Change*, 173, 1-14.
- 1673 Miao, L., Moczyłowska, M., Zhu, S., Zhu, M., 2019. New record of organic-walled, morphologically  
 1674 distinct microfossils from the late Paleoproterozoic Changcheng Group in the Yanshan Range, North  
 1675 China. *Precambrian Research* 321, 172–198.
- 1676 Mitchell, R.N., 2014. True polar wander and supercontinent cycles: implications for lithospheric  
 1677 elasticity and the triaxial earth. *American Journal of Science*, 514, 966-979.
- 1678 Mitchell, R.N., Kilian, T.M., Evans, D.A.D., 2012. Supercontinent cycles and the calculation of  
 1679 absolute palaeolongitude in deep time: *Nature*, 482, 208-211
- 1680 Mitchell, R.N., Spencer, C.J., Kirscher, U., He, X.-F., Murphy, J.B., Li, Z.X., Collins, W.J., 2019.  
 1681 Harmonic hierarchy of mantle and lithospheric convective cycles: Time series analysis of hafnium  
 1682 isotopes of zircon. *Gondwana Research*, 75, 239-248.
- 1683 Moreira, H., Seixas, L., Storey, C., Fowler, M., Lasalle, S., Stevenson, R., Lana, C., 2018. Evolution of  
 1684 Siderian juvenile crust to Rhyacian high Ba-Sr magmatism in the Mineiro Belt, southern São  
 1685 Francisco Craton. *Geoscience Frontiers*, 9, 977-995, doi: 10.1016/j.gsf.2018.01.009.
- 1686 Nagovitsin, K., 2009. *Tappania*-bearing association of the Siberian platform: Biodiversity, stratigraphic  
 1687 position and geochronological constraints. *Precambrian Research*, 173, 137-145.
- 1688 Nance, R.D., Murphy, J.B., 2018. Supercontinents and the case for Pannotia. In: Wilson, R.W.,  
 1689 Houseman, G.A., McCaffrey, K.J.W., Doré, A.G., Buiter, S.J.H. (Eds.), *Fifty Years of the Wilson  
 1690 Cycle Concept in Plate Tectonics* 470, Geological Society, London, Special Publications, 470, 65-86.
- 1691 Nance, R.D., Worsley, T.R., Moody, J.B., 1986. Post-Archean biogeochemical cycles and long-term  
 1692 episodicity in tectonic processes. *Geology*, 14, 514-518.
- 1693 Nelson, L.L., Smith, E.F., Hodgkin, E.B., Crowley, J.L., Schmitz, M.D., Macdonald, F.A., 2020.  
 1694 Geochronological constraints on Neoproterozoic rifting and onset of the Marinoan glaciation from the  
 1695 Kingston Peak Formation in Death Valley, California (USA). *Geology*, 48, doi:10.1130/G47668.1.
- 1696 O’Neil, J., Carlson, R. W., Francis, D., Stevenson, R. K. (2008). Neodymium-142 Evidence for Hadean  
 1697 Mafic Crust. *Science*, 321, 1828–1832.
- 1698 O’Neil, J., Carlson, R. W., Paquette, J. L., & Francis, D. (2012). Formation age and metamorphic history  
 1699 of the Nuvvuagittuq Greenstone Belt. *Precambrian Research*, 220–221, 23–44.
- 1700 O’Neill, C., Lenardic, A., Condie, K.C., 2015. Earth’s punctuated tectonic evolution: cause and effect.  
 1701 In: Roberts, N.M.W., Ven Kranendonk, M.J., Parman, S., Shirey, S., Clift, P.D. (Eds.), *Continental  
 1702 Formation Through Time* 389, Geological Society, London, Special Publications, pp. 17-40.



- 1703 Ossa Ossa, F., Hofmann, A., Spangenberg, J.E., Poulton, S.W., Stueeken, E.E., Schoenberg, R.,  
 1704 Eickmann, B., Wille, M., Butler, M., Bekker, A., 2019. Limited oxygen production in the  
 1705 Mesoarchean ocean. *Proceedings of the National Academy of Sciences*, 116, 6647-6652.
- 1706 Ostrander, C.M., Nielsen, S.G., Owens, J.G., Kendall, B., Gordon, G.W., Romaniello, S.J., Anbar,  
 1707 A.D., 2019. Fully oxygenated water columns over continental shelves before the Great Oxidation  
 1708 Event. *Nature Geoscience*, 12, 186-191.
- 1709 Ouyang, G. She, Z., Papineau, D., Wang, X., Luo, G., Li, C., 2020. Dynamic carbon and sulfur cycling  
 1710 in the aftermath of the Lomagundi-Jatuli Event: Evidence from the Paleoproterozoic Hutuo  
 1711 Supergroup, North China Craton. *Precambrian Research* 337, 105549.
- 1712 Page et al., 2000.
- 1713 Pang, K., Tang, Q., Wan, B., Yuan, X., 2020. New insights on the palaeobiology and biostratigraphy  
 1714 of the acritarch *Trachyhystrychosphaeraaimika*: a potential late Mesoproterozoic to Tonian index  
 1715 fossil. *Palaeoworld*, doi:10.1016/j.palwor.2020.02.003.
- 1716 Papineau, D., 2010. Global biogeochemical change at both ends of the Proterozoic: Insights from  
 1717 phosphorites. *Astrobiology*, 10: 165-181.
- 1718 Parfrey, L.W., Lahr, D.J.G., Knoll, A.H., Katz, L.A., 2011. Estimating the timing of early eukaryotic  
 1719 diversification with multigene molecular clocks. *Proceedings of the National Academy of Sciences*  
 1720 108, 13624–13629.
- 1721 Park, H.U., Zhai, J.H., Peng, P., Kim, J.N., Zhang, Y.B., Kim, M.C., Park, U., Feng, L.J., 2016.  
 1722 Deposition age of the Sangwon Supergroup in the Pyongnam basin (Korea) and the early Tonian  
 1723 negative carbon isotope interval. *Acta Petrologica Sinica*, 32, 2181-2195.
- 1724 Partin, C.A., Bekker, A., Planavsky, N.J., Scott, C.T., Gill, B.C., Li, C., Podkovyrov, V., Maslov, A.,  
 1725 Konhauser, K.O., Lalonde, S.V., Love, G.D., 2013. Large-scale fluctuations in Precambrian  
 1726 atmospheric and oceanic oxygen levels from the record of U in shales. *Earth and Planetary Science*  
 1727 *Letters*, 369, 284-293.
- 1728 Partin, C.A., Bekker, A., Sylvester, P.J., Wodicka, N., Stern, R.A., Chacko, T., Heaman, L.M., 2014.  
 1729 Filling the juvenile magmatic gap: Evidence of uninterrupted Paleoproterozoic plate tectonics. *Earth*  
 1730 *and Planetary Science Letters*, 388, 123-124.
- 1731 Patterson, C., 1956. Age of meteorites and the Earth. *Geochimica et Cosmochimica Acta*, 10, 230–237,
- 1732 Payne, J.L., Hand, M., Barovich, K.M., Reid, A., and Evans, D.A.D., 2009, Correlations and  
 1733 reconstruction models for the 2500-1500 Ma evolution of the Mawson Continent, *in* Reddy, S.M.,  
 1734 Mazumder, R., Evans, D.A.D., and Collins, A.S., eds., *Palaeoproterozoic Supercontinents and Global*  
 1735 *Evolution*: Geological Society, London, Special Publications, v. 323, p. 319-355.
- 1736 Peng, P., 2015. Precambrian mafic dyke swarms in the North China Craton and their geological  
 1737 implications. *SCES*, doi: 10.1007/s11430-014-5026-x.
- 1738 Peng, S., Babcock, L., Ahlberg, P., 2020. The Cambrian Period. From: F.M. Gradstein, J.G. Ogg, M.  
 1739 Schmitz, G. Ogg). *The Geologic Time Scale 2020*. Elsevier Science Limited, in press.

- 1740 Philippot, P., Avila, J.N., Killingsworth, B.A., Tessalina, S., Baton, F., Caquineau, T., Muller, E.,  
1741 Pecoits, E., Cartigny, P., Lalonde, S.V., Ireland, T.R., Thomazo, C., van Kranendonk, M.J., Busigny,  
1742 V., 2018. Globally asynchronous Sulphur isotope signals require re-definition of the Great Oxidation  
1743 Event. *Nature Communications*, 9(1), 1-10 doi: 10.1038/s41467-018-04621.
- 1744 Pietrzak-Renaud, N., Davis, D., 2014. U-Pb geochronology of baddeleyite from the Belleview  
1745 metadiabase: Age and geotectonic implications for the Negaunee Iron Formation, Michigan.  
1746 *Precambrian Research*, 250, 1-5.
- 1747 Pimentel, M.M., Heaman, L., Fuck, R.A., Marini, O.J. 1991. U-Pb zircon geochronology of  
1748 Precambrian tin-bearing continental-type acid magmatism in central Brazil. *Precambrian Research*  
1749 52, 321-335, 1991.
- 1750 Pisarevsky, S.A., Elming, S.-Å., Pesonen, L.J., Li, Z.-X., 2014. Mesoproterozoic paleogeography:  
1751 Supercontinent and beyond. *Precambrian Research*, 244, 207-225.
- 1752 Planavsky, N.J., Rouxel, O.J., Bekker, A., Lalonde, S.V., Konhauser, K.O., Reinhard, C.T., Lyons,  
1753 T.W., 2010. The evolution of the marine phosphate reservoir. *Nature*, 467, 1088-1090.
- 1754 Planavsky, N.J., Reinhard, C.T., Qiang, X., Thomson, D., McGoldrick, P., Rainbird, R.H., Johnson, T.,  
1755 Fischer, W.W., Lyons, T.W., 2014. Low mid-Proterozoic atmospheric oxygen levels and the delayed  
1756 rise of animals. *Science*, 346, 635-638.
- 1757 Plumb, K.A., 1991. New Precambrian time scale. *Episodes*, 14, 139-140.
- 1758 Plumb, K.A., 1992. New Precambrian time scale – reply. *Episodes*, 15(2), 124-125.
- 1759 Plumb, K.A., James, H.L., 1986. Subdivision of Precambrian time: recommendations and suggestions  
1760 by Subcommission on Precambrian stratigraphy. *Precambrian Research* 32, 65-92.
- 1761 Porter, S.M., 2016. Tiny vampires in ancient seas: evidence for predation via perforation in fossils from  
1762 the 780-740 million-year-old Chuar Group, Grand Canyon, USA. *Proceedings of the Royal Society*  
1763 B 283, 20160221.
- 1764 Poulton, S.W., Canfield, D.E., 2011. Ferruginous conditions: A dominant feature of oceans  
1765 throughout Earth's history. *Elements*, 10.2113/gselements.7.2.107.
- 1766 Poulton S.W., Fralick, P.W., Canfield, D.E., 2010. Spatial variability in oceanic redox structure 1.8  
1767 billion years ago, *Nature Geoscience*, 3, 486-490.
- 1768 Porter, S.M., Knoll, A.H., 2000. Testate amoebae in the Neoproterozoic Era: evidence from vase-  
1769 shaped microfossils in the Chuar Group, Grand Canyon. *Paleobiology* 26, 360-385.
- 1770 Porter, S.M., Meisterfeld, R., Knoll, A.H., 2003. Vase-shaped microfossils from the Neoproterozoic  
1771 Chuar Group, Grand Canyon: a classification guided by modern testate amoebae. *Journal of*  
1772 *Paleontology* 77, 409-429.
- 1773 Porter, S.M., Riedman, L.A., 2016. Systematics of organic-walled microfossils from the c. 780-740 Ma  
1774 Chuar Group, Grand Canyon, Arizona. *Journal of Paleontology* 90, 815-853.
- 1775 Poulton, S.W., Fralick, P.W., Canfield, D.E., 2004. The transition to a sulphidic ocean approximately  
1776 1.84 billion years ago, *Nature*, 431, 173-177.

- 1777 Pourteau, A., Smit, M.A., Li, Z.X., Collins, W.J., Nordsvan, A.R., Volante, S., Li, J., 2018. 1.6 Ga  
 1778 crustal thickening along the final Nuna suture: *Geology*, 46, 959-962.
- 1779 Prave, A.R., Condon, D.J., Hoffmann, K.H., Tapster, S., Fallick, A.E., 2016. Duration and nature of the  
 1780 end-Cryogenian (Marinoan) glaciation. *Geology* 44, 631–634.
- 1781 Prince, J.K.G., Rainbird, R. H., Wing, B.A., 2019. Evaporite deposition in the mid-Neoproterozoic as  
 1782 a driver for changes in seawater chemistry and the biogeochemical cycle of sulfur. *Geology*, 47(4),  
 1783 291-294. doi: 10.1130/G45464.1,
- 1784 Puetz, S.J., Condie, K., 2019. Time series analysis of mantle cycles Part 1: Periodicities and correlations  
 1785 among seven global isotopic databases. *Geoscience Frontiers*, 10, 1305-1326.
- 1786 Qu et al., 2014.
- 1787 Rainbird, R.H., Jefferson, C.W., Young, G.M., 1996. The early Neoproterozoic sedimentary succession  
 1788 B of northwestern Laurentia: Correlations and paleogeographic significance. *Geological Society of  
 1789 America Bulletin*, 108, 454–470.
- 1790 Ranjan, S., Upadhyay, D., Pruseth, K.L., Nanda, J.K., 2020. Detrital zircon evidence for change in  
 1791 geodynamic regime of continental crust formation 3.7-3.6 billion years ago. *Earth and Planetary  
 1792 Science Letters*, 538, 116206 doi: 10.1016/j.epsl.2020.116206.
- 1793 Rasmussen, B., Buick, R., 1999. Redox state of the Archean atmosphere: evidence from detrital heavy  
 1794 minerals in ca. 3250-2750 Ma sandstones from the Pilbara Craton, Australia. *Geology*, 27, 115-118.
- 1795 Rawlings, D.J., 1999. Stratigraphic resolution of a multiphase intracratonic basin system: the McArthur  
 1796 Basin, northern Australia. *Australian Journal of Earth Sciences*, 46(5), 703-723. doi: 10.1046/j.1440-  
 1797 0952.1999.00739.x.
- 1798 Ray, J.S., 2006. Age of the Vindhyan Supergroup: A review of recent findings. *Journal of Earth System  
 1799 Science* 115, 149–160.
- 1800 Reusch, H., 1891. SkuringmaerkerogmoraenguseftervistiFinnmarkenfraenperiodemegetaeldre end  
 1801 'istiden' (Glacial striae and boulder-clay in Norwegian Lapponie from a period much older than the  
 1802 last ice age). *Norges Geologiske Undersøkelse* 1, 78–85, 97–100.
- 1803 Riding, R., 2008. Abiogenic, microbial and hybrid authigenic carbonate crusts: components of  
 1804 Precambrian stromatolites. *Geologia Croatia*, 61, 73-103.
- 1805 Riding, R., Fralick, P., Liang, L., 2014. Identification of an Archean marine oxygen oasis. *Precambrian  
 1806 Research* 251, 232-237.
- 1807 Riedman, L.A., Porter, S., 2016. Organic-walled microfossils of the mid-Neoproterozoic Alinya  
 1808 Formation, Officer Basin, Australia. *Journal of Paleontology* 90, 854-887.
- 1809 Riedman, L.A., Porter, S.M., Calver, C.R., 2018. Vase-shaped microfossil biostratigraphy with new  
 1810 data from Tasmania, Svalbard, Greenland, Sweden and the Yukon. *Precambrian Research* 319, 19-  
 1811 36.
- 1812 Riedman, L.A., Sadler, P.M., 2018. Global species richness record and biostratigraphic potential of  
 1813 early to middle Neoproterozoic eukaryote fossils. *Precambrian Research* 319, 6-18.

- 1814 Rivers, T., 2015. Tectonic Setting and Evolution of the Grenville Orogen: An Assessment of Progress  
 1815 Over the Last 40 Years. *Geoscience Canada*, 42(1), 77-124, doi:10.12789/geocanj.2014.41.057
- 1816 Rogers, J.J.W., Santosh, M., 2002. Configuration of Columbia: a Mesoproterozoic supercontinent.  
 1817 *Gondwana Research*, 5: 5-22.
- 1818 Rooney, A.D., Strauss, J.V., Brandon, A.D., Macdonald, F.A., 2015. A Cryogenian chronology: Two  
 1819 long-lasting synchronous Neoproterozoic glaciations. *Geology* 43, 459–462.
- 1820 Rooney, A.D., Yang, C., Condon, D.J., Zhu, M., Macdonald, F.A., 2020. U-Pb and Re-Os  
 1821 geochronology tracks stratigraphic condensation in the Sturtian snowball Earth aftermath. *Geology*,  
 1822 48(6), 625-629. doi: 10.1130/G47246.1
- 1823 Roscoe, S.M., 1969. Huronian rocks and uraniferous conglomerates in the Canadian Shield Geological  
 1824 Survey of Canada Special Paper, 68-40, 217pp.
- 1825 Safanova, L., Maruyama, S., 2014. Asia: a frontier for a future supercontinent Amasia. *International*  
 1826 *Geology Reviews*, 56: 1051-1071.
- 1827 Sánchez-Baracaldo, P., Raven, J.A., Pisani, D., Knoll, A.H., 2017. Early photosynthetic eukaryotes  
 1828 inhabited low-salinity habitats. *Proceedings of the National Academy of Sciences*, 114(37), pp.E7737-  
 1829 E7745.
- 1830 Satkoski, A.M., Lowe, D.R., Beard, B.L., Coleman, M.L., Johnson, C.M., 2016. A high continental  
 1831 weathering flux into Paleoarchean seawater revealed by strontium isotope analysis of 3.26 Ga barite.  
 1832 *Earth and Planetary Science Letters*, 454: 28–35.
- 1833 Scott, C., Lyons, T.W., Bekker, A., Shen, Y.A., Poulton, S.W., Chu, X.L., Anbar, A.D., 2008. Tracing  
 1834 the stepwise oxygenation of the Proterozoic ocean. *Nature*, 452, 456-459.
- 1835 Schroeder, S., Bekker, A., Beukes, N.J., Strauss, H., van Niekerk, H.S., 2008. Rise in seawater sulphate  
 1836 concentrations associated with the Paleoproterozoic positive carbon isotope excursion: evidence from  
 1837 sulphate evaporites in the ~2.2-2.1 Gyr shallow-marine Lucknow Formation, South Africa. *Terra*  
 1838 *Nova*, 20, 108-117.
- 1839 Schulze, D.J., Harte, B., Edinburgh Ion Microprobe Facility Staff, Page, Z., Valley, J.W., Channer,  
 1840 D.M., Jaques, A.L., 2013. Anticorrelation between low  $\delta^{13}\text{C}$  of eclogitic diamonds and high  $\delta^{18}\text{C}$   
 1841 of their coesite and garnet inclusions requires a subduction origin. *Geology* 41, 455-458.
- 1842 Sedgwick, A., 1845. On the Older Palæozoic (Protozoic) Rocks of North Wales. *Quarterly Journal of*  
 1843 *the Geological Society*, 1, 5-22.
- 1844 Semikhatov, M.A., Kuznetsov, A.B., Chumakov, N.M., 2015. Isotope age boundaries between the  
 1845 general stratigraphic subdivisions of the upper Proterozoic (Riphean and Vendian) in Russia: The  
 1846 evolution of opinions and the current estimate. *Stratigraphy and Geological Correlation*, 23, 568-579.
- 1847 Sergeev, V.N., Vorob'eva, N.G., Petrov, P.Y., 2017. The biostratigraphic conundrum of Siberia: do true  
 1848 Tonian–Cryogenian microfossils occur in Mesoproterozoic rocks? *Precambrian Research* 299, 282–  
 1849 302.

- 1850 Shang, M., Tang, D., Shi, X., Zhou, L., Zhou, X., Song, H., Jiang, G., 2019. A pulse of oxygen increase  
 1851 in the early Mesoproterozoic ocean at ca. 1.57-1.56 Ga. *Earth and Planetary Science Letters*, 527,  
 1852 115797.
- 1853 Sharma, Mukund, Shukla, Y. 2009. Taxonomy and affinity of Early Mesoproterozoic megascopically  
 1854 helically coiled and related fossils from the Rohtas Formation, the Vindhyan Supergroup, India.  
 1855 *Precambrian Research*, 173, 105–122.
- 1856 Shen, Y., Canfield, D. E. and Knoll, A. H. 2002. Middle Proterozoic ocean chemistry: evidence from  
 1857 the McArthur Basin, northern Australia. *American Journal of Science*, 302, 81-109.
- 1858 Shields, G.A., 2002. ‘Molar-tooth microspar’: a chemical explanation for its disappearance ~750 Ma.  
 1859 *Terra Nova*, 14, 108-113.
- 1860 Shields, G.A., 2007. A normalised seawater strontium isotope curve: possible implications for  
 1861 Neoproterozoic-Cambrian weathering rates and the further oxygenation of the Earth. *eEarth*, 2: 35-  
 1862 42.
- 1863 Shields, G.A., Halverson, G.P., Porter, S.M., 2018. Descent into the Cryogenian. *Precambrian Research*  
 1864 319, 1–5.
- 1865 Shields, G.A., Mills, B.J.W., 2017. Tectonic controls on the long-term carbon isotope mass balance.  
 1866 *PNAS*, doi:10.1073/pnas.1614506114.
- 1867 Shields, G.A., Mills, B.J.W., Zhu, M., Daines, S., Lenton, T.M., 2019. Unique Neoproterozoic carbon  
 1868 isotope excursions sustained by coupled evaporite dissolution and pyrite burial. *Nature Geoscience*,  
 1869 12, 823-827. doi: 10.1038/s41561-019-0434-3.
- 1870 Shields, G., Veizer, J., 2002, *Precambrian marine carbonate isotope database: Version 1.1:*  
 1871 *Geochemistry Geophysics Geosystems*, 3(6), 1–12, doi: 10.1029/2001GC000266.
- 1872 Shields-Zhou, G.A., Hill, A.C., Macbabbann, B.A., 2012. The Cryogenian Period. Chapter 17 in F.M.  
 1873 Gradstein, J. G. Ogg, M. Schmitz, and G. Ogg (Eds.), *The Geological Time Scale 2012* (vol. 1).  
 1874 Elsevier, pp. 393–411.
- 1875 Shields-Zhou, G., Porter, S.A., Halverson, G.P., 2016. A new rock-based definition for the Cryogenian  
 1876 Period (circa 720–635 Ma). *Episodes* 39, 3–9.
- 1877 Shirey, S.B., Richardson, S.H., 2011. Start of the Wilson Cycles at 3 Ga shown by Diamonds from  
 1878 Subcontinental Mantle. *Science*, 333, 434-458.
- 1879 Singh, V. K., Sharma Mukund, Sergeev V. N. 2019. A New Record of Acanthomorphic Acritarch  
 1880 *Tappania* Yin from the Early Mesoproterozoic Saraipali Formation, Singhora Group, Chhattisgarh  
 1881 Supergroup, India and its Biostratigraphic Significance. *Journal of the Geological Society of India*,  
 1882 94, 471-479.
- 1883 Sircombe, K.N., Bleeker, W., Stern, R.A., 2001. Detrital zircon geochronology and grain-size analysis  
 1884 of a ~2800 Ma Mesoarchean proto-cratonic succession, Slave Province, Canada. *Earth and Planetary*  
 1885 *Science Letters*, 189, 207-220.

- 1886 Slack, J.F., Grenne, T., Bekker, A., Rouxel, O.J., Lindberg, P.A., 2007. Suboxic deep seawater in the  
1887 late Paleoproterozoic: evidence from hematitic chert and Fe formation related to seafloor  
1888 hydrothermal sulfide deposits, central Arizona, USA. *Earth and Planetary Science Letters*, 255, 243-  
1889 256.
- 1890 Spencer, C.J., Hawkesworth, C., Cawood, P.A., Dhuime, B., 2013. Not all supercontinents are created  
1891 equal: Gondwana-Rodinia case study. *Geology*, 41(7), 795–798.
- 1892 Spencer, C.J., Murphy, J.B., Kirkland, C.L., Liu, Y., Mitchell, R.M., 2018. A Palaeoproterozoic tecton-  
1893 magmatic lull as a potential trigger for the supercontinent cycle. *Nature Geoscience*, 11: 97-101.
- 1894 Spencer, C.J., 2020. Continuous continental growth as constrained by the sedimentary record. *American*  
1895 *Journal of Science*, 320, 373-401.
- 1896 Sprigg, R.C., 1947. Early Cambrian (?) jellyfishes from the Flinders Ranges, South Australia.  
1897 *Transactions of the Royal Society of South Australia*, 71, 212–224.
- 1898 Stern, R.A., Bleeker, W., 1998. Age of the world’s oldest rocks refined using Canada’s SHRIMP:  
1899 Acasta Gneiss Complex, Northwest Territories. *Geoscience Canada*, 25, 27-31.
- 1900 Stockwell, C.H., 1961. Structural provinces, orogenies, and time classification of rocks of the Canadian  
1901 Precambrian Shield. *Geol. Surv. Canada. Paper*, 61-17, 108-118.
- 1902 Stockwell, C.H., 1982. Proposals for time classification and correlation of Precambrian rocks and  
1903 events in Canada and adjacent areas of the Canadian Shield. Part 1: A time classification of  
1904 Precambrian rocks and events. *Geol. Surv. Can. Pap.* 80-19.
- 1905 Stolper, D.A., Brenhin-Keller, C., 2018. A record of deep-ocean dissolved O<sub>2</sub> from the oxidation  
1906 state of iron in submarine basalts. *Nature*, doi:10.1038/nature/25009.
- 1907 Strachan, R., Murphy, J.B., Darling, J., Storey, C., Shields, G.A., 2020. Precambrian (4.56–1.0 Ga).  
1908 From: F.M. Gradstein, J.G. Ogg, M.D. Schmitz, G.M. Ogg (Eds.). *The Geologic Time Scale 2020*  
1909 volume 1. Elsevier Science Limited, 481-493pp.
- 1910 Strauss, J.V., Rooney, A.D., Macdonald, F.A., Brandon, A.D., Knoll, A.H., 2014. 740 Ma vase-shaped  
1911 microfossils from Yukon, Canada: implications for Neoproterozoic chronology and biostratigraphy:  
1912 *Geology*, 42, 659–662.
- 1913 Swanson-Hysell, N. L., Maloof, A. C., Condon, D. J., Jenkin, G. R. T., Alene, M., Tremblay, M. M.,  
1914 Tesema, T., Rooney, A. D., Haileab, B., 2015. Stratigraphy and geochronology of the Tambien Group,  
1915 Ethiopia: Evidence for globally synchronous carbon isotope change in the Neoproterozoic. *Geology*  
1916 43, 323–326.
- 1917 Swanson-Hysell, N. L., Maloof, A. C., Kirschvink, J. L., Evans, D. A. D., Halverson, G. P., Hurtgen,  
1918 M. T., 2012. Constraints on Neoproterozoic paleogeography and Paleozoic orogenesis from  
1919 paleomagnetic records of the Bitter Springs Formation, central Australia. *American Journal of Science*  
1920 312, 817–884.
- 1921 Tang, H., Chen, Y., 2013. Global glaciations and atmospheric change at c. 2.3 Ga. *Geoscience Frontiers*,  
1922 4: 583-596.

- 1923 Tang, Q., Pang, K., Xiao, S., Yuan, X., Ou, Z., Wan, B., 2013. Organic-walled microfossils from the  
 1924 early Neoproterozoic Liulaobei Formation in the Huainan region of North China and their  
 1925 biostratigraphic significance. *Precambrian Research* 236, 157–181.
- 1926 Tang, Q., Pang, K., Yuan, X., Wan, B., Xiao, S., 2015. Organic-walled microfossils from the  
 1927 TonianGouhou Formation, Huaibei region, North China Craton, and their biostratigraphic  
 1928 implications. *Precambrian Research* 266, 296–318.
- 1929 Tang, D., Shi, X., Wang, X., Jiang, G., 2016. Extremely low oxygen concentration in mid-Proterozoic  
 1930 shallow seawaters. *Precambrian Research*, 276, 145-157.
- 1931 Tang, Q., Pang, K., Yuan, X., Xiao, S., 2020. A one-billion-year-old multicellular chlorophyte. *Nature*  
 1932 *Ecology and Evolution*, doi: 10.1038/s41559-020-1122-9.
- 1933 Teixeira, W., Geraldes, M.C., Matos, R., Salina Ruiz, A., Saes, G., Vargas-Mattos, G., 2010. A review  
 1934 of the tectonic evolution of the Sunsas Belt, SW Amazonian craton. *Journal of South American Earth*  
 1935 *Sciences*, 29, 47-60.
- 1936 Thomazo, C., Pinto, D.L., Busigny, V., Ader, M., Hashizume, K., Philippot, P., 2009. Biological  
 1937 activity and the Earth’s surface evolution: insights from carbon, sulfur, nitrogen and iron stable  
 1938 isotopes in the rock record. *Comptes Rendus Palevol*, 8, 665-678.
- 1939 Thomson, J., 1871. On the stratified rocks of Islay. Report of the 41st Meeting of the British Association  
 1940 for the Advancement of Science, Edinburgh, John Murray, London, pp. 110-111.
- 1941 Thomson, J., 1877. On the geology of the island of Islay. *Transactions of the Geological Society of*  
 1942 *Glasgow* 5, 200-222.
- 1943 Thomson, D., Rainbird, R.H., Planavsky, N., Lyons, T.W., Bekker, A., 2015. Chemostratigraphy of the  
 1944 Shaler Supergroup, Victoria Island, NW Canada: a record of ocean composition prior to the  
 1945 Cryogenian glaciations. *Precambrian Research*, 263, 232-245.
- 1946 Torres, M.A., Paris, G., Adkins, J.F., Fischer, W.W., 2018. Riverine evidence for isotopic mass balance  
 1947 in the Earth’s early sulfur cycle. *Nature Geoscience*, 11, 661-664.
- 1948 Trendall, A.F., 1966. Towards rationalism in Precambrian stratigraphy. *Geol. Soc. Austr. J.*, 13, 517-  
 1949 522.
- 1950 Trendall, A.F., 1991. The “Geological Unit” (g.u.) – A suggested new measure of geologic time.  
 1951 *Geology*, 19, 195.
- 1952 Trendall et al. (2004)
- 1953 Tsikos, H., Matthews, A., Erel, Y., Moore, J.M., 2010. Iron isotopes constrain biogeochemical redox  
 1954 cycling of iron and manganese in a Palaeoproterozoic stratified basin. *Earth and Planetary Science*  
 1955 *Letters*, 298, 125-134.
- 1956 Tyrell, T. 1999. The relative influences of nitrogen and phosphorus on oceanic primary production.  
 1957 *Nature* 400, 525–531.
- 1958 Van Kranendonk, M.J., Altermann, W., Beard, B.L., Hoffman, P.E., Johnson, C.J., Kasting, J.F.,  
 1959 Melezhik, V.A., Nutman, A.P., Papineau, D., Pirajino, F., 2012. A chronostratigraphic division of the

- 1960 Precambrian: possibilities and challenges. In: Gradstein, F.M., Ogg, J.G., Schmitz, M., Ogg, G.,  
 1961 (Coordinators). *The Geologic Time Scale 2012*. Elsevier Publ., pp. 299-392.
- 1962 Van Kranendonk, M.J., Kirkland, C.L., 2016. Conditioned duality of the Earth system: Geochemical  
 1963 tracing of the supercontinent cycle through Earth history. *Earth-Science Reviews*, 160: 171-187.
- 1964 Veizer, J., 1989. Strontium isotopes in seawater through time. *Annual Reviews of Earth and Planetary  
 1965 Sciences*, 17, 141-167.
- 1966 Vermeesch, P., Resentini, A., and Garzanti, E., 2016. An R package for statistical provenance analysis:  
 1967 *Sedimentary Geology*, 336, 14–25, <https://doi.org/10.1016/j.sedgeo.2016.01.009>
- 1968 Walker, J.C.G., Hays, P.B., and Kasting, J.F., 1981. A negative feedback mechanism for the long-term  
 1969 stabilization of Earth's surface temperature: *Journal of Geophysical Research*, 86, 9776,  
 1970 doi:10.1029/JC086iC10p09776.
- 1971 Walter, M. R., Oehler, J. H., and Oehler, D. Z. 1976. Megascopic algae 1300 million years old from the  
 1972 Belt Supergroup, Montana: a reinterpretation of Walcott's Helminthoidichnites. *Journal of  
 1973 Paleontology* 50, 872–881.
- 1974 Wang, X. C., Li, Z. X., Li, X. H., Li, Q. L., Zhang, Q.-R., 2011. Geochemical and Hf-Nd isotope data  
 1975 of Nanhua rift sedimentary and volcanoclastic rocks indicate a Neoproterozoic continental flood basalt  
 1976 provenance. *Lithos*, 427–440.
- 1977 Wang, C., Peng, P., Wang, X., Yang, S., 2016. Nature of three Proterozoic (1680 Ma, 1230 Ma and 775  
 1978 Ma) mafic dyke swarms in North China: Implications for tectonic evolution and paleogeographic  
 1979 reconstruction. *Precambrian Research*, 285, 109-126.
- 1980 Wang, D., Zhu, X.-K., Zhao, N., Yan, B., Li, X.-H., Shi, F., Zhang, F., 2019. Timing of the termination  
 1981 of Sturtian glaciation: SIMS U-Pb zircon dating from South China. *Journal of Asian Earth Sciences*  
 1982 177, 287–294.
- 1983 Ward, L.M., Kirschvink, J.L., Fischer, W.W., 2016. Timescales of oxygenation following the evolution  
 1984 of oxygenic photosynthesis. *Origin of Life and Evolution of the Biosphere*, 46, 51-65.
- 1985 Warke, M.R., Strauss, H., Schröder, S., 2020a. Positive cerium anomalies imply pre-GOE redox  
 1986 stratification and manganese oxidation in Paleoproterozoic shallow marine environments.  
 1987 *Precambrian Research*, 344, 105767.
- 1988 Warke, M.R., Di Rocco, T., Zerkle, A.L., Lepland, A., Prave, A.R., Martin, A.P., Ueno, Y., Condon,  
 1989 D.J., Claire, M.W., 2020b. The Great Oxidation Event preceded a Paleoproterozoic Snowball Earth.  
 1990 *Proceedings of the National Academy of Sciences*, 117, 13314-13320.
- 1991 Whitmeyer, S.J., Karlstrom, K.E., 2007. Tectonic model for the Proterozoic growth of North America.  
 1992 *Geosphere*, 3: 220-259.
- 1993 Worsley, T.R., Nance, R.D., Moody, J.B., 1985. Proterozoic to recent tectonic tuning of biogeochemical  
 1994 cycles. In: Sunquist, E.T., Broecker, W.S. (Eds.), *The Carbon Cycle and Atmospheric CO<sub>2</sub>: Natural  
 1995 Variations Archean to Present*. American Geophysical Union, *Geophysical Monographs*, 32: 561-572.



- 1996 Xiao, S., Narbonne, G.M., 2020. The Ediacaran Period. From: F.M. Gradstein, J.G. Ogg, M.D. Schmitz,  
 1997 G.M. Ogg (Eds.). The Geologic Time Scale 2020 volume 1. Elsevier Science Limited 521-560pp.
- 1998 Xiao, S., Tang, Q., 2018. After the boring billion and before the freezing millions: evolutionary patterns  
 1999 and innovations in the Tonian Period: Emerging Topics in Life Sciences, 2, 161-171, doi:  
 2000 10.1042/ETLS20170165.
- 2001 Yang, B., Collins, A.S., Blades, M.L., Capogreco, N., Payne, J.L., Munson, T.J., Cox, G.M., 2019.  
 2002 Middle-late Mesoproterozoic tectonic geography of the North Australia Craton: U–Pb and Hf isotopes  
 2003 of detrital zircons in the Beetaloo Sub-basin, Northern Territory, Australia. Journal of the Geological  
 2004 Society, London, 176, 771-784.
- 2005 Yang, B., Collins, A.S., Cox, G.M., Jarrett, A.J.M., Denyszyn, S., Blades, M.L., Farkaš, J., Glorie, S.,  
 2006 2020. Using Mesoproterozoic Sedimentary Geochemistry to Reconstruct Basin Tectonic Geography  
 2007 and Link Organic Carbon Productivity to Nutrient Flux from a Northern Australian Large Igneous  
 2008 Province. Basin Research, 2020; 00: 1–17. <https://doi.org/10.1111/bre.12450>.
- 2009 Yin, L. 1997. Acanthomorphic acritarchs from Meso-Neoproterozoic shales of the Ruyang Group,  
 2010 Shanxi, China. Rev. Palaeobot. Palynol., 98: 15-25.
- 2011 Yin, L., Changtai, N., Kong, F.-F. 2018. A Review of Proterozoic Organic walled Microfossils –  
 2012 *Tappania* and Its Biologic and Geologic Implication. Acta Palaeontol. Sinica, 57: 147-156.
- 2013 Young, G.M., 2013. Precambrian supercontinents, glaciations, atmospheric oxygenation, metazoan  
 2014 evolution and an impact that may have changed the second half of Earth history. Geoscience Frontiers,  
 2015 4: 247-261.
- 2016 Young, G.M., 2019. Aspects of the Archean-Proterozoic transition: How the great Huronian Glacial  
 2017 Event was initiated by rift-related uplift and terminated at the rift-drift transition during break-up of  
 2018 Lauroscandia. Earth Science Reviews, 190, 171-189.
- 2019 Zalasiewicz, J. Smith, A., Brenchley, P., Evans, J., Knox, R., Riley, N., Gale, A., Gregory, F.J.,  
 2020 Rushton, A., Gibbard, P., Hesselbo, S., Marshall, J., Oates, M., Rawson, P., Trewin, N., 2004.  
 2021 Simplifying the stratigraphy of time. Geology, 32, 1-4.
- 2022 Zhai, M.G., Hu, B., Zhao, T.P., Peng, P., Meng, Q.R., 2015. Late Paleoproterozoic-Neoproterozoic  
 2023 multi-rifting events in the North China craton and their geological significance: a study advance and  
 2024 review. Tectonophysics, 662, 153-166.
- 2025 Zhang, K., Zhu, X., Wood, R., Shi, Y., Gao, Z., Poulton, S.W., 2018. Oxygenation of the  
 2026 Mesoproterozoic ocean and the evolution of complex eukaryotes. Nature Geoscience, 11: 345-350.
- 2027 Zhang, S., Wang, X., Wang, H., Bjerrum, C.J., Hammerlund, E.U., Mafalda Costa, M., Connelly, J.N.,  
 2028 Zhang, B., Su, J., Canfield, D.E., 2016. Sufficient oxygen for animal respiration 1,400 million years  
 2029 ago. Proceedings of the National Academy of Science, 113, 1731-1736.
- 2030 Zhang, S., Ernst, R.E., Pei, J., Zhao, Y., Zhou, M., Hu, G., 2018. A temporal and causal link between  
 2031 c. 1380 Ma large igneous provinces and black shale: Implications for the Mesoproterozoic time scale  
 2032 and paleoenvironment. Geology, 46: 963-966.

- 2033 Zhao, G., Cawood, P.A., 2012. Precambrian geology of China. *Precambrian Research*, 222-223, 13-54.
- 2034 Zhao, G., Cawood, P.A., Wilde, S.A., Sun, M., 2002. Review of global 2.1-1.8 Ga orogens: implications  
2035 for a pre-Rodinia supercontinent. *Earth-Science Reviews*, 59, 125-162.
- 2036 Zhou, C.M., Huyskens, M.H., Lang, X.G., Xiao, S.H., Yin, Q.Z., 2019. Calibrating the terminations of  
2037 Cryogenian global glaciations: *Geology*, 47, 251–254, doi: 10.1130/G45719.1.
- 2038 Zhou, Y., Pogge von Strandmann, P.A.E., Zhu, M., Ling, H., Manning, C., Li, D., He, T., Shields, G.A.,  
2039 2020. Reconstructing Tonian seawater  $^{87}\text{Sr}/^{86}\text{Sr}$  using calcite microspar. *Geology*, doi:  
2040 10.1130/G46756.1.
- 2041 Zhu, S., Zhu, M., Knoll, A.H., Yin, Z., Zhao, F., Sun, S., Qu, Y., Shi, M., Liu, H., 2016. Decimetre-  
2042 scale multicellular eukaryotes from the 1.56-billion-year-old Gaoyuzhuang Formation in North China.  
2043 *Nature Communications*, doi: 10.1038/ncomms11500.
- 2044 Zumberge, J.A., Rocher, D., Love, G.D., 2019. Free and kerogen-bound biomarkers from late Tonian  
2045 sedimentary rocks record abundant eukaryotes in mid-Neoproterozoic marine communities.  
2046 *Geobiology*, doi: 10.1111/gbi.12378.
- 2047
- 2048

2049 **Figure captions**

2050

2051 **Fig. 1A.** Current geological time scale; **1B.** Timescale proposal of van Kranendonk et al. (2012). Golden  
2052 spike symbols represent ratified (yellow) and potential (pale) GSSP levels. Clock symbols represent  
2053 ratified Proterozoic and recommended Archean GSSAs.

2054

2055 **Fig. 2.** Evolution of stratigraphic terminology for the Neoproterozoic Era. Note that age ranges for  
2056 earlier subdivisions are based on current age estimates. Triangle symbol ( $\Delta$ ) denotes the approximate  
2057 levels of glaciations relevant to the time scale subdivisions. \* Denotes the term “Ediacarian” introduced  
2058 by Cloud and Glaessner (1982).

2059

2060 **Fig. 3.** Peaks in the distribution ( $1\sigma$  error) of U–Pb zircon ages for orogenic granitoids and detrital  
2061 zircon grains match intervals of supercontinent assembly, whereas troughs correspond to intervals of  
2062 supercontinent tenure and break-up (from Condie and Aster 2010; Condie, 2014). Black: Total ages ( $n$   
2063 = 37,830); Green: detrital ancient sedimentary rocks ( $n$  = 21,849); Blue: detrital modern sediments ( $n$   
2064 = 7053;  $2x$ ); Red: orogenic granitoids ( $n$  = 8928). N (vertical axis) is the number of zircon ages as a  
2065 function of time for a Gaussian kernel bandwidth of three standard deviations (30 m.y.).

2066

2067 **Fig. 4.** The Neoproterozoic geological time scale (after Halverson et al., 2020). Negative  
2068 carbon isotope anomalies (BSA = Bitter Springs Anomaly; RA = Russøya anomaly; GA =  
2069 Garvellach anomaly; TA = Trezona Anomaly; SA = Shuram Anomaly; E-CA = Ediacaran-  
2070 Cambrian boundary anomaly). Minimum biostratigraphic ranges are also shown for  
2071 *Trachyhystrichosphaera aimika*, *Cerebrosphaera globosa* (*C. buickii*), and the *Cycliocyrrillium*  
2072 *simplex* assemblage. Geochronological age constraints for the Tonian and Cryogenian periods  
2073 (along with ages from the early Ediacaran Period that provide minima on the Cryogenian-  
2074 Ediacaran boundary) are shown (in open squares) by type of age determination. **4B.** Expanded  
2075 view of the age constraints that establish the synchronous onset and end of the Cryogenian  
2076 glaciations.

2077

2078 **Fig. 5.** Neoproterozoic seawater strontium isotope curve (blue line) superimposed on known large  
2079 igneous provinces (red bars) and the carbon isotope record (after Zhou et al., 2020).

2080 **Fig. 6A.** Current geological time scale; **6B.** Proposed chronostratigraphic subdivision of the geological  
2081 time scale – this paper. Note that era and period boundary ages are approximate ages only and would  
2082 inevitably change in any internationally agreed chronostratigraphic scheme. Period names in italics  
2083 represent suggested changes to existing nomenclature. If the first period of the Paleoproterozoic Era

2084 were renamed (here as the *Scourian* Period, cf. Oxygenian Period of van Kranendonk et al., 2012), we  
2085 note that the term ‘Siderian’ would likely be retained for the final period of the Archean Eon.

2086

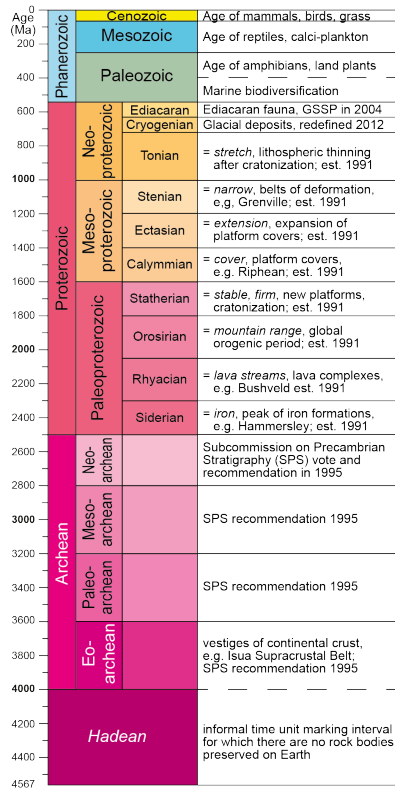
2087

# A community effort towards an improved geological time scale

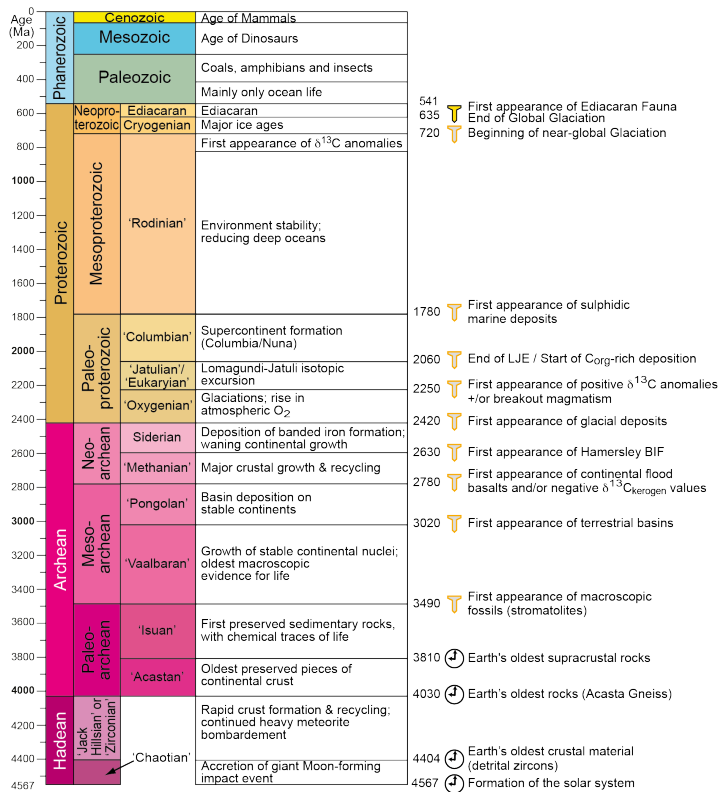
2088 Figure 1

2089

(A) Current subdivision of the Geological Time Scale



(B) Alternative Geological Time Scale from GTS2012



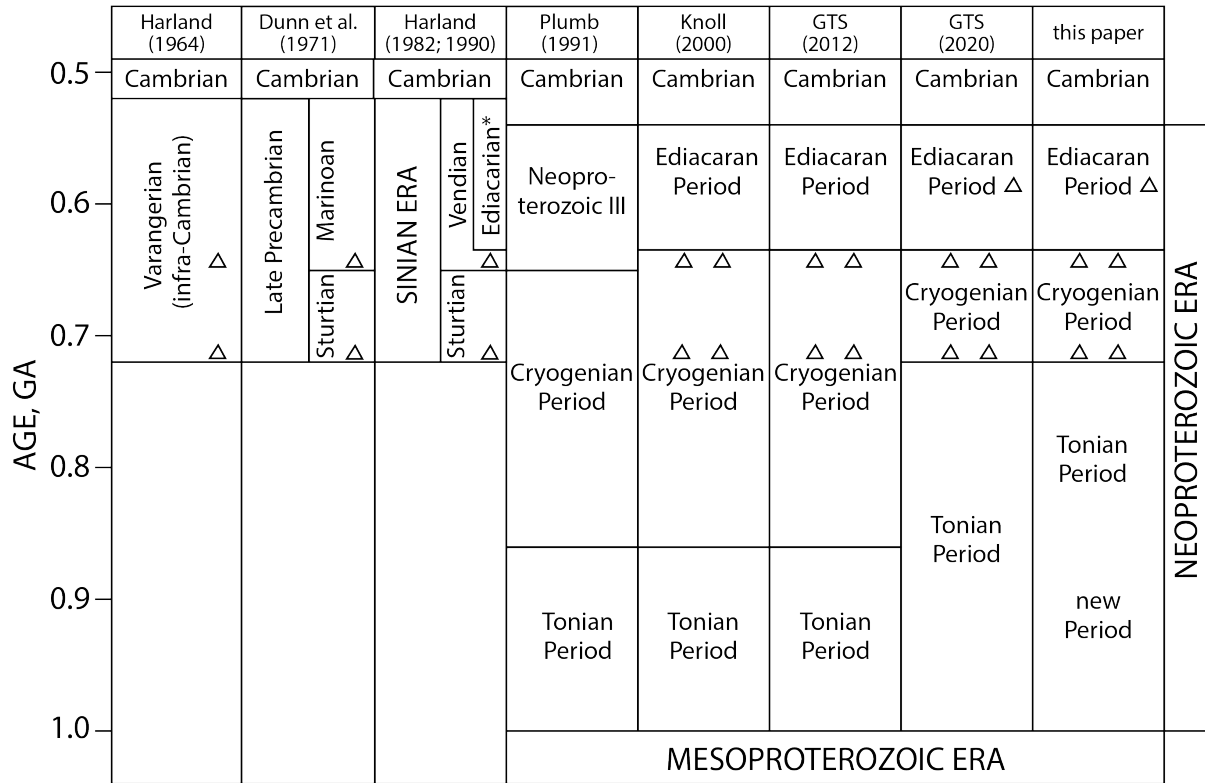
2090

2091

2092

2093 **Figure 2**

2094



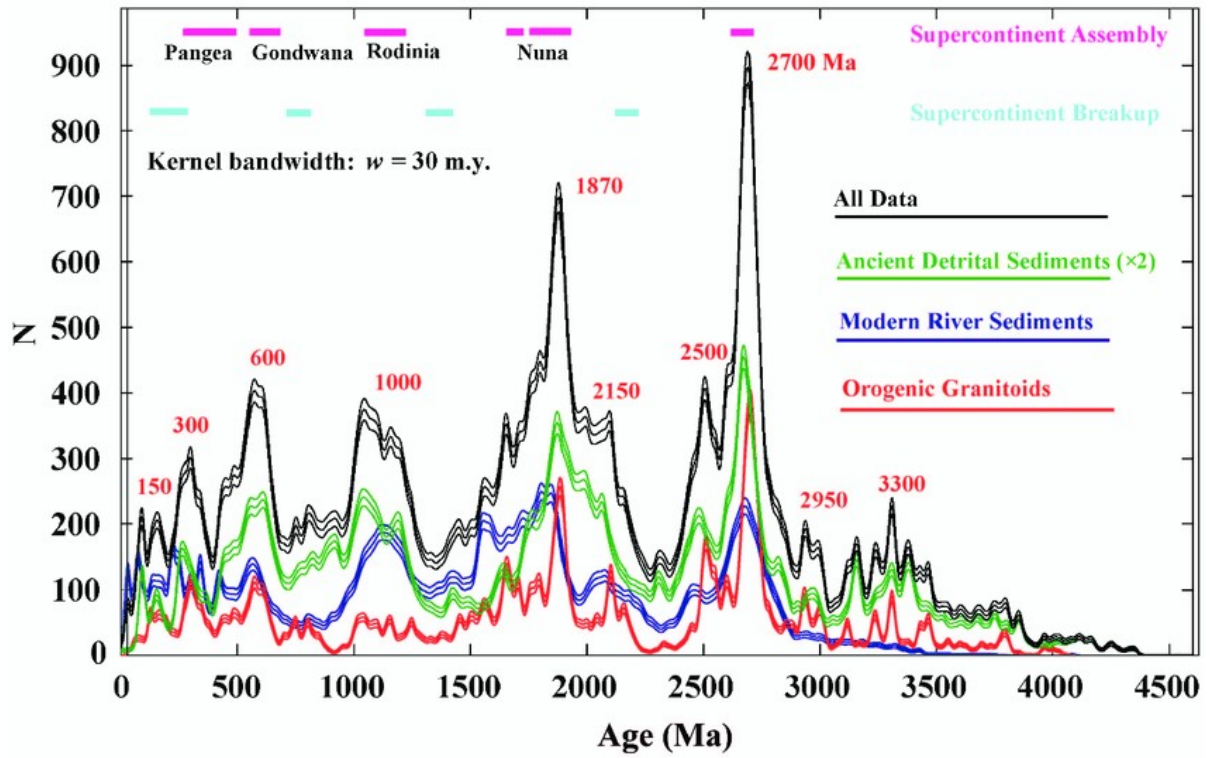
2095

2096

2097

2098 Figure 3

2099



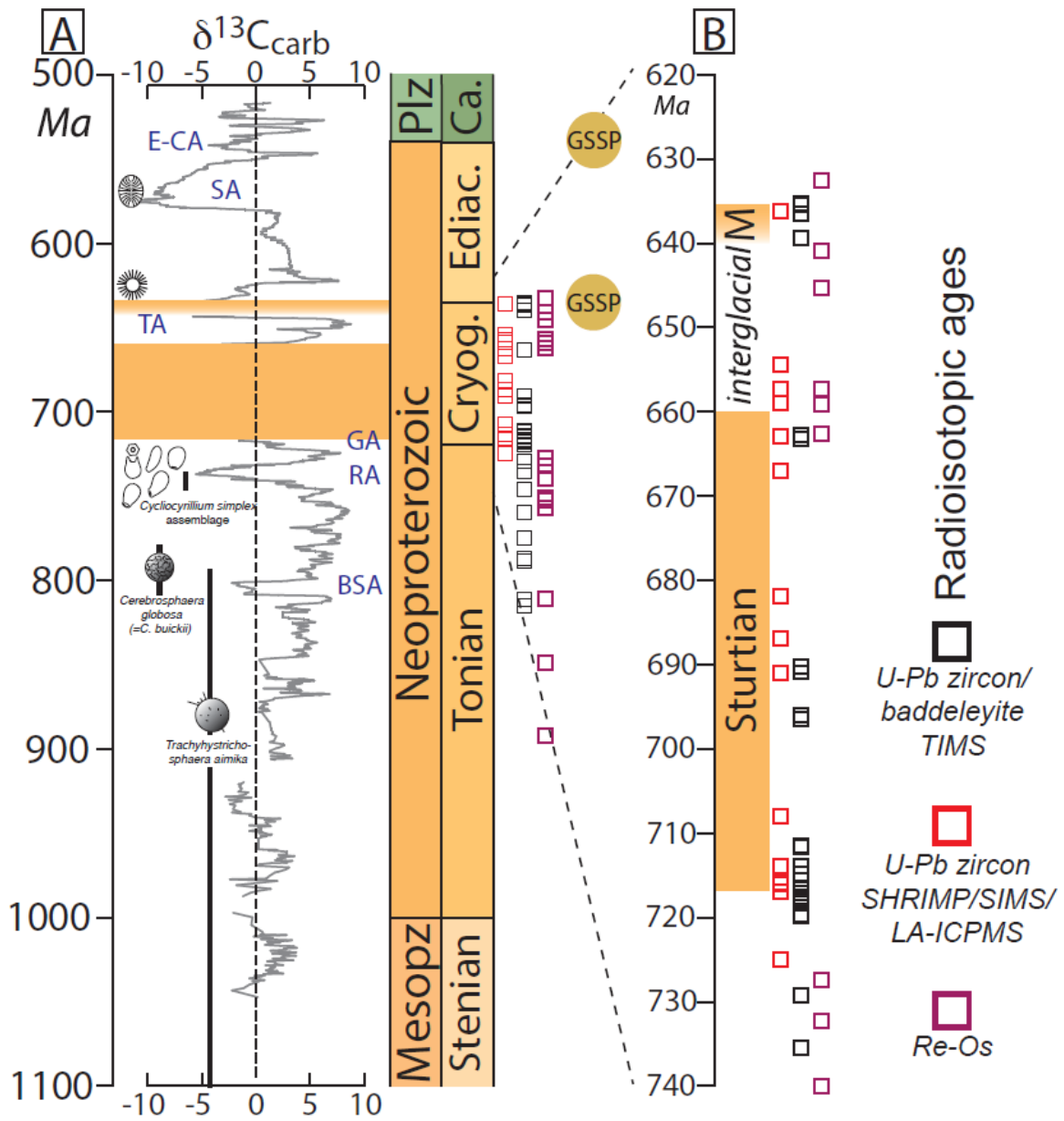
2100

2101

2102

2103 Figure 4

2104



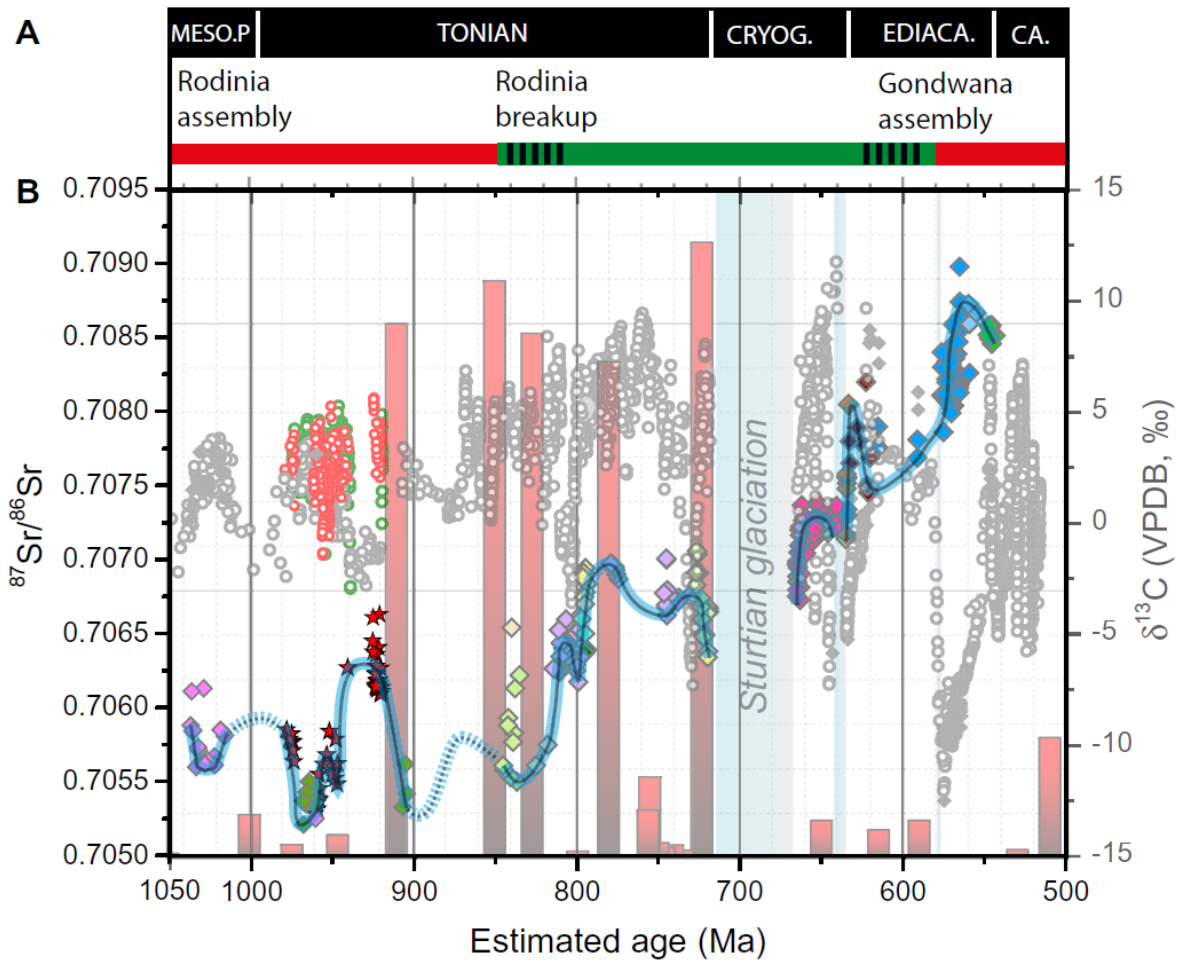
2105

2106

2107



2108 Figure 5  
 2109  
 2110

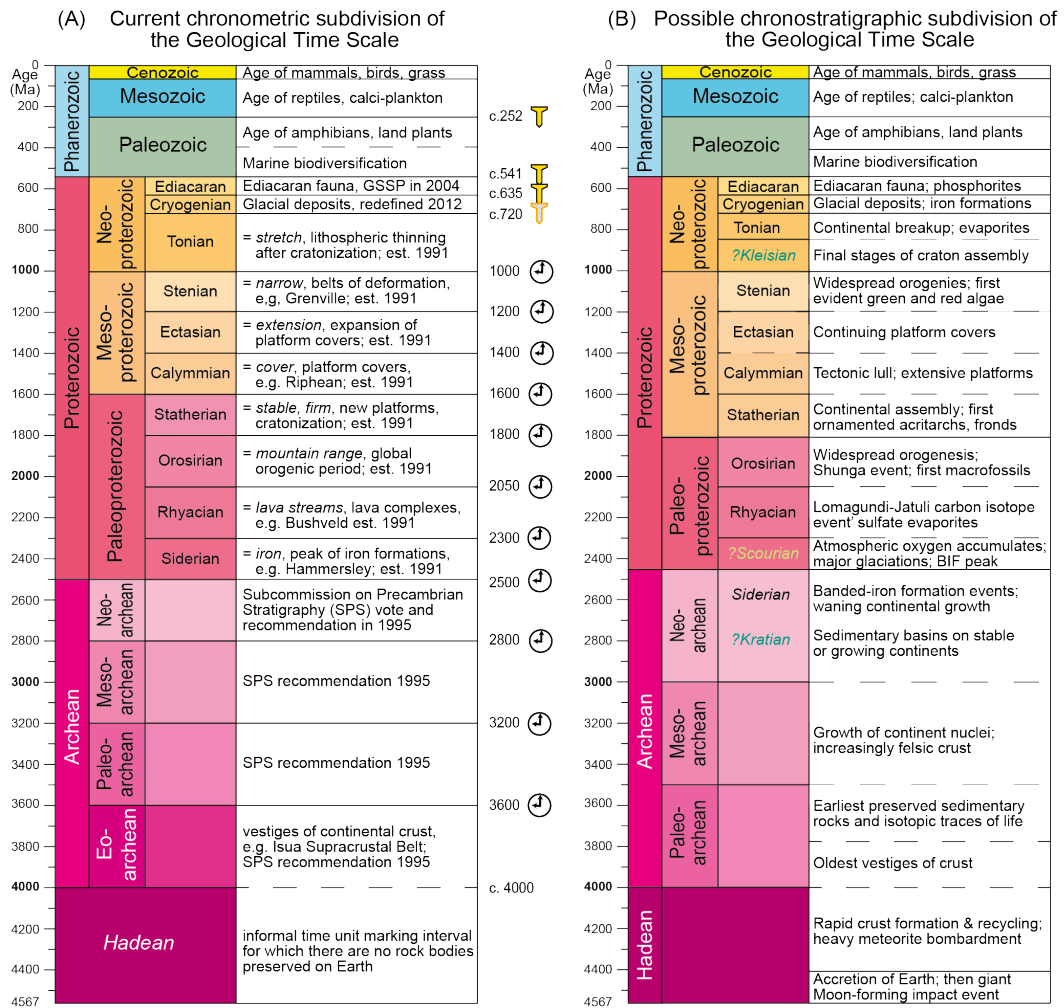


2111  
 2112

# A community effort towards an improved geological time scale

2113 **Figure 6**

2114



2115

2116

2117